WNT SIGNALING IN THE MOUSE SMALL INTESTINE

by

Adria Decker Dismuke

A DISSERTATION

Presented to the Department of Molecular and Medical Genetics

And the Oregon Health and Science University

School of Medicine

In partial fulfillment of the requirements for the degree of

Doctor of Philosophy

July 2009

School of Medicine
Oregon Health and Science University

CERTIFICATE OF APPROVAL

This is to certify that the Ph.D. thesis of

Adria Decker Dismuke

has been approved

Mentor/Advisor

Committee Chair

Member

Member

Member

Member

TABLE OF CONTENTS

LIST OF FIGURES

CHAPTER 1

CHAPTER 2

CHAPTER 3

CHAPTER 4

CHAPTER 5

APPENDIX 1

APPENDIX 2

APPENDIX 3

ABBREVIATIONS

ALCAM	Activated leukocyte cell adhesion molecule
APC/Apc	Adenomatous Polyposis Coli
BM	Bone Marrow
BMDC	Bone Marrow Derived Cells
Bmp	Bone morphogenetic protein
BrdU	5-Bromo-2-deoxyuridine
β-gal	beta-galactosidase
CamKII	Ca2+/calmodulin-dependent protein kinase
CBC cell	Crypt-Base Columnar cell
CIC	Cancer-initiating cells
CKI	Casein Kinase I
CRC	Colorectal Cancer
CRD	Cysteine Rich Domain
CSC	Cancer stem cell
CT	Cycle Threshold
Dkk	Dickkopf
Dsh	Disheveled
DSI	Distal Small Intestine
DsRed	*Discosoma sp*. red fluorescent protein
EDTA	ethylenediaminetetraacetic acid
eGFP	Enhanced Green Fluorescent Protein
ES cell	Embryonic Stem cell
ESA	Epithelial Surface Antigen
FACS	Fluorescence Activated Cell Sorting
FISH	Fluorescent *in situ* hybridization
FGF	Fibroblast Growth Factor
Gapdh	Glyceraldehyde 3-phosphate dehydrogenase
GFP	Green Fluorescent Protein
GI	Gastrointestinal
GSK3β	Glycogen synthase kinase 3 beta
H&E	Hematoxylin and Eosin
HBSS	Hank's Buffered Saline Solution
HIV	Human Immunodeficiency Virus
FACS	Fluorescence-activated cell sorting
FAP	Familial Adenomatous Polyposis
Fz	Frizzled
Jnk	Jun kinase
LEF	Lymphoid Enhancer-Binding Factor
Lrp	Low-density lipoprotein receptor-related protein
LTR	Long terminal repeat
MIN	Multiple Intestinal Neoplasia
mRNA	Messenger Ribonucleic Acid
MSI	Medial Small Intestine
Msi-1	Musashi-1

NFAT	Nuclear Factor of Activated T Cell
PBS	Phosphate Buffered Saline
PCP	Planar Cell Polarity
PCR	Polymerase Chain Reaction
PKC	Protein Kinase C
PSI	Proximal small intestine
qPCR	Quantitative polymerase chain reaction
qRT-PCR	Quantitative reverse transcriptase polymerase chain reaction
sFRP	Secreted Frizzled-related protein
Shh	Sonic hedgehog
SIN	Self-inactivating
Std	Standard deviation
TA-cell	Transient amplifying cell
Tcf	T-cell factor
Tgf-β	Transforming growth factor beta
VSV	Vesicular stomatitis virus
X-gal	bromo-chloro-indolyl-galactopyranoside

ACKNOWLEDGEMENTS

I am so lucky to have an excellent support system in both my personal and professional life, without which I surely would not be writing this dissertation. I am grateful to have this opportunity to thank them all.

First and foremost, I would like to thank my mentor, Dr. Melissa Wong. Missy taught me that when your experiments are going well in the lab, you have to work as hard as you possibly can because you never know when they are going to stop working – but when things aren't going well, you have to work even harder. She is a fantastic role model as a woman scientist, showing that it is possible to balance family life and work life, and excel at both. She tirelessly encouraged me to keep pushing through when experiments failed and ended all of our meetings with instructions to "Go! Fight! Win!". I sincerely appreciate the hundreds of hours she has spent helping me think critically about my research, planning the next steps, reading my grants and manuscripts, and teaching me how to present my work effectively. Any graduate student would be lucky to have such a dedicated mentor, and I thank her from the bottom of my heart.

I also thank the other members of the Wong lab, past and present, for their support, help, and insight. I am grateful to Paige Davies for her good example and hard work, especially as the first author of the paper that lay the foundation for my thesis and her critical reading of my dissertation. I am thankful for my fellow graduate students: Annie Powell for her friendship, support, and FACS expertise, and Trevor Levin for his creative and entertaining mind. Christy Glynn was indispensable for her help maintaining the mouse colony and as an

extra pair of hands to aid me with analysis. Thanks also to John Swain as the original Wong lab member: he taught me how to dissect a mouse intestine, a skill I will treasure for the rest of my life.

I must also thank my friends and family. Firstly, I am so grateful to my amazing husband Daniel for his love and support. He is my foundation. Dan, thanks for taking care of me even when I'm cranky. I am thankful to my family: my parents Laurel and Randy Decker, for their unconditional love and support and generally being the best parents a person could ask for; my brilliant sister Amelia (sorry sweetie, I get to have the Dr. title first); and my loving and ingenious brother Alex. Jennifer Johnson was the first friend I made when I moved to Oregon from Arizona, and she has saved my sanity many times throughout the years. I treasure her friendship dearly.

Finally, thank you to all the students, faculty, and staff at OHSU that have helped me along the way. Thank you to Dr. Susan Olson and the MMG department for their support. Thanks to Dr. Peter Kurre for agreeing to be my committee chairperson. And lastly, many thanks to my Thesis Advisory Committee, Dr. Markus Grompe, Dr. Mike Liskay, Dr. Rosalie Sears, and Dr. Scott Stadler, for their scientific insight over the years and critical reading of my dissertation.

ABSTRACT

The Wnt signaling pathway is an essential regulator of the intestinal epithelium, during development and throughout adulthood. Inappropriate activation of this pathway leads to over-proliferation of the epithelium and intestinal cancer, whereas inhibition causes a loss of stem cells and collapse of the intestinal epithelium. To date, there are 19 Wnt ligands that have been identified in both mice and humans, several of which are expressed in the intestine. However, not all Wnt ligands serve to activate the canonical pathway that signals through β-catenin, and the functional role of the various ligands in the intestinal epithelium has not been conclusively determined.

In the mature intestine, proliferation is confined to the relatively quiescent stem cells and the rapidly cycling transient-amplifying cells within the intestinal crypts. Although the Wnt signal has previously been reported to regulate all proliferating intestinal cells, this has not been definitively demonstrated. A precise understanding of how the canonical pathway is regulated and what role the β-catenin independent Wnt ligands play in intestinal epithelial homeostasis has important implications for intestinal function, especially during epithelial expansion or regeneration, and warrants an extensive characterization of Wnt-activated cells. We found that Wnt-positive cells were restricted to the base of the small intestinal and colonic crypts. Intriguingly, the majority of the Wnt-reporter-expressing cells did not overlap with the transient-amplifying cell population, and expressed stem cell markers but not differentiation markers. Further, the number of Wnt-activated intestinal crypt cells increased in response to γ-irradiation.

Though Wnt activation was not seen endogenously in the rapidly proliferating transient-amplifying population, overexpression of human WNT1 did stimulate mitosis, resulting in an expansion of the proliferation zone in the crypts and intestinal polyps. This supports the notion that, though it is not the sole regulator of proliferation during crypt homeostasis, over-stimulated Wnt signaling is capable of inducing proliferation and speaks to the importance of tight regulation of the Wnt ligands.

Wnt5a, a ligand that signals independently of β-catenin and is normally expressed in the mouse small intestinal mesenchyme, negatively regulates the canonical Wnt pathway in some receptor contexts. Here we show that Wnt activation is inhibited when Wnt5a is ectopically expressed in the intestine, both by changes in reporter gene expression and by the aberrant localization of differentiated Paneth cells. Furthermore, analyses of damage and disease models suggest that Wnt5a may exist in a negative feedback loop with the canonical pathway. These studies have important implications about the essential role of Wnt signaling in the intestinal epithelium, the manner in which it is required for stem cell regulation, and a mechanism of canonical Wnt regulation in damage and disease.

CHAPTER 1

BACKGROUND AND INTRODUCTION

I. The Structure of the Small Intestine

II. The Canonical Wnt Pathway

III. Wnt5a and β-catenin-independent Wnt Signaling Pathways

IV. Tools for Studying the Wnt Signaling Pathway *In Vivo*

V. Hypothesis and Rationale

CHAPTER 1: Background and Introduction

I. The Structure of the Small Intestine

The gastrointestinal (GI) tract is a tube-like structure that extends from the oral cavity to the anus and encompasses organs including the esophagus, stomach, small intestine, large intestine, pancreas and liver (Figure 1.1). In the adult human, the GI tract is greater than 22 feet long and is efficiently coiled within the peritoneal cavity. Each region of the GI tract conveys a specialized function that is dictated by its diverse physiology. The mammalian small intestine is a complex and dynamic organ that serves a dual-functional role. The most commonly associated function of the epithelial cell layer that lines the small intestine is for proper nutritional absorption of digested food into the bloodstream. However, it also acts as a primary barrier between the organism and the external environment. If either of these essential functions are compromised, the survival of the organism is at risk. A breach of the epithelium can result in bacterial infection of the bloodstream, termed sepsis, which can rapidly cause severe illness and death. Additionally, if the intestine cannot appropriately absorb nutrients from digested food, the organism is subject to wasting and will eventually die from malnutrition or starvation. Therefore, a healthy and functional small intestine is absolutely essential for the survival of the organism.

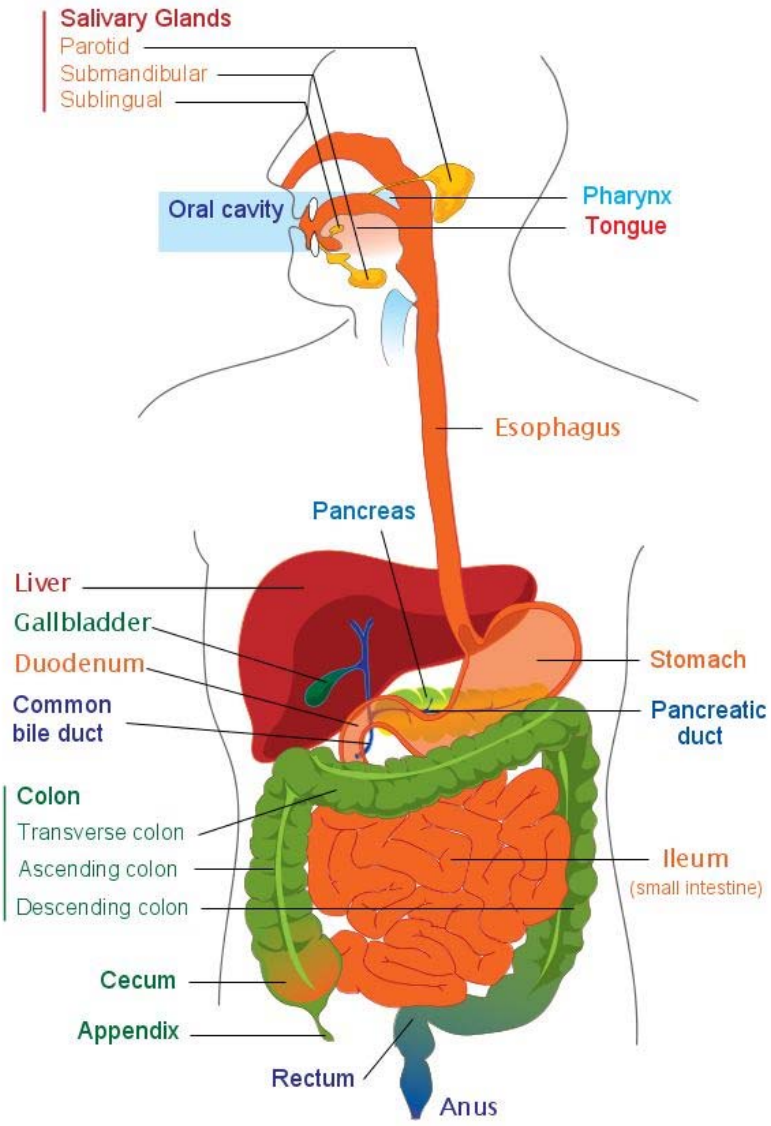

Figure 1.1. The upper and lower human gastrointestinal tract. The GI tract is a tubal structure that extends from the mouth to the anus and includes the small intestine. Open source image used under Creative Commons license.

The intestinal epithelial lining is organized in a contiguous monolayer of columnar cells. These cells line the flask-like invaginations, called the crypts of Lieberkühn, and the adjacent finger-like lumenal projections called villi (Figure 1.2). This secondary structure allows for maximal absorptive capacity, effectively increasing the intestinal surface area approximately 600-fold in humans (Wilson 1967). Not surprisingly, the villi house the majority of functionally differentiated cells specialized for nutrient absorption. The crypts residing on the floor of the small intestine, interspersed between villi, house the proliferative epithelial cell population. A multipotent epithelial progenitor (or stem cell) is located within the protective crypt niche. This stem cell can asymmetrically divide and give rise to a transit amplifying population that divides more rapidly, the progeny of which go on to make up the terminally differentiated intestinal epithelium.

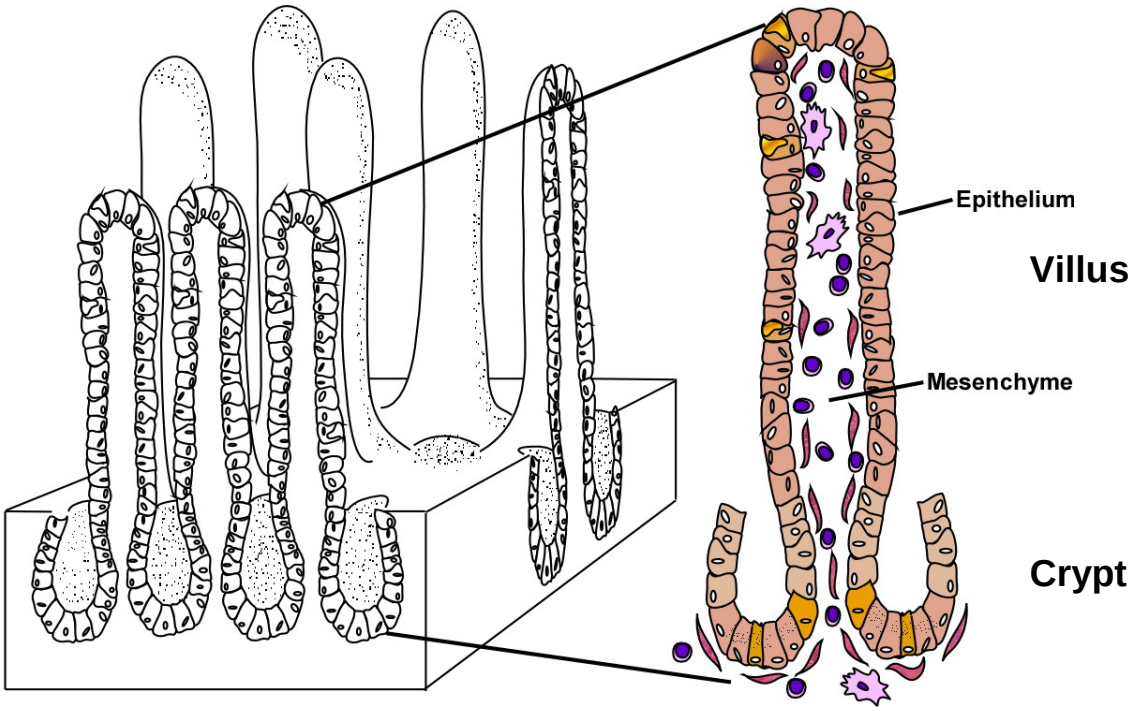

Figure 1.2. The intestinal crypt-villus unit. The intestinal epithelium is organized into differentiated finger-like luminal projections called villi and proliferative flask-shaped invaginations called crypts which surround an intricate mesenchymal compartment.

The adult mouse intestine is highly similar to the human intestine and has been used as a scientific model for understanding intestinal development, function and disease. With a tremendous capacity for proliferation, the mature mouse intestine contains approximately 1.1 million crypts (Hagemann et al., 1970), with each crypt containing as many as 530 cells in the proximal small intestine (duodenum) and approximately 340 cells in the distal small intestine (ileum). This difference in cell numbers reflects a gradient of proliferation corresponding to differential function down the length of the small intestine. The stem cells near the base of the crypt proliferate relatively slowly, but give rise to a more rapidly proliferating transient amplifying population that produces about 13-16 new cells per hour per crypt (Potten and Bullock 1983). These proliferating cells accommodate complete epithelial turnover every 5 days (Barker 2008). This continual epithelial renewal provides protection to the organism by reducing accumulation of acquired cell mutations in the face of exposure to environmental assault in the intestinal lumen.

The mouse small intestine is an ideal model system to study epithelial proliferation, stem cell determination, lineage differentiation, and regulation of the cell signaling pathways that control these processes. The intestinal epithelium contains a tightly regulated proliferation-to-differentiation program along the radial axis (crypt-villus axis) coincident with upward cellular migration. This unique structure of the intestinal epithelium recapitulates these important developmental programs where key signaling pathways important in

developmental biology underlie the mesenchyme-to-epithelial communication essential for maintaining this gradient.

Proliferation and self-renewal of the epithelium is driven by a multipotent stem cell that resides in the crypt. However, the identity of the intestinal stem cell remains somewhat debatable because definitive molecular markers have not yet been identified. While the consensus in the field is that each crypt contains between four and six ancestral stem cells (Hendry et al., 1992; Barker 2008), two opposing models have arisen regarding the location and identity of these cells: the "+4 position" model and the "stem cell zone" model (Figure 1.3). The "+4 position" model was first established in the 1950's describing a potential stem cell residing at the fourth cell position when counting up from the base of the crypt. Potten and colleagues further described this model by demonstrating that label-retaining cells exist at this position using both BrdU and H^3-thymidine (Potten 1974) and that +4 cells are particularly radiation-sensitive (Potten 1977). However, opponents of this model point out that these +4 cells cannot be experimentally linked to all cell lineages in the epithelium, and as such cannot be definitively placed in the epithelial hierarchy.

A more recent viewpoint suggests that the Crypt Base Columnar (CBC) cells, described as small, wedge-shaped, undifferentiated cycling cells that are somewhat obscured between the large cryptal Paneth cells, are the true intestinal epithelial stem cells and give rise to the +4 cells (Cheng and Leblond 1974; Cheng and Leblond 1974; Bjerknes and Cheng 1981; Bjerknes and Cheng 1981; Stappenbeck et al., 2003). A number of putative stem cell markers exist for

both of the reported stem cell populations, including Musashi-1 (Kayahara et al., 2003; Potten et al., 2003; Asai et al., 2005), β1-integrin (Fujimoto et al., 2002), DCAMKL1(May et al., 2008), Bmi-1(Reinisch et al., 2006), and a Wnt target gene that encodes an orphan G-protein-coupled receptor, Lgr5 (Barker et al., 2007).

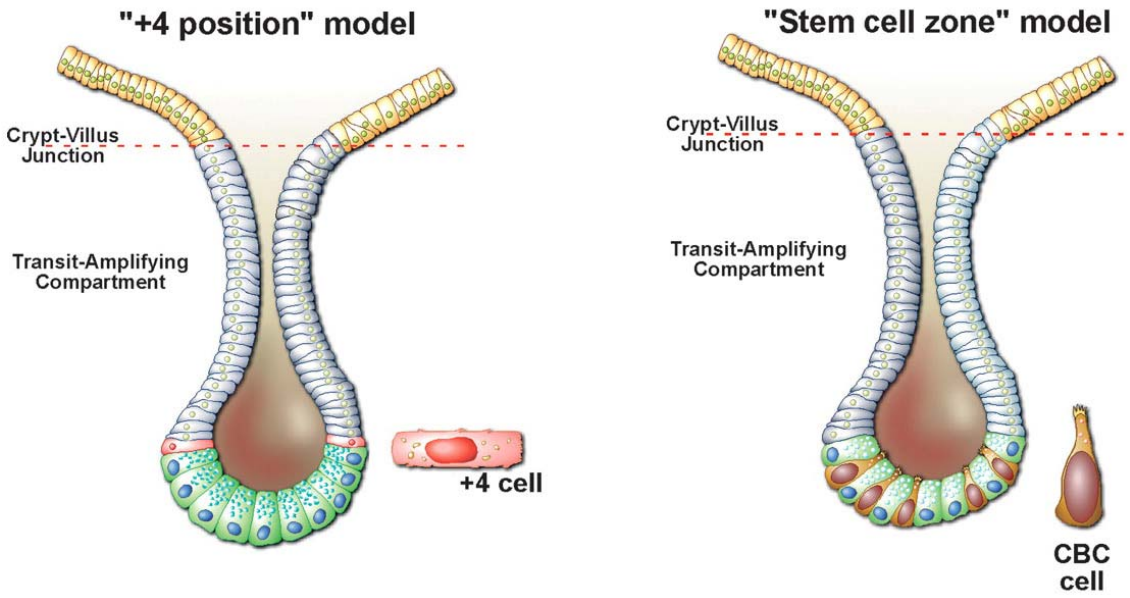

Figure 1.3. The two different proposed intestinal stem cell populations. It is a matter of some debate whether or not the ancestral intestinal stem cell resides at the "+4 position" in the crypt, or is instead a crypt-based columnar (CBC) cell located between the Paneth cells. Modified and reprinted with permission: Barker *et al.*, *Genes and Development* 15;22(14):1856-64, ©2008.

The Lgr5 protein, identified as a potential intestinal stem cell marker by Hans Clever's group in 2007, is an intriguing candidate. Lgr5 mRNA expression is restricted to columnar cells in the crypt base, lending support to the CBC stem cell model. Lineage studies with Lgr5 promoter knock-in mice show that Lgr5-expressing cells can give rise to all differentiated cell types of the intestinal epithelium (Barker et al., 2007). This is especially interesting in light of the fact that Lgr5 is a target of the canonical Wnt signaling pathway, which is known to be important in the establishment and maintenance of the intestinal epithelial stem cell, and is discussed in more depth later in this chapter.

Recently, in vitro culture conditions have been established that allow a single Lgr5+ cells to give rise to crypt/villus containing intestinal organoids validating the progenitor capacity of Lgr5 expressing intestinal epithelial cells (REF). Most interestingly, in this experiment, single cells FACS isolated from the Lgr5:GFP reporter mouse required only four supplemental factors to drive organogenesis in the absence of a mesenchymal niche (Sato et al., 2009). Crypt-like structures were established from a single Lgr5+ cell, which subsequently underwent multiple crypt fission events while simultaneously generating differentiated villus-like epithelial domains. This marks the first time that intestinal epithelial organoids have been successfully cultured. Importantly, organoid formation derived from a single cell implies that there is autonomy intrinsic to the intestinal stem cell, allowing it to retain its identity outside of the stem cell niche. It also suggests that asymmetric stem cell division does not depend upon morphogen gradients but rather is intrinsically instructed.

While the *in vitro* culturing of intestinal epithelium is an exciting advancement in intestinal biology, the identity of the intestinal stem cell still remains completely resolved. This is based upon the observation only 6% of all isolated Lgr5+ cells resulted in organoid formation. This important point emphasizes that Lgr5 expression may also encompass more differentiated cells as well as intestinal stem cells, necessitating further evaluation of stem cell markers to definitively identify the stem population. However, while the discrete identity of the ancestral stem cell remains unresolved, it is functionally defined by its ability to ultimately give rise to fully differentiated cells within the crypt-villus unit.

The terminally differentiated intestinal epithelium is comprised of four principal cell lineages – the absorptive enterocytes, mucous-producing goblet cells, hormone-producing enteroendocrine cells, and the lysozyme and defensin-producing Paneth cells (Figure 1.4). Epithelial cell differentiation is tightly controlled and coupled to cell migration. Three of the four cell types, the enterocyte, goblet, and enteroendocrine cells, differentiate as they migrate out of the crypt and onto the villus. The migration rate from crypt to villus tip is rapid, and has been shown to be as fast as 3 days in H^3-thymidine labeling studies (Potten and Bullock 1983). Once cells reach the apical tip of the villus, they undergo programmed cell death or are sloughed off into the intestinal lumen (Potten and Allen 1977). Paneth cells, however, undergo a downward migration where they reside in their fully differentiated state at the base of the crypt for

approximately 3 weeks. At the end of their lifetime, Paneth cells are removed from the crypt base by phagocytosis (Crosnier et al., 2006).

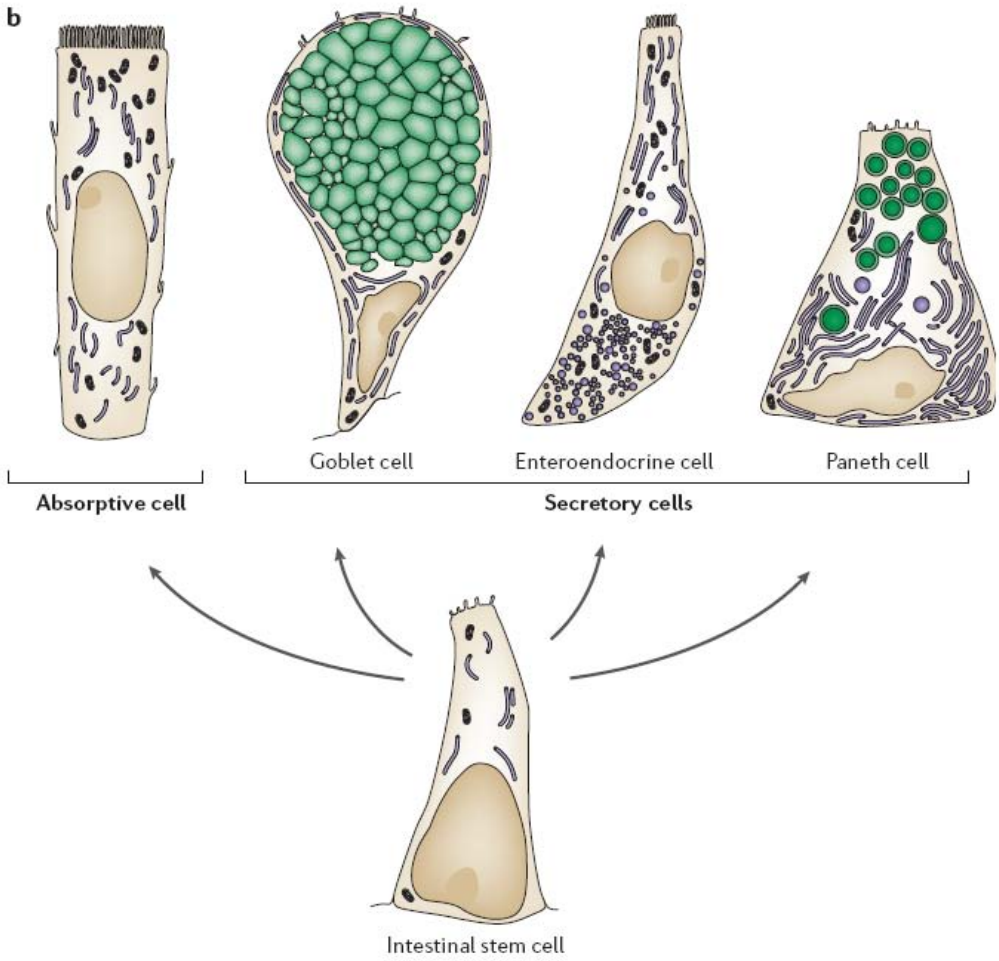

Figure 1.4. Differentiated epithelial cell types arise from a common intestinal stem cell. The ancestral intestinal stem cell gives rise to absorptive and secretory cell types of the intestinal epithelium. Reprinted by permission from Macmillan Publishers Ltd: Crosnier *et al., Nature Reviews Genetics* 7, 349–359. © May 2006

This perpetual process of cell renewal, differentiation and death of the intestinal epithelium make it an attractive model for studying the mechanisms that regulate proliferation and mitosis, asymmetric cell division, lineage commitment and differentiation, and apoptotic-mediated death. Based upon these features, it is clear that the processes involved in homeostatic epithelial renewal have much in common with embryonic development. Not surprisingly, this process is also regulated by many of the same developmentally important signaling factors, including the Wnt signaling pathway, the Notch pathway, the Hedgehog pathway and the TGF-β pathway (Scoville et al., 2008). These pathways and molecules have been largely characterized in mice using transgenic and chimeric models.

II. The Canonical Wnt Pathway

One of the primary signaling pathways responsible for regulating the intestinal epithelium is the canonical Wnt pathway (Fig. 1.5). The term “Wnt” is an amalgamation of the *wingless* (wg) gene discovered in *Drosophila melanogaster*, and *Int-1*, the first Wnt gene discovered in the mouse (Nusse and Varmus, 1982; Nusse and Varmus, 1992). *Int-1* was initially described as a proto-oncogene based upon its preferential integration site for the Mouse Mammary Tumor Virus. The combined observations of epistatic gene relationships in mouse and *Drosophila* elucidated a complex, highly conserved pathway in which the Wnt protein is a secreted, glycosylated ligand. Since the first discovery of Wnt1, a total of 19 Wnt ligand-encoding genes have been identified and described in both the mouse and human genomes (Nusse, 2008).

In the most well-characterized mode of signaling by Wnt ligands known as the “canonical” Wnt signaling pathway (Figure 1.5), Wnt ligands have been described to interact in either a paracrine or autocrine fashion with cell surface Frizzled (Fz) receptors, which are seven-pass transmembrane proteins (Klingensmith and Nusse, 1994; Bhanot et al., 1996; Kennerdell and Carthew, 1998; Bhanot et al., 1999; Chen and Struhl, 1999). There are 10 Fz receptor genes in both the mouse and human (Nusse, 2008). The Wnt ligands bind to the N-terminal cysteine-rich domain (CRD) on the extracellular region of the Fz receptor (Bhanot et al., 1996). During this interaction, Fz receptors cooperate with the LRP5/6 protein, a single pass transmembrane protein required for canonical Wnt signaling, known as *arrow* in *Drosophila* (Wehrli et al., 2000). Wnt

ligands, Fz receptors, LRP co-receptors, and Wnt inhibitors are tightly regulated at both the transcriptional and translational modification level, allowing for cell- and tissue-specific regulation.

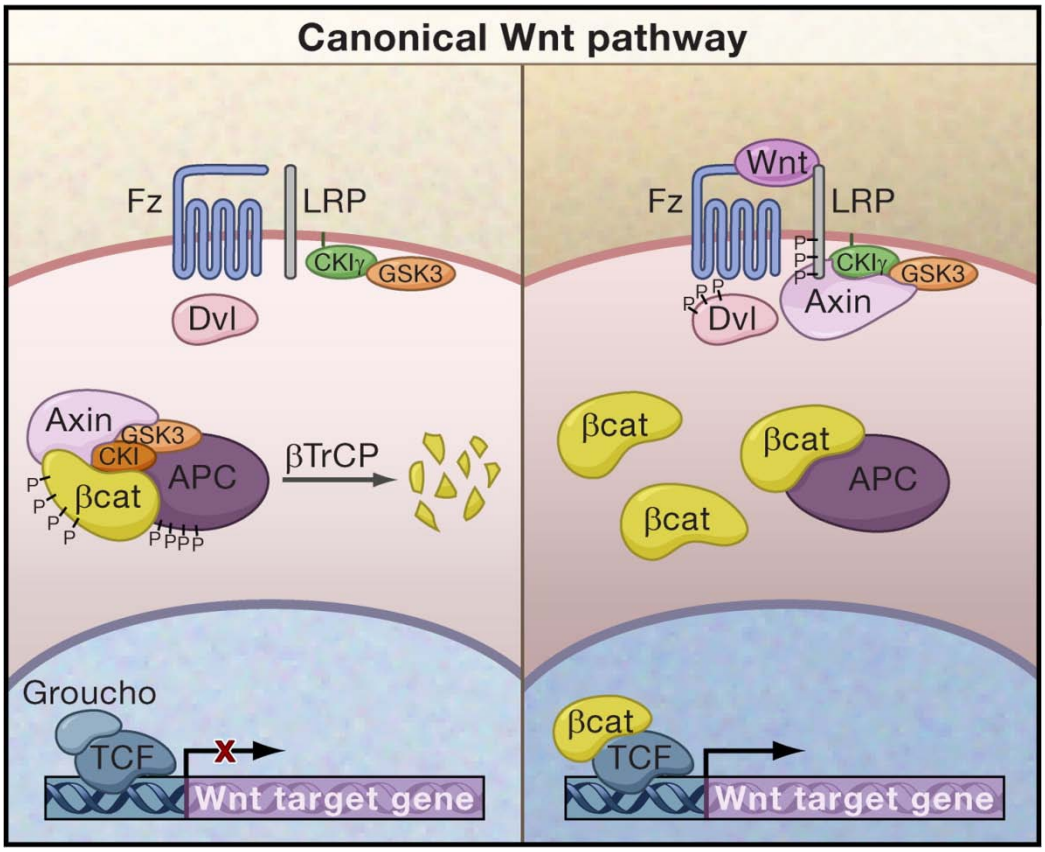

Figure 1.5. The Canonical Wnt Signaling Pathway. Wnt target gene expression relies on the stabilization of β-catenin through inhibition of the Axin/Apc/GSK-3β complex. Reprinted with permission from Clevers, *Cell* 127, 469-480, © 2006.

The central player and a potent regulator of Wnt target gene regulation is β-catenin, a cytoplasmic protein that is also important in adherens junctions (Nusse, 1999). The stability of this protein is actively regulated by the proteasomal destruction complex. In the absence of a Wnt signal, the Axin/GSK-3/CK1/APC destruction complex binds and phosphorylates β-catenin, targeting it for ubiquitination by β-TrCP and subsequent degradation by the proteasome (Aberle et al., 1997). Axin acts as the scaffold for this complex, as it has been shown to directly interact with all of the components. The Adenomatous Polyposis Coli (Apc) protein is known to be necessary for proper activity of this complex, and in fact acts as a Wnt pathway-activating oncogene when mutated, but there is no consensus on the mechanism of its activity within the complex (Clevers 2006). CK1 and GSK3 are the kinases responsible for phosphorylating β-catenin at a series of highly conserved Ser/Thr residues near its N-terminus (Amit et al., 2002; Liu et al., 2002; Yanagawa et al., 2002). However, once the Fz/LRP coreceptor complex is bound by a Wnt ligand, it activates the canonical Wnt signaling pathway by recruiting and physically interacting with the Dishevelled (Dsh) protein, a cytoplasmic protein that recruits the Axin/GSK-3 kinase complex. It has been shown that the LRP5/6 coreceptor interacts with Axin in a Wnt-ligand regulated fashion with five phosphorylated PPP(S/T)P repeats located on its cytoplasmic tail (Davidson et al., 2005; Zeng et al., 2005). The recruitment of Axin away from its complex with APC allows β-catenin to escape ubiquitination and degradation, subsequently allowing it to accumulate in the cytoplasm.

Upon accumulation of β-catenin in the cytosol, it translocates to the nucleus by a poorly-understood process unrelated to the Nuclear Localization Signal/importin mechanism (Fagotto et al., 1998). When in the nucleus, β-catenin transcribes target genes by binding to the Tcf/LEF transcription factors. In the absence of β-catenin, Tcf acts as a transcriptional repressor in a complex with the Groucho protein (Cavallo et al., 1998; Roose et al., 1998). However, once β-catenin physically displaces Groucho, Tcf is converted into a transcriptional activator and activates Wnt-mediated transcriptional programs essential for morphogenesis, proliferation, and stem cell regulation (Clevers, 2006).

In addition to all of its positive regulators, the Wnt pathway is also regulated by a number of inhibitors. The secreted Wnt antagonist Dickkopf (Dkk) binds to LRP5/6 and prevents its interaction with Fz/Wnt, thus inhibiting a transduced Wnt signal (Glinka et al., 1998). Another set of Wnt inhibitory factors, the Soluble Frizzled-Related Proteins (SFRPs), function by a competition mechanism by utilizing their CRD resembling that of functional Fz receptors to bind and sequester Wnt ligands (Hoang et al., 1996).

In the intestine, the Wnt pathway is known to play a major role during development and throughout adult epithelial homeostasis. Further, defects in the Wnt pathway are often indicated in intestinal disease (Nishisho et al., 1991; Wehkamp et al., 2007) and activated during epithelial regeneration (Davies et al., 2008). Current studies suggest that Wnt signaling is a major factor in driving progenitor proliferation and in directing cell fate decisions along the crypt-villus axis (Nakamura et al., 2007). Nuclear accumulation of β-catenin, a hallmark of

canonical Wnt signaling, is observed in crypt-based cells of both the small intestine and colon, corresponding with the location of stem/progenitor cell populations (Batlle et al., 2002; van de Wetering et al., 2002). Additionally, intestines from Wnt-reporter mice exhibit β-galactosidase-positive cells near the base of normal crypts (Davies et al., 2008). Taken together, these two observations suggest that the stem cell requires a Wnt signal for either maintenance or for entry into a proliferative state. Further, transgenic expression of the Wnt inhibitor, *Dkk-1*, in the adult mouse intestine results in the loss of crypts and ablation of the secretory cell lineage (Pinto et al., 2003). These findings correlate with developmental studies in fetal mice in which the intestinal Tcf/Lef family member, Tcf-4, has been ablated. In this setting, embryonic-lethal Tcf-null mutant mice display loss of intestinal stem cells and a failure to expand the epithelial population (Korinek et al., 1998). Together, these loss of function studies support the important role for Wnt signaling in maintaining intestinal proliferation.

Conversely, chronic activation of the Wnt pathway caused by ablation of the Apc tumor suppressor gene is the most common early mutation in intestinal carcinogenesis in humans, including both sporadic and hereditary forms. (Kinzler et al., 1991; Nishisho et al., 1991). Several animal models exist for one of the most prevalent genetic forms, Familial Adenomatous Polyposis (FAP) which is characterized by inherited mutations in the APC gene. Dove and colleagues first described the Multiple Intestinal Neoplasia (MIN) mouse, which carries a stop codon in the Apc gene ($Apc^{MIN/+}$) and develop numerous epithelial adenomas in

the small intestine that recapitulate early disease in FAP patients (Su et al., 1992). Further, inactivation of Apc mediated by inducible Cre recombination in the adult mouse intestine results in repopulation of the villus epithelium by crypt-like proliferative cells (Sansom et al., 2004). Combined with the ablative studies, this data implicates Wnt signaling as an absolutely necessary component to drive and maintain the proliferative crypt compartments and the stem/progenitor cells within them – and is therefore essential for successfully maintaining the intestinal epithelium. Further, data presented in both Chapters 2 and 4 shows that the Wnt pathway is activated in response to intestinal damage by both irradiation and ischemia, and may be essential for effective repair of damaged epithelium.

Based on the vast knowledge of the Wnt signaling pathway in the intestine, a model for its role in patterning the crypt-villus axis emerges. In the crypts, Wnt expression stabilizes β-catenin and partners with Tcf-4 to drive a proliferation gene program. Based upon the restriction of Wnt activated cells within the proliferative zone of the intestine (Davies et al., 2008), this allows for a discrete proliferative compartment and regulation of differentiation as cells migrate away from the proliferative zone. Additionally, Wnt signaling is also involved in establishing cellular positioning along the crypt-villus axis by directly regulating the expression of EphB/ephrinB receptors and ligands. The Eph/ephrins restrict Paneth cell positioning to the base of the crypt in the small intestine (Batlle et al., 2002) and are involved in the establishment of the crypt/villus boundary. Tight regulation of Wnt signaling along the crypt-villus axis is essential to the maintenance of the proliferative zone and differentiation

program. This explains the necessity for discrete expression domains of Wnt ligands, Fz and LRP receptors, and Wnt inhibitory factors within the epithelium and the adjacent mesenchyme (Gregorieff et al., 2005) (Figure 1.6).

Wnt ligands that are known to stimulate the canonical β-catenin-dependent pathway, including Wnt3, Wnt6, and Wnt9b, as well as the receptor Fz7, have an expression pattern restricted to the base of the intestinal crypts. Because the canonical Wnt signaling pathway is known to regulate functions within the crypt, localization of these pathway components support their role in maintaining the intestinal epithelium. The inhibitor Dkk3 is expressed at the crypt-villus junction, and potentially restricts active Wnt signaling to the crypt base. Interestingly, other Wnt ligands and receptors are expressed on the villus. It is known that the balance of these factors is of utmost importance in maintaining the proper gradient of Wnt activation, but the described expression pattern does not offer an entirely clear functional picture of intestinal Wnt regulation.

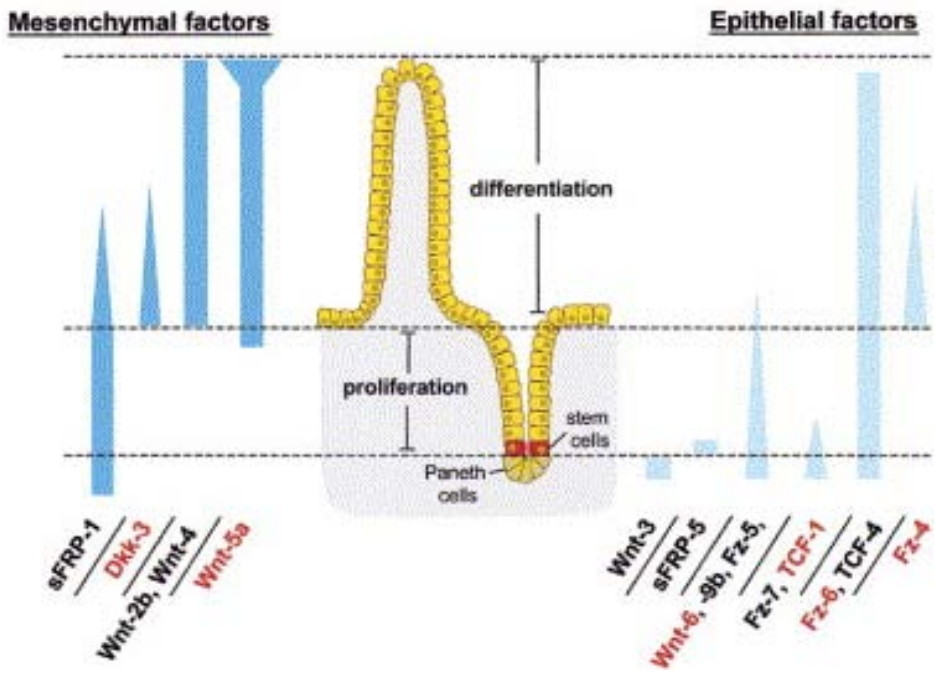

Figure 1.6. Expression pattern of Wnt ligands, receptors, and inhibitory factors in the intestinal epithelial and mesenchymal compartments. Some Wnt ligands and receptors are restricted to the proliferative crypts, while others are expressed on the differentiated villi. Adapted with permission from Gregorieff et al., Gastroenterology © 2005.

III. Wnt5a and β-catenin-independent Wnt Signaling Pathways

Despite the clear role of canonical Wnt ligands in β-catenin-dependent signaling, not all Wnt ligands function to activate β-catenin. Initially, individual Wnts were defined by functional assays. Injection of high amounts of mRNA from most Wnt genes results in duplication of the dorsal-ventral axis in early *Xenopus* embryos (McMahon and Moon, 1989; Christian and Moon ,1993; Wolda et al., 1993). Further, overexpression of most Wnt ligands in C57MG mammary epithelial cells is sufficient to drive transformation to an immortalized cancer-like state (Wong et al., 1994). Wnt genes capable of inducing these two specific phenotypes were later shown to activate the canonical (β-catenin-dependent) Wnt pathway and were categorized as such. However, three Wnt ligands, Wnt4, Wnt5a, and Wnt11, do not elicit either of these phenotypes when subjected to such assays (Wong et al., 1994; Du et al., 1995). Furthermore, the Xenopus gene Xwnt5a has been shown to antagonize the activity of other Wnts, including Xwnt1, Xwnt3a, and Xwnt8 to induce Xenopus axis duplication (Torres et al., 1996), suggesting the existence of alternative Wnt signaling pathways.

Experiments in zebrafish and *Xenopus* embryos suggest that Wnt5a is capable of stimulating a flux in intracellular calcium (Ca^{2+}), leading to the stimulation of downstream effector molecules such as calcium/calmodulin-dependent kinase II (CamKII), protein kinase C (PKC), and nuclear factor associated with T-cells (NFAT) (Slusarski et al., 1997; Sheldahl et al., 1999; Kuhl et al., 2000; Kuhl et al., 2000). However, this phenomenon has not yet been confirmed in a mammalian context, either by cell culture or *in vivo* studies.

Alternatively, other evidence shows that Wnt5a plays a role in the Planar Cell Polarity (PCP) pathway and the regulation of convergence and extension movements in *Xenopus* and *Drosophila* during gastrulation through mediation of Jun kinase (Jnk), and RhoA GTPase (Yamanaka et al., 2002; Zhu et al., 2006; Schambony and Wedlich, 2007).

Furthermore, the interaction of Wnt5a with the canonical pathway remains controversial. Conflicting data for this interaction exists in different model systems, complicating the relevance of these data. In human colon carcinoma Caco-2BBE cells, an intestinal cell line, over-expression of Wnt5a has been shown to repress canonical Wnt signaling through the Ror2 receptor (Figure 1.7), which is expressed in the intestinal epithelium (Pacheco and Macleod, 2008). However, conflicting data from additional *in vitro* studies co-overexpressing a specific co-receptor combination, Fz4 and LRP5, both of which are expressed in the intestine (Gregorieff et al., 2005), show that Wnt5a is capable of stimulating the canonical pathway (Mikels and Nusse, 2006). Both of these studies make use of over-expression of Wnt5a and its receptors by transfection in a transformed cell line at beyond physiologically normal levels, making interpretation of a physiological relevance difficult. Significantly, a role for Wnt5a in modulating the canonical pathway has not been shown *in vivo*. Therefore, the question remains as to what the role of Wnt5a is in the adult intestine.

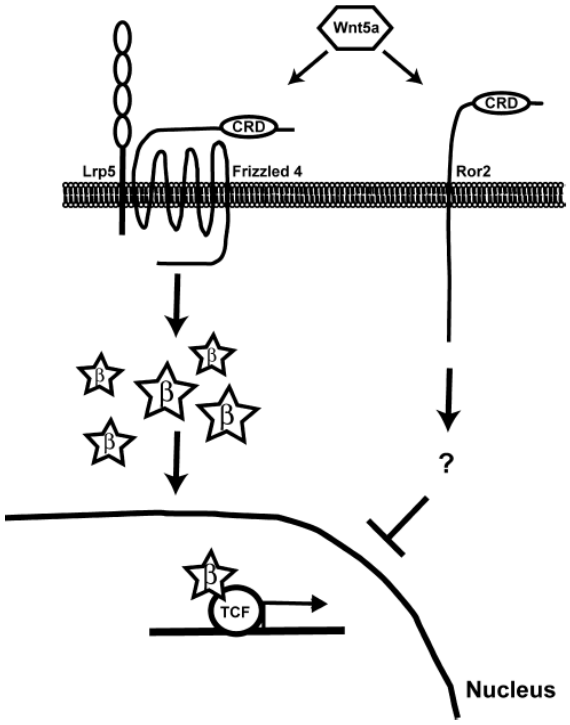

Figure 1.7. Wnt5a has been shown to activate or suppress the canonical pathway depending upon receptor context. The role of Wnt5a remains controversial, as it has been shown to either stimulate β-catenin signaling through the Fz4/Lrp5 coreceptors or repress β-catenin signaling through the Ror2 receptor. Adapted under the Creative Commons license from Mikels and Nusse, PLoS Biology 2006.

Wnt5a knockout mice are embryonic-lethal and exhibit a profound defect in anterior-posterior axis elongation as well as morphogenesis of outgrowing limb buds and other structures (Yamaguchi et al., 1999). Recent studies of the Wnt5a$^{-/-}$ embryonic intestine demonstrate the requirement of Wnt5a for proper intestinal development (Cervantes et al., 2009). These knockout mice display dramatic shortening of the small intestine and defective closure of the primitive gut tube at E10 resulting in an aberrant bifurcation of the midgut (Figure 1.8). Interestingly, all of the differentiated cell types normally present by E18.5 still exist in the

Wnt5a$^{-/-}$ mice, suggesting that the ligand is not required for differentiation programs at this developmental stage. However, Wnt5a expression remains in the intestinal mesenchyme throughout adulthood, suggesting it may play a role in the regulation of a Wnt-associated pathway(Gregorieff et al., 2005).

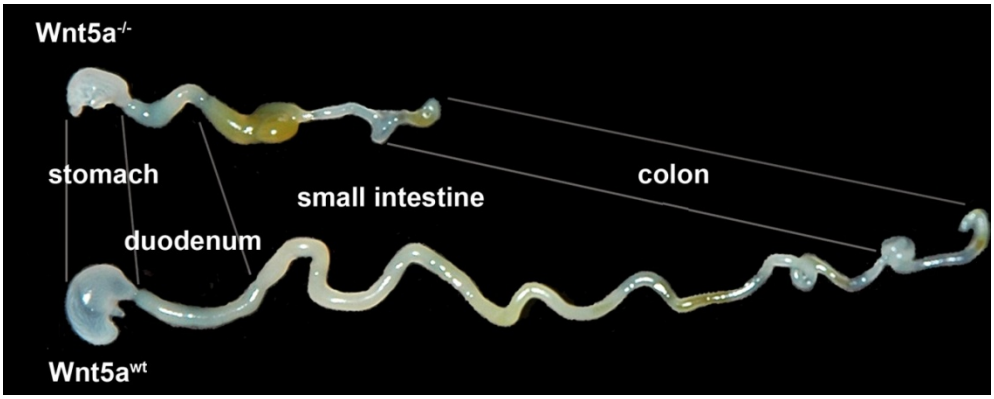

Figure 1.8. The E18.5 Wnt5a$^{-/-}$ intestine is severely foreshortened and has an aberrant bifurcation in the midgut. Adapted and reprinted from Developmental Biology, 326, Cervantes et al., Wnt5a is essential for intestinal elongation in mice, 285-289, © 2009, with permission from Elsevier.

IV. Tools for studying the Wnt signaling pathway *in vivo*

Several tools have been developed to facilitate the study of endogenous Wnt signaling in mice. The TOPGAL reporter mouse (DasGupta and Fuchs 1999), for example, allows for the identification of cells actively receiving a Wnt signal by expression of a reporter that can be detected at the mRNA (*LacZ*) or protein (β-galactosidase; β-gal) level. This model was first described in skin, where a distinct role for Wnt signaling was identified in the initiation of hair follicle morphogenesis (DasGupta and Fuchs, 1999). Similar to the TOPFLASH luciferase assay extensively used in cell culture models, the TOPGAL mouse harbors a transgene in which the *LacZ* gene is under control of a LEF/Tcf and β-catenin-inducible promoter (Fig. 1.9) (Molenaar et al., 1996). Expression of the reporter can be quantified and compared using quantitative reverse-transcriptase polymerase chain reaction (qRT-PCR), identified with antibodies to β-gal by immunofluorescence in tissue sections, or by detecting enzymatic activity with the substrate 5-bromo-4-chloro-3-indolyl-beta-D-galactopyranoside (X-gal) (Fig. 1.10). Several iterations of this Wnt-reporter mouse have been generated. A similar model exists in the BAT-gal mouse, which i has 7 LEF/Tcf binding sites upstream of LacZ, but our preliminary studies detected no discernable difference in intestinal expression between the two mouse models (data not shown). Additionally, a TOPEGFP model, expressing enhanced green fluorescent protein (eGFP) in response to a Wnt signal, has also been described (Moriyama et al., 2007).

Despite the existence of successful systems for detecting and monitoring endogenous Wnt signaling, methods for introducing exongenous Wnt ligands into live animals are less well-defined. In cell culture models, Wnt ligands are over-stimulated by the addition of recombinant protein or Wnt-conditioned media (Willert et al., 2003). However, targeting Wnt proteins to the intestinal mesenchyme is problematic as no tissue-specific promoters have as yet been identified. A method for overcoming this pitfall, described in Chapter 3, takes advantage of lentivirus-mediated gene delivery and lentiviral vectors to express multiple Wnt ligands in the blood-derived intestinal mesenchyme.

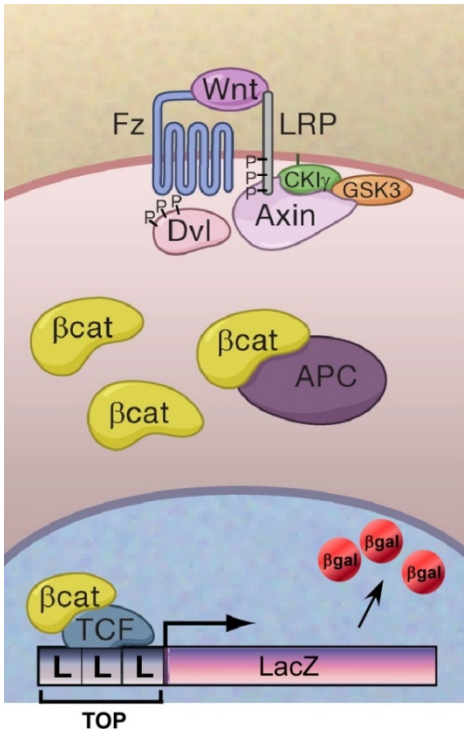

Figure 1.9. The TOPGAL reporter transgene. The TOPGAL reporter mouse harbors 3 Lef/TCF binding sites upstream of the LacZ reporter gene, which is activated upon canonical Wnt stimulation. Adapted with permission from DasGupta and Fuchs, *Development* 126, 4557-4568 (1999) and from Clevers, *Cell* 127, 469-480 (2006).

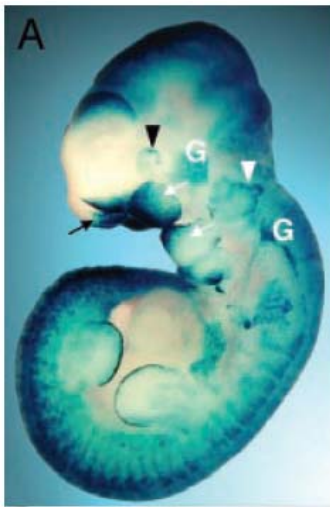

Figure 1.10. X-gal staining in a BAT-gal mouse embryo. Wnt-reporter expression is labeled in blue. Reprinted from PNAS, Vol. 100 no. 6, Silvia Maretto, Michelangelo Cordenonsi, Sirio Dupont, Paola Braghetta, Vania Broccoli, A. Bassim Hassan, Dino Volpin, Giorgio M. Bressan, and Stefano Piccolo, 3299-3304. Mapping Wnt/β-catenin signaling during mouse development and in colorectal tumors. © 2003, National Academy of Sciences, U.S.A.

Although there are several transgenic mouse lines that modify components of the Wnt signaling pathway, most rely on the perturbation of downstream components, including β-catenin and Apc. These models cannot illuminate the role of individual Wnt ligands as they affect the pathway downstream of the ligand/receptor level. Furthermore, the limited number of ligand knockout mouse lines in existence are embryonic lethal and therefore uninformative in the adult animal (McMahon and Bradley 1990; Takada et al., 1994; Yamaguchi et al., 1999). Tissue-specific analyses are impeded by the lack of available knockout mice with conditional alleles, and models that over-express Wnt ligands are also not readily available. Generating mouse lines with individual Wnt ligands and receptors ablated in different tissues or cellular compartments

would be very costly and time consuming, thus leading us to utilize viral vectors as a means to investigate the role of Wnt5a in the intestine.

Lentiviral vectors were developed by Luigi Naldini and collegues as a means for viral gene therapy (Naldini et al., 1996). Previous to their 1996 report in *Science*, gene therapy protocols often relied upon cationic liposomes or adenoviruses, which only offered transient expression of transgenes. Alternatively, retroviruses were often used, which stably integrate transgenes into the genome, but have the caveat that they only infect dividing cells (Copreni et al., 2004). Naldini et al., based their replication-deficient lentiviral vector on the Human Immunodeficiency Virus (HIV), which could integrate into the genome of non-proliferating cells, and used the envelope from the vesicular stomatitis virus (VSV)-G protein. A second generation of this system reduced the HIV packaging component to the *gag*, *pol*, *tat*, and *rev* genes, while the virulent *env*, *vif*, *vpu*, and *nef* genes were deleted (Zufferey et al., 1997). To improve the biosafety of these vectors even further, a third generation of lentiviral vectors was developed such that the tat-dependent U3 sequence from the 5'-long terminal repeat (LTR) was replaced by strong heterologous promoter sequences and the expression of *rev in trans* (Dull et al., 1998). Finally, a deletion in the U3 region of the 3'-LTR resulted in a self-inactivating (SIN) vector, by abolishing the transcriptional activity of the LTR (Zufferey et al., 1998) (Figure 1.11).

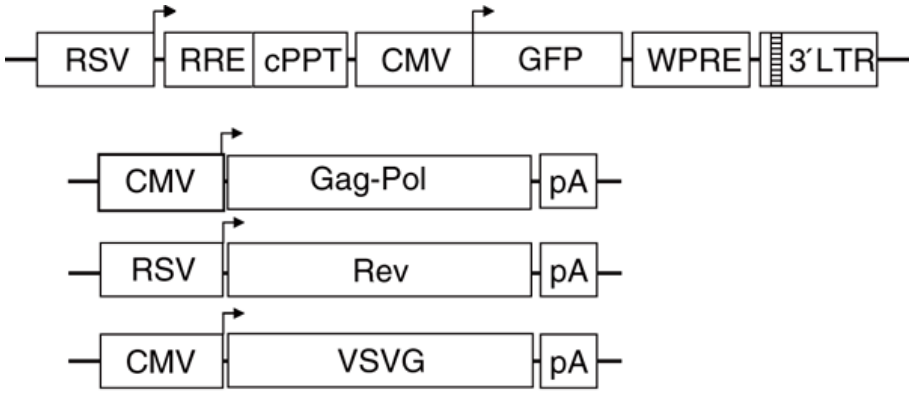

Figure 1.11. Schematic representation of the third generation lentiviral system. The essential genes for lentiviral production are separated on four different plasmid constructs. Co-transfection of these plasmids results in a functional lentiviral vector that is in itself unable to self-replicate. Reprinted by permission from Macmillan Publishers Ltd: Nature Protocols; **1**, 241-245, ©2006.

Viral delivery methods represent an attractive alternative approach for transgene expression over generation of a transgenic animal., Advances in the biosafety of lentiviral vectors make this approach an appealing option for expressing transgenes, because non-replicative, self-inactivating viruses now cause little to no adverse effects on the infected subject (Dull et al., 1998; Naldini 1998; Zufferey et al., 1998). Previous studies have successfully demonstrated lentiviral-mediated gene delivery in embryonic stem cells and somatic cells from a variety of organs (Fassler 2004; Skarsgard et al., 2005). This delivery system represents a powerful tool for the study of signaling pathways in complex tissues, as it offers an ideal approach for expressing ligands for paracrine or autocrine signaling.

V. Hypothesis and Rationale

The overall goal of my thesis research is to understand how Wnt signaling is regulated in the mouse small intestine. It is known that canonical Wnt signaling is essential for proper development and homeostasis of the mouse intestinal epithelium, and that Wnt signaling must be tightly controlled along the crypt-villus axis by an array of different ligands, receptors, and repressors. Specifically studying the role of the Wnt5a ligand in adult intestinal tissue homoestasis will provide a better understanding of how mesenchymal-to-epithelial signaling can be manipulated and how the canonical Wnt pathway is modulated along the proliferation-to-differentiation axis of the intestinal epithelium.

Hypothesis: Wnt5a functions as a paracrine canonical Wnt repressor to effectively maintain proper signaling in the adult mouse small intestine during homeostasis and in response to epithelial damage and disease states. In addition, Wnt5a acts to counterbalance increased canonical Wnt signaling and allow for tight and rapid regulation of the pathway. To test this hypothesis, I have addressed these research aims:

1. Identify the intestinal phenotype elicited by over-expression of the Wnt5a ligand using lentiviral vectors.

2. Determine the relationship between endogenous Wnt5a expression and stimulation of the canonical Wnt signaling pathway in response to intestinal damage by γ-irradation and ischemia.

3. Identify the expression of Wnt5a in response to a heightened canonical Wnt signaling environment of a tumor setting.

CHAPTER 2

Wnt reporter expression in the mouse small intestine

CHAPTER 2

Wnt-reporter expression pattern in the mouse intestine during homeostasis

Paige S. Davies[1], Adria D. Dismuke[2], Anne E. Powell[3], Kevin H. Carroll[1] and Melissa H. Wong[1]

[1]Department of Dermatology, Oregon Cancer Center, Oregon Stem Cell Center; [2]Department of Molecular and Medical Genetics; [3]Department of Cell and Developmental Biology; Oregon Health & Science University, Portland, OR.

BMC Gastroenterology, 8: 57 (2008).

PSD and MHW participated in planning of all experiments within the study, as well as the writing of the manuscript. ADD planned and performed primer design and qRT-PCR analyses, and participated in writing and editing of the manuscript. AEP and KHC performed IHC analyses.

Abstract

Background: The canonical Wnt signaling pathway is a known regulator of cell proliferation during development and maintenance of the intestinal epithelium. Perturbations in this pathway lead to aberrant epithelial proliferation and intestinal cancer. In the mature intestine, proliferation is confined to the relatively quiescent stem cells and the rapidly cycling transient-amplifying cells in the intestinal crypts. Although the Wnt signal is believed to regulate all proliferating intestinal cells, surprisingly, this has not been thoroughly demonstrated. This important determination has implications on intestinal function, especially during epithelial expansion and regeneration, and warrants an extensive characterization of Wnt-activated cells. Methods: To identify intestinal epithelial cells that actively receive a Wnt signal, we analyzed intestinal Wnt-reporter expression patterns in two different mouse lines using immunohistochemistry, enzymatic activity, *in situ* hybridization and qRT-PCR, then corroborated results with reporter-independent analyses. Wnt-receiving cells were further characterized for co-expression of proliferation markers, putative stem cell markers and cellular differentiation markers using an immunohistochemical approach. Finally, to demonstrate that Wnt-reporter mice have utility in detecting perturbations in intestinal Wnt signaling, the reporter response to gamma-irradiation was examined.

Results: Wnt-activated cells were primarily restricted to the base of the small intestinal and colonic crypts, and were highest in numbers in the

proximal small intestine, decreasing in frequency in a gradient toward the large intestine. Interestingly, the majority of the Wnt-reporter-expressing cells did not overlap with the transient-amplifying cell population. Further, while Wnt-activated cells expressed the putative stem cell marker Musashi-1, they did not co-express DCAMKL-1 or cell differentiation markers. Finally, gamma-irradiation stimulated an increase in Wnt-activated intestinal crypt cells.

Conclusions: We show, for the first time, detailed characterization of the intestine from Wnt-reporter mice. Further, our data show that the majority of Wnt-receiving cells reside in the stem cell niche of the crypt base and do not extend into the proliferative transient-amplifying cell population. We also show that the Wnt-reporter mice can be used to detect changes in intestinal epithelial Wnt signaling upon physiologic injury. Our findings have an important impact on understanding the regulation of the intestinal stem cell hierarchy during homeostasis and in disease states.

Introduction

It is well established that the canonical Wnt signaling pathway plays a critical role in regulating intestinal proliferation at the level of the stem cell(Kinzler and Vogelstein, 1996; Korinek et al., 1998; Bienz and Clevers, 2000; Booth and Potten, 2000; Pinto et al., 2003; Kuhnert et al., 2004) and has been inferred to regulate proliferation of all intestinal crypt-based cells including the bulk of proliferative cells, the transient-amplifying-cell (TA-cell) population(Kinzler and Vogelstein, 1996; Korinek et al., 1998; Bienz and Clevers, 2000; Booth and Potten, 2000; Pinto et al., 2003; Kuhnert et al., 2004; Van der Flier et al., 2007). Surprisingly, the proliferative influence of the Wnt signal on discrete cell populations within the crypt has not been previously characterized. Confounding issues for making these distinctions is that manipulation of Wnt signaling in the stem cell population will invariably affect the downstream TA-cell population, complicating interpretation. Further, there is precedence for a Wnt signal acting as a global regulator of proliferation in development prior to the establishment of the stem cell hierarchy(Korinek et al., 1998). However, there is also evidence that proliferative control of crypt-based cells may be more multi-faceted than originally thought. Most interestingly, the TA-cell population does not express the recently identified Wnt-target stem cell marker, Lgr5(Barker et al., 2007), nor does it harbor nuclear β-catenin staining, a hallmark of activated Wnt signaling(Batlle et al., 2002; van de Wetering et al., 2002). In addition, Wnt signaling has been shown to differentially regulate stem cell and TA-cell populations in other epithelial systems such as the skin(DasGupta and Fuchs, 1999; Blanpain et al.,

2007), suggesting that a more complex regulation of proliferation may exist. Therefore, determining the influential distinction of the Wnt signal within the different proliferative intestinal cell populations is important for understanding epithelial homeostasis, regeneration after injury, and cellular dynamics during proliferative diseases.

Epithelial proliferation is confined to the intestinal crypts. The proliferative capacity of the intestine is defined by approximately 4-6 active stem cells and a second rapidly proliferating crypt population made up of the TA-cells that is situated adjacent to the stem cells. Multiple signaling cascades, including the Wnt, Notch, and Sonic Hedgehog pathways(Radtke et al., 2006), converge within the crypt niche to regulate the gradient of proliferation-to-differentiation. The canonical Wnt signaling pathway is well established as an important regulator of intestinal epithelial proliferation(Korinek et al., 1998) and homeostasis(Korinek et al., 1998; Lickert et al., 2001; Gregorieff and Clevers, 2005; Muncan et al., 2006). During mouse intestinal development, ablation of the downstream transcription factor, Tcf4 links loss of Wnt signaling with a loss of epithelial proliferation(Korinek et al., 1998). In the adult mouse, a proliferative role for this pathway is recapitulated when the Wnt inhibitor Dickkopf-1 is over-expressed, leading to collapse of the crypt structure(Kuhnert et al., 2004), and most notably in disease, where mutations in this pathway result in epithelial hyperproliferation leading to colorectal cancer(Kinzler and Vogelstein, 1996).

The canonical Wnt signal is conveyed through the binding of a soluble ligand to cell surface co-receptors, Frizzled and Lrp5/6(Logan and Nusse, 2004),

then propagated by inhibiting the degradation of β-catenin, which stimulates the transcription of target genes(Molenaar et al., 1996; Gordon and Nusse, 2006, Molenaar, 1996 #39). The Wnt target gene Lgr5 is a putative stem cell marker based upon its crypt mRNA localization and a functional knock-in reporter experiment(Barker et al., 2007). Interestingly, Lgr5 is expressed only in epithelial columnar cells, but not higher up in the crypt within the TA-cell population. This suggests that Wnt signals may influence discrete cell populations rather than act as a global proliferative regulator within the crypt. Therefore, it is possible that proliferation of stem cells and the TA-cell population are differentially controlled.

In other systems, such as the hematopoietic system, the Wnt signal also provides proliferative cues to progenitor cells(Staal and Clevers, 2005). Self-renewal of both the hematopoietic stem cells and their TA-cell populations are thought to be regulated by the Wnt pathway. Conversely, in epithelial systems such as the skin, stem and TA-cell populations appear to be differentially activated by Wnt signals(DasGupta and Fuchs, 1999; Blanpain et al., 2007). In the intestine, however, definitive stem cell markers have been slow to be established. The absence of these markers and the inability to accurately distinguish stem and progenitor populations within the intestinal crypt presents an obstacle for determining if Wnt acts as a global regulator of cell proliferation. One approach to establishing the role of Wnt signaling on the discrete intestinal crypt cell populations is to characterize cells within the crypt that are Wnt-activated. Here, we validate for the first time, the Wnt-reporter mouse as a useful resource for evaluation of Wnt-activation within the intestine. Further, we establish that

during intestinal homeostasis, activation of the Wnt pathway occurred primarily in an intestinal progenitor cell and not in the actively cycling TA-cell population. Our data validates the Wnt-reporter mouse as a functional tool for detecting changes in Wnt signaling within the intestinal epithelium. We show that the canonical Wnt pathway is stimulated in response to gamma-irradiation-induced apoptosis both by an increased expression of the Wnt-reporter as well as Wnt ligands and the *c-Myc* target gene. The characterization of Wnt signaling within the intestine provides an important foundation for understanding the regulation of the intestinal stem cell hierarchy during homeostasis and in disease states.

Materials and Methods

Mice

Mice were housed in a specific pathogen-free environment under strictly controlled light cycle conditions, fed a standard rodent Lab Chow (#5001 PMI Nutrition International, Brentwood, MO), and provided water ad libitum. All procedures were performed in accordance to the OHSU Animal Care and Use Committee. The Wnt-reporter TOPGAL(DasGupta and Fuchs, 1999), C57Bl/6, and Apc^{MIN-}(Moser et al., 1990) mice were obtained from The Jackson Laboratory (Bar Harbor, ME) and the BAT-Gal Wnt-reporter mice were a kind gift from Dr. Stefano Piccolo(Maretto et al., 2003).

Analyses of Wnt-responsive intestinal cells

Immunohistochemical analyses. Wnt signaling activity was characterized in adult TOPGAL, BAT-Gal, and C57Bl/6 mouse intestines. The entire length of the intestine was prepared for frozen or paraffin sectioning and the methods used for single and multi-label immunohistochemical staining are previously described(Wong et al., 1998). The following antisera were used: anti-β-galactosidase (β-gal; Immunology Consultants Laboratory, Inc.; Newberg, OR; 1:500 dilution), anti-Musashi-1 (#14H-1; a gift from Dr. H. Okano, Keio University, Tokyo; 1:500), UEA-1 (Sigma; St. Louis, MO; 1:500), anti-cryptidin (a kind gift from Andy Oulette, University of California - Irvine; 1:25) and anti-5-HT (Serotonin; Incstar; Stillwater, MN; 1:500). Primary antibodies were detected with species appropriate secondary antibodies conjugated to Cy3, FITC (Jackson ImmunoResearch; West Grove, PA) or Alexa-488 (Molecular Probes; Eugene, OR). Tissues were counterstained with Hoechst (33258; Sigma; St. Louis, MO; 0.1 μg/ml). Paraffin embedded tissue sections were stained with antibodies for β-catenin (Transduction Labs; Lexington, KY; 1:500 dilution) to detect nuclear localization. Staining was performed as described previously(Sansom et al., 2007). Biotinylated secondary antibodies and Diaminobenzidine (DAB) were employed for visualization. Images were captured on a DMR microscope and DC500 digital camera with IM50 Image Manager Software (Leica Microsystems; Bannockburn, IL). Cy3 images were captured as grayscale and digitally converted to red images.

Quantification of β-gal-positive cells. To establish the percentage of β-gal-positive crypts and villi down the length of the intestine, tissue sections from mice stained with antibodies to β-gal as described above were quantified. At least 1500 crypts or villi were screened from n = 2-5 mice and reported as a percentages. For a more detailed analysis of the location of β-gal-positive cells within the crypt, the proximal small intestinal crypts were divided into equal thirds. β-gal-positive cells for each region (upper, middle and lower third) were tallied and compared to the total number of β-gal-positive crypt cells (>1500 crypts; n = 2 mice). To determine the percentage of dual-labeled β-gal-expressing Paneth cells, tissue sections were co-stained with UEA-1 and β-gal antibodies as described above. A total of >1500 crypts/mouse were screened (n = 3 mice).

β-gal enzymatic activity. Five µm frozen sections were washed in phosphate buffered saline and prepared for 5-bromo-4-chloro-3-inodyl β-D-galactoside (X-gal) detection followed by nuclear-fast red counterstain modified from previously described protocols(Wong et al., 1996).

Assessment of proliferative status. To detect proliferating cells, 5 µm frozen tissue sections were stained with antibodies against Ki67 (Abcam #ab15580; Cambridge, MA; 1:250) and appropriate fluorescent-conjugated secondary antibodies. Alternatively, mice were injected with 5-bromo-2'deoxyuridine/5-fluoro-2'deoxyuridine (BrdU/FrdU, 120/12 mg/kg body weight; Sigma; St. Louis, MO) 48h prior to sacrifice. Tissue sections were co-stained sequentially with antibodies to BrdU and β-gal. For BrdU staining a modified protocol from the Abcam Resources website was used (www.abcam.com).

Briefly, tissues were washed in phosphate buffered saline and incubated in blocking buffer (1% BSA, 0.3% Triton X-100, 1mM $CaCl_2$) prior to staining with antibodies to BrdU(Wong et al., 1998) (a gift from Dr. Jeffrey Gordon, Washington University School of Medicine, St. Louis, MO; 1:1000) and detected with fluorescent secondary antibodies. The tissue was imaged after each step and the acquired images overlayed using Canvas software (ACD Systems; Miami, FL). To quantify β-gal and BrdU expression, >1000 crypts per animal (n = 3) were scored for crypts containing co-labeled cells.

Wnt signaling response to intestinal damage

Irradiation-induced epithelial damage. TOPGAL and C57Bl/6 mice were exposed to 12Gy and sacrificed at 1, 12, 24, 48, and 72h post-irradiation. Intestinal tissue was harvested and processed as described above and stained with Hematoxylin & Eosin (H&E) or with antibodies for β-gal or β-catenin. The number of β-gal-positive crypts were counted and compared to the total number of crypts in each tissue section (≥1300 crypts counted/time point). Intestinal samples from at least three mice per time point were analyzed (n = 19 mice total). Further, for untreated and 24h post-irradiation time points, the number of β-gal-positive cells per crypt (1, 2 or >2) was also tallied and normalized to the total number of crypts (>1500 crypts counted/time point; n = 2 mice each). The number of cells co-stained with antibodies for Ki67 and β-gal were also determined for both non-irradiated (n = 2) and 24h-post-irradiated intestines (n = 2; ≥2000 crypts/animal). Average values were represented ± standard deviation.

Statistical significance was determined by unpaired *t*-tests assuming equal variances using Microsoft Excel. *p* values < 0.05 were considered significant.

mRNA expression

In situ hybridization. To validate the gene expression pattern of *lacZ*, RNA *in situ* hybridization was performed as previously described(Murtaugh et al., 1999) using digoxigenin-labeled LacZ riboprobes (1µg/µl), alkaline-phosphatase-conjugated anti-digoxigenin antibody and BM Purple substrate (Roche; Indianapolis, IN).

Quantitative analysis of mRNA expression from isolated intestinal cell populations. β-gal mRNA has a shorter half-life than the protein(Bachmair et al., 1986; Selinger et al., 2003) and can provide a more precise detection of Wnt-activated cells. A modified Weiser preparation(Weiser, 1973; Weiser, 1973) was used to isolate crypt and villus epithelium from adult Wnt-reporter mouse small intestine. Differentiated epithelial cells were removed in 1mM EDTA and 1mM DTT, where crypt epithelium was isolated in 1 mM EDTA and 5 mM DTT. Total RNA was purified from the isolated villus and crypt cell populations and cDNA was synthesized as we have previously described(Wong et al., 2000). Quantitative RT-PCR was performed using a SYBR Green-based assay, primers to β-gal and a 7900HT Sequence Detector according to established protocols(Wong et al., 2000; Hooper et al., 2001). Each cDNA sample was analyzed in triplicate, along with triplicate samples of the endogenous reference gene, Glyceraldehyde-3-phosphate dehydrogenase. Each assay for *lacZ*

expression was performed at least three independent times on n = 3 mice. The fold-change was determined using established methods(Wong et al., 2000; Hooper et al., 2001) and reported relative to levels in crypts.

To demonstrate intestinal Wnt-responsiveness in the TOPGAL model, mice were irradiated as described above and sacrificed 24h later. Crypt epithelial cells were isolated from the small intestine as described above and evaluated by qRT-PCR for gene expression of three Wnt ligands (*Wnt3*, *Wnt6*, *Wnt9b*), a secreted Wnt inhibitor (*sFrp2*), and a Wnt target gene (*c-Myc*) (n = 2 non-irradiated, n = 3 irradiated). For Wnt9b, only distal small intestinal crypt epithelium was surveyed, due to its restricted expression to this region(Gregorieff et al., 2005). Primer sequences are presented in Table 2.1.

Table 2.1 Primer sequences for qRT-PCR

Gene	Forward Sequence	Reverse Sequence
lacZ	5'-GATCTTCCTGAGGCCGATACTG-3'	5'-GGCGGATTGACCGTAA TGG-3'
gapdh	5'-TGGCAAAGTGGA GATTGTTGCC-3'	5'-AAGATGGTGATGGGCTTCCCG-3'
wnt3	5'-CAAGCACAACAATGAAGCAGGC-3'	5'-TCGGGACTCACGGTGTTTCTC-3'
wnt6	5'-TGCCCGAGGCGCAAGACTG-3'	5'-ATTGCAAACACGAAAGCTGTCTCTC-3'
wnt9b	5'-AAGTACAGCACCAAGTTCCTCAGC-3'	5'-GAACAGCACAGGAGCCTGACAC-3'
sfrp2	5'-AGGTCCTTTGATGCTGACTGTAAA-3'	5'-TCGGCTTCACCTTTTTGCA-3'
c-myc	5'-AGCTTCGAAACTCTGGTGCATAA-3'	5'-GGCTTTGGCATGCATTTTAATT-3'

Results

Activation of Wnt signaling in single cells within the intestinal crypt.

To identify the intestinal epithelial cell population that actively receives a Wnt signal, we surveyed the entire length of the intestine from two independently established Wnt-reporter mouse lines, TOPGAL and BAT-Gal(DasGupta and Fuchs, 1999; Maretto et al., 2003), in addition to C57Bl/6 mice. TOPGAL and BAT-Gal transgenic mice express the reporter, β-galactosidase (β-gal), in response to reception and processing of an endogenous canonical Wnt signal, marking cells activated by the signaling cascade(DasGupta and Fuchs, 1999; Maretto et al., 2003). Both mouse reporter lines displayed a similar pattern (Figure 2.1A,B), therefore TOPGAL mouse intestines are depicted unless otherwise noted. In the Wnt-reporter mouse intestine, we found strong β-gal expression in epithelial cells within the crypt base (Figure 2.1A,B,D). Typically, positive crypts within the proximal small intestine (PSI) contained only one or two β-gal-positive cells (Figure 2.1A,B), although some crypts were uniformly populated with β-gal-positive cells that extended into the TA-cell region (Figure 2.1C) and onto the adjacent villi. The reporter protein expression pattern was confirmed by detecting β-gal expression by enzymatic activity using the substrate, X-gal (Figure 2.1E). Interestingly, while single cells within the crypt base were detected, no crypts with the broader expression pattern, nor villus epithelial expression were observed. We corroborated our findings in the Wnt-reporter mice with identification of crypt cells harboring nuclear β-catenin in wild-type mice, a hallmark of Wnt activation (Figure 2.1F). The nuclear β-catenin

staining pattern recapitulated the Wnt-reporter protein expression pattern (Figure 2.1A,B,D). Because of the discrepancy between the β-gal protein expression on the villus detected by antibodies (Figure 2.1C and 2.2D) and the crypt-based expression of β-gal enzymatic activity (Figure 2.1E), we analyzed reporter RNA expression. Both *in situ* hybridization (Figure 2.1G&H) and qRT-PCR for the *lac*Z gene in isolated crypt or villus epithelial populations (Figure 2.1I) demonstrated that Wnt-activated cells were restricted to the crypt base. An indepth examination of the crypt localization of β-gal-positive cells revealed that the majority resided in the base of the crypt (79.6%), the stem cell niche and the location of differentiated Paneth cells, while fewer β-gal-positive cells were located in the middle third (17.4%) or the upper third of the crypt (3.0%; Figure 2.1J).

Interestingly, a gradient of Wnt-activated, β-gal-positive cells existed in the intestine, with 15.2% of crypts containing a Wnt-activated cell in the PSI compared to 0.8% of colonic crypts (Figure 2.1K). Additionally, villi with β-gal-positive epithelium were also detected in a decreasing gradient down the length of the small intestine (Figure 2.1L). This pattern of Wnt-activated cells parallels the decreasing gradient in cell turnover and proliferation rates that exist down the length of the small intestine and colon(Lipkin, 1985).

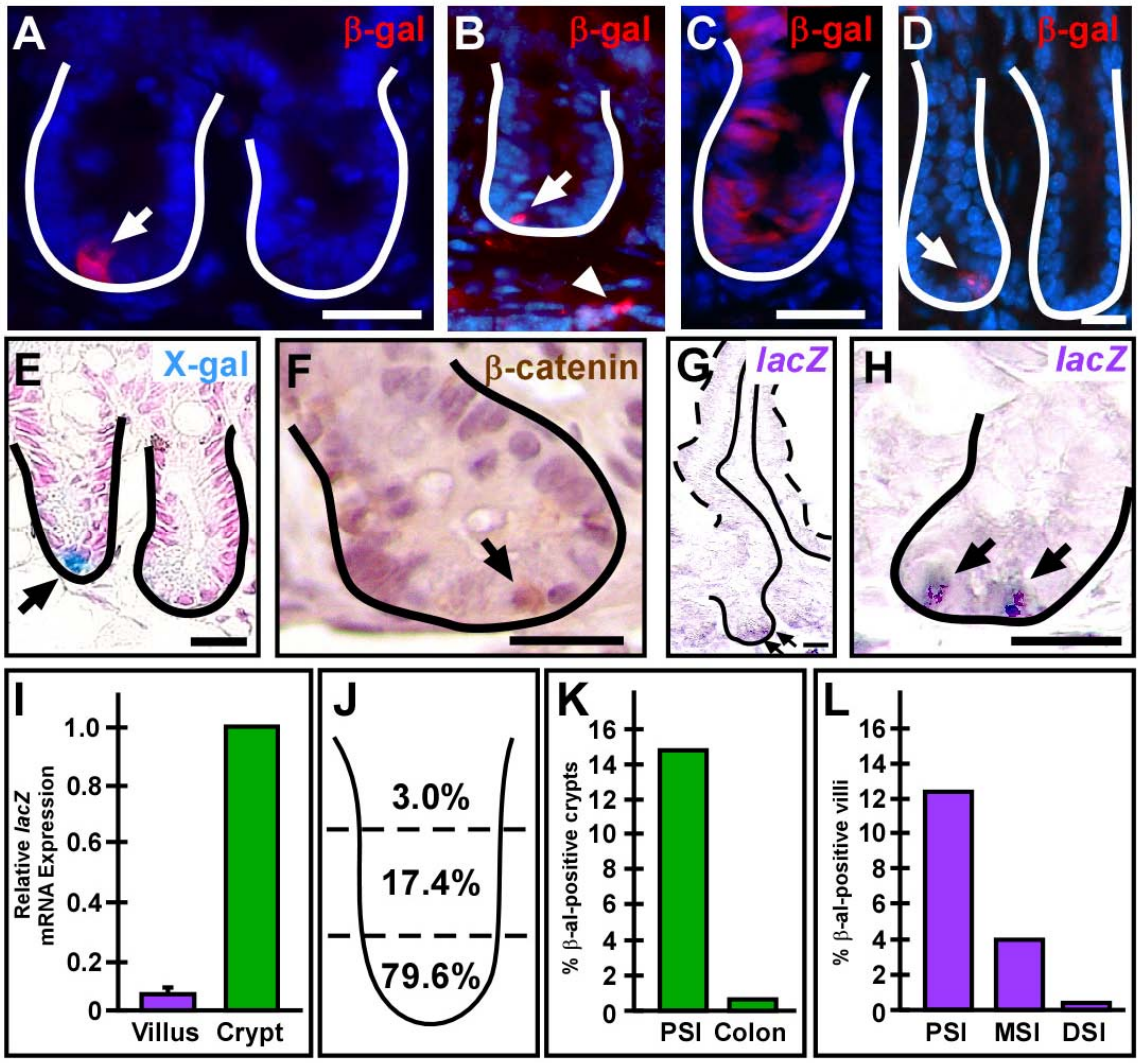
A
β-gal
B
β-gal
C
β-gal
D
β-gal
E
X-gal
F
β-catenin
G
lacZ
H
lacZ
I
Relative lacZ mRNA Expression
1.0
0.8
0.6
0.4
0.2
0
Villus
Crypt
J
3.0%
17.4%
79.6%
K
% β-al-positive crypts
16
14
12
10
8
6
4
2
0
PSI
Colon
L
% β-al-positive villi
16
14
12
10
8
6
4
2
0
PSI
MSI
DSI

Figure 2.1

Figure 2.1 Adult mouse expression pattern of Wnt-receiving epithelial cells. (A,C,D) Cryopreserved adult TOPGAL mouse proximal small intestinal (PSI) or colonic and (B) BAT-Gal mouse PSI tissue sections were stained with antibodies against β-galactosidase (β-gal, red) and counterstained with Hoechst dye (blue). (A&B) The majority of crypts in the PSI contained only one Wnt-activated cell or was devoid of positive cells (arrow). There were occasional mesenchymal cells positive for β-gal (arrowhead) in BAT-Gal intestines (B). (C) Occasionally, β-gal-expressing cells were detected throughout the crypt epithelium and on adjacent villi. (D) Colonic crypts contained only rare single β-gal positive cells near the crypt base. (E) Wnt-receiving cells detected by enzymatic activity, X-gal staining (blue, arrow). (F) Adult wild-type mouse PSI was stained with antibodies against β-catenin (brown; arrow) to detect nuclear expression and counterstained with Hematoxylin. (G-I) Analyses of reporter RNA expression pattern and localization was determined by *in situ* hybridization (G,H; purple, arrow) and are consistent with the expression pattern in (A). (I) qRT-PCR for *lacZ* gene expression in isolated crypt or villus epithelial cells from TOPGAL PSI demonstrated expression in the crypts. (J) The crypt localization of β-gal-positive cells was highest in the lower third and decreased in numbers in the middle and upper third. (K) Crypts with Wnt-receiving cells in TOPGAL intestinal sections were higher in the PSI (15.2%) and decreased down the length of the intestine to 0.8% in the colon. (L) The number of β-gal-positive villi also reflected a decreasing gradient with the highest numbers in the PSI (12.3%), less in the the middle small intestine (MSI; 4.0%) and the least in the distal small intestine (DSI; 0.2%). Solid white or black line demarks the epithelial-mesenchymal boundary. Dashed line outlines the apical epithelial border. Bar = 25 μm.

Wnt-receiving cells express cell proliferation markers but are not located in the TA-cell region.

The majority of β-gal-positive cells reside in the base of the intestinal crypt, suggesting that Wnt signaling may influence proliferation in the progenitor population and not the TA-cell population. To distinguish if the Wnt signal conveys a restricted rather than global proliferative response within the intestinal crypt, intestines from Wnt-reporter mice were co-stained with antibodies to β-gal and the proliferation marker Ki67, which designates cells undergoing late G1, S, G2 or M phases of the cell cycle. Ki67-positive cells were located in the middle portion of the crypts and extended toward the lower third, consistent with the location of both the TA-cell population and crypt progenitor cells. Analysis was restricted to crypts containing one or two β-gal positive cells. In most of these crypts, the majority of the Ki67 staining did not co-localize with β-gal-positive cells (Figure 2.2A-C, arrow). Occasionally, β-gal-expressing crypt cells were also Ki67-positive (7.1%), potentially indicating that this Wnt-activated cell was actively dividing (Figure 2.2A-C, arrowhead).

To determine if the Wnt-activated cells were label-retaining cells, we performed BrdU label-retaining assays by injecting BrdU into TOPGAL mice 48h prior to analysis. This timeframe is sufficient for BrdU-labeled epithelial cells to give rise to BrdU-positive descendents that have migrated up the villus (Figure 2.2D, lagging edge BrdU-cell marked by green arrow). At this analytical time point, the BrdU-labeled progeny have migrated away from the BrdU-label-retaining stem cell in the crypt (Figure 2.2D-G, white asterisk), as apparent by the

intervening BrdU-negative cells (Figure 2.2D&E). The β-gal-positive villus epithelial cells overlap with the BrdU-positive villus cells (Figure 2.2D, red bracket) suggesting that they might be derived from the dual BrdU-positive, β-gal positive cell in the crypt. Approximately 7.5% of crypts contained cells with co-localized β-gal and BrdU (Figure 2.2F&G and Figure 2.3), suggesting that a subset of β-gal-positive cells were also crypt label-retaining cells.

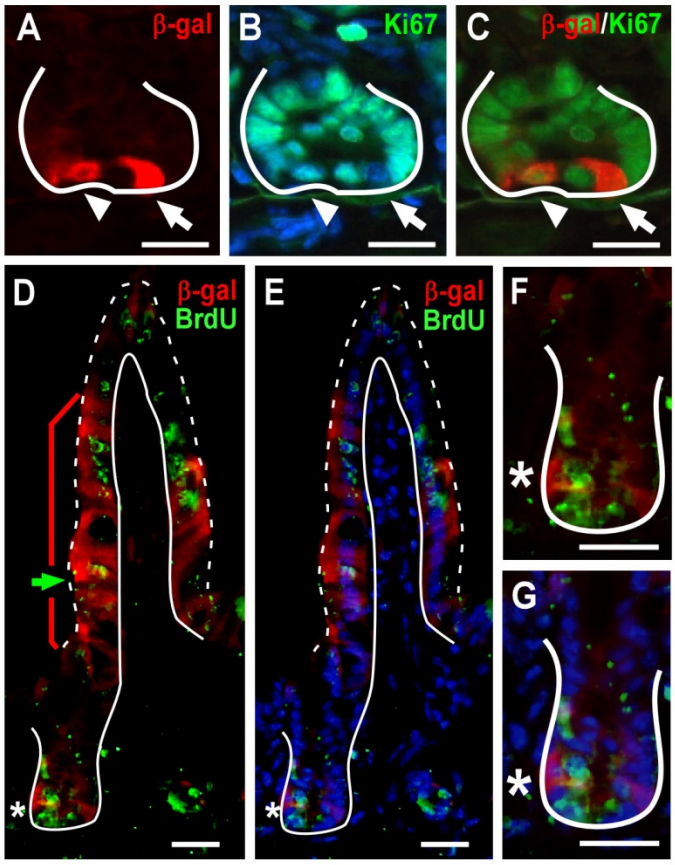

Figure 2.2 Wnt-activated cells represent progenitor cells within the intestinal crypt. (A-C) Cryopreserved intestinal tissue sections from TOPGAL adult mice co-stained with antibodies to β-gal (red) and Ki67 (green) then counter-stained with Hoechst (blue). Arrow indicates a cell with β-gal staining and arrowhead designates a cell co-staining for both markers. (D-G) Co-localization of BrdU (green) and β-gal (red) expression in crypt and villus epithelial cells from adult TOPGAL mice injected with BrdU 2 days prior to sacrifice. Green arrow denotes β-gal-positive cells at the lagging edge of migrating BrdU-positive cells up the villus. Red bracket indicates β-gal-positive villus epithelium. White asterisk marks β-gal and BrdU double-positive crypt cells. (F&G) Higher magnification of crypt regions in D&E. Solid white line demarks the epithelial-mesenchymal boundary. Dashed white line outlines the apical epithelial border. Counter-stained with Hoechst dye (blue). Bar = 25 μm.

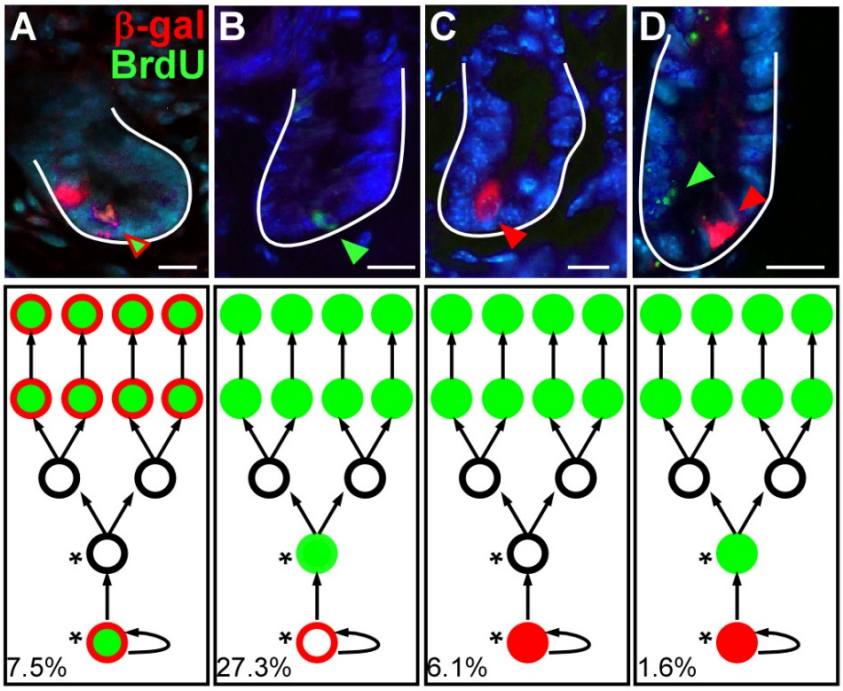

Figure 2.3 β-gal and BrdU co-staining scenarios. Wnt-reporter mouse intestines were injected with BrdU 2 days prior to analyses to assess the proliferative status of the β-gal positive crypt-based cells. (A) Approximately 7.5% of crypts contained a cell that was dual-labeled for β-gal and BrdU, reflecting cells that have been retained within the crypt (label-retaining cells) and that were Wnt-activated. (B) Approximately 27.3% of crypts contained a single BrdU-positive cell, possibly representing a “stem cell” that is not designated by the Wnt signaling pathway. This would be in line with the recently identified Bmi-1 positive stem cell. (C) 6.1% of crypts contained a single positive β-gal cell. This cell likely represents a cell that is activated by the Wnt signal after the effective BrdU labeling half-life in the animal. Finally, (D) a small percentage of crypts, 1.6%, contained a β-gal-positive cell and a BrdU-positive cell distinct from one another, likely representing a combination of the described scenarios. These scenarios are schematized in cartoon form beneath the corresponding fluorescent image that describes our perception of what each scenario may represent. In classical stem cell hierarchy, the lowest circle represents a progenitor cell residing near the base of the crypt and upper circles represent the progeny. Solid green circles represent BrdU-positive cells, solid red circles represent an activated Wnt cell, open red circles represent a cell that may have been Wnt-activated prior to BrdU labeling. These many different scenarios reflect the complex nature of the role of Wnt signaling on the stem cell hierarchy within the intestinal crypt.

To determine if Wnt-receiving crypt cells might share expression with stem or early progenitor cells, Wnt-reporter mouse intestines were stained with antibodies for a putative intestinal epithelial stem cell marker, Musashi-1 (Msi-1)(Kayahara et al., 2003; Potten et al., 2003; He et al., 2004). Although Msi-1 and β-gal co-localized (Figure 2.4A&B), the Msi-1 antibody displayed a broader staining pattern within the crypt, also encompassing the TA-cell population. DCAMKL-1 is an alternative putative stem cell marker(May et al., 2008), however Wnt-activated cells did not co-express DCAMKL-1 (Figure 2.4C-E).

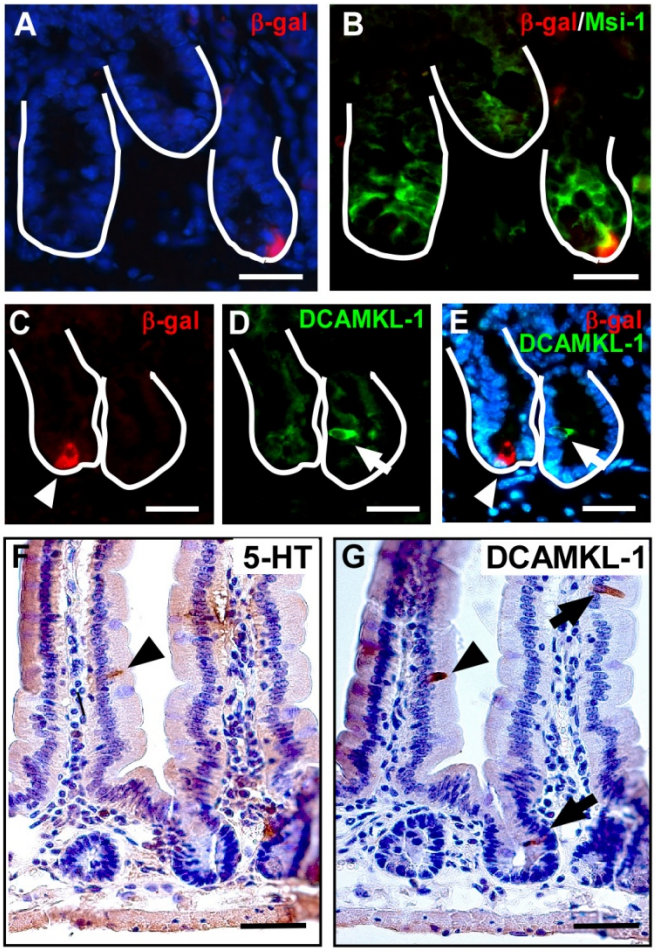

Figure 2.4. Characterization of putative stem cell markers in Wnt-activated cells. (A&B) The putative stem cell marker, Musashi-1 (Msi-1; green) had broad expression within the crypt and co-localized with crypt β-gal-expressing cells (red). (C-E) β-gal-positive cells (red) do not co-localize with another putative stem cell marker, DCAMKL1 (green). Solid white line marks the epithelial-mesenchymal boundary of the intestinal crypt. (F&G) DCAMKL-1 is expressed in a subset of enteroendocrine cells. Serial sections of mouse PSI were stained for serotonin (5-HT, an enteroendocrine marker; F) or DCAMKL-1 (G), a proposed intestinal stem cell marker. Arrowheads mark a single cell that co-labeled with both antibodies. Arrows mark DCAMKL-1-positive cells that do not express serotonin. Bar = 25 μm.

Progenitor cell populations are not the only residents within the intestinal crypt. In the small intestine, differentiated Paneth cells reside at the crypt base, and differentiating goblet and enteroendocrine cells are also scattered within the crypt. Interestingly, a recent study implicated Wnt signaling in Paneth cell differentiation(van Es et al., 2005). To determine if Ki67-negative/β-gal-positive cells were differentiated cells that resided at the crypt base(Cheng, 1974), we stained Wnt-reporter mouse intestines with antibodies raised against epithelial differentiation markers. Co-localization of β-gal and the lectin, UEA-1, a dual goblet and Paneth cell marker, revealed that approximately 40.7% of the β-gal-positive cells possessed overlapping Paneth cell expression (Figure 2.5A-C; arrowhead), while 59.3% were distinct from Paneth cells (Figure 2.5A-C; arrow). Further, dual-labeling with antibodies to β-gal and cryptidin, a Paneth cell-specific marker, revealed similar findings (Figure 5D-F). It is possible that Wnt-activated, differentiated Paneth cells that retain β-gal protein are progeny from a Wnt-activated stem cell in a similar fashion as the β-gal-positive villus epithelial cells. Additionally, β-gal-positive cells were distinct from enteroendocrine cells when tissue sections were co-stained for the serotonin marker 5-HT (Figure 2.5G-I), and distinct from crypt-based goblet cells (data not shown).

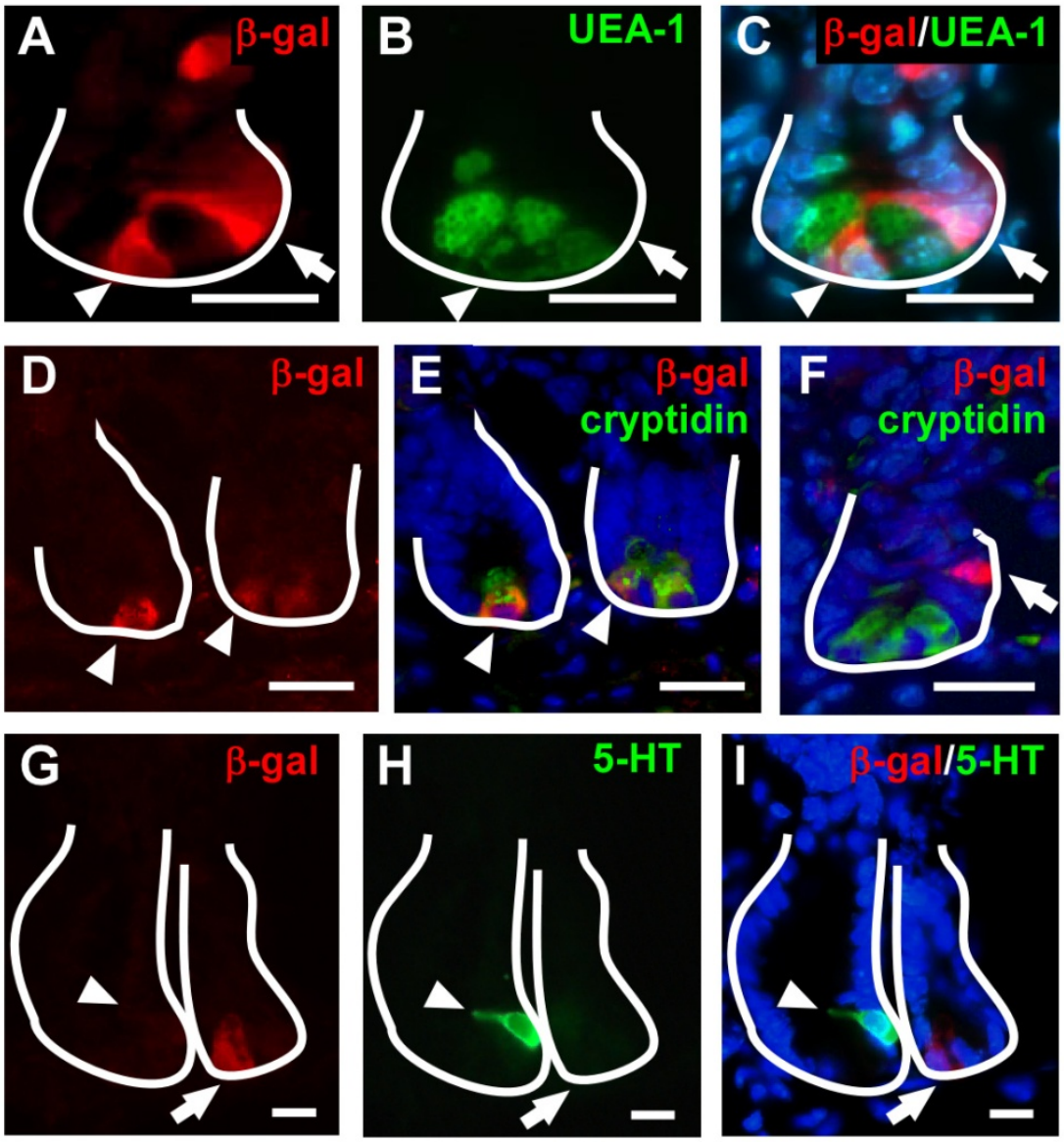

Figure 2.5 Characterization of epithelial differentiation markers in Wnt-activated cells. (A-C) Co-incubation of antibodies to β-gal (red) and UEA-1 (green), a lectin to mark Paneth and goblet cells, identifies distinct Wnt-activated cells (arrow) and overlapping expression (arrowhead). (D-F) Similar results are observed for the Paneth-cell-specific marker, cryptidin (green) when co-stained with β-gal (red). (G-I) Co-localization is not observed with dual staining of β-gal (red) and the enteroendocrine marker serotonin (5-HT; green). Solid white line marks the epithelial-mesenchymal boundary of the intestinal crypt. Bar = 25 μm.

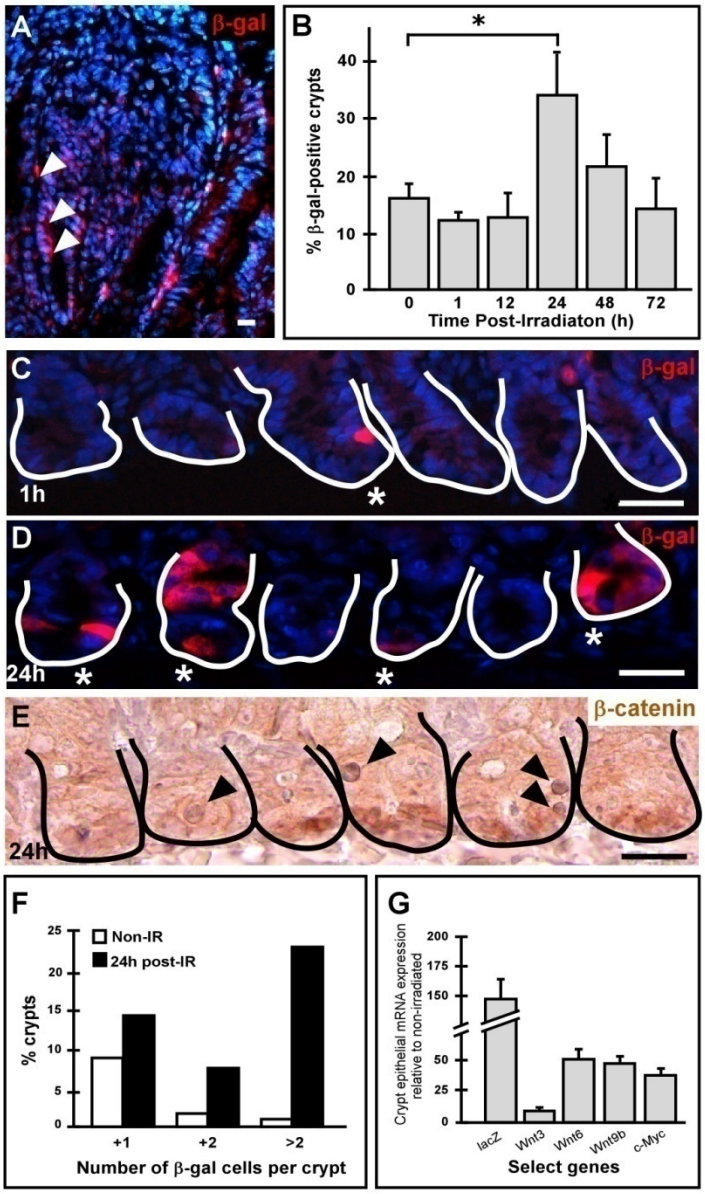

Figure 2.6 Wnt activity increases after γ-irradiation. (A) An increased number of Wnt-activated cells are detected in an intestinal adenoma from a progeny of a BAT-Gal and Apc^{MIN} mouse mating. β-gal-positive cells are in red (arrows). Wnt signaling is stimulated in response to gamma-irradiation-induced injury. (B) Intestinal tissue sections from lethally irradiated TOPGAL mice harvested at various timepoints were stained with antibodies to β-gal (red) and quantified. At 24 h post-irradiation, the number of crypts harboring Wnt-receiving cells significantly increased (p = 0.004; asterisk) relative to non-irradiated controls. (C&D) Comparison of representative intestinal tissue sections from lethally irradiated TOPGAL mice stained with antibodies to β-gal (red) and

counterstained with Hoechst dye (blue) at 1 h post-irradiation (C) and 24 h post-irradiation (D). (E) Wild type mice, 24 h post-irradiation, were examined with antibodies to β-catenin (brown) and counterstained with Hematoxylin (purple). Solid line marks the epithelial-mesenchymal boundary of the intestinal crypts. At 1 h post-irradiation, the number of β-gal-expressing cells was similar to the 0h control, but increased in 24 h post-irradiated tissues. Asterisks denote β-gal or nuclear β-catenin positive crypts; black arrowheads denote apoptotic cells. Bar = 25 μm. (F) The number of β-gal-positive cells per crypt was scored in both non-irradiated (Non-IR) and 24 h post-irradiated (post-IR) intestines. The percentage of crypts with 1, 2 or greater than 2 β-gal-positive cells are shown. (G) qRT-PCR performed on mRNA from small intestinal crypt fractions of TOPGAL mice 24 h post-irradiation revealed an increase in the *lacZ* reporter gene compared to non-irradiated samples. In addition, three Wnt ligands known to be expressed in the intestinal epithelium (*Wnt3*, *Wnt6*, and *Wnt9b*) and a Wnt target gene (*c-Myc*) increased in response to the irradiation stimulus.

Wnt-reporter mouse intestine responded to physiologic increase in Wnt signaling.

In some intestinal diseases, such as colorectal cancer, the Wnt signaling pathway is aberrantly stimulated in epithelial cells resulting in uncontrolled hyperproliferation. This establishes a role for Wnt signaling in epithelial proliferation and highlights the importance of the Wnt signal in maintaining epithelial homeostasis. It has previously been shown, and we demonstrate here, that BAT-Gal reporter mice display an increase in Wnt signaling readout when crossed to tumor-forming Apc^{MIN} mice that overstimulate the Wnt pathway(Maretto et al., 2003) (Figure 2.6A). To investigate if the Wnt-reporter mice are useful tools for increased Wnt signaling readout during tissue repair after injury, we examined the reporter response to intestinal gamma-irradiation exposure, which is known to stimulate an epithelial proliferative response.

Exposure to gamma-irradiation elicits massive crypt cell apoptosis, coincident with proliferative changes that peak within the first 24 hours (Potten, 1990). To determine if activation of Wnt signaling is important in a regenerative response and if it can be monitored in a Wnt-reporter mouse, we subjected TOPGAL mice to 12Gy of gamma-irradiation. Intestinal tissues were processed and analyzed 1, 12, 24, 48, and 72h after irradiation (Figure 2.6B). At 1h post-irradiation, the intestinal epithelium appeared relatively normal. Wnt-responsive cells, as detected by protein levels, were still present in low numbers in the crypts of the PSI (Figure 2.6B&C). However, by 24h post-irradiation, near the peak of the apoptotic response, a significant increase in the number of crypts with Wnt-

receiving cells was detected (p = 0.004, Figure 2.6B,D,E). Additionally, we observed more Wnt-receiving cells per crypt (Figure 2.6D-F) compared to non-irradiated controls (Figure 2.1A) or to the 1h post-irradiation time point (Figure 2.6C). The most striking increase was represented by β-gal-positive crypts harboring greater than two Wnt-activated cells (Figure 2.6F). The Wnt response returned to non-irradiated, homeostatic levels by 72h (Figure 2.6B).

Interestingly, the increase in Wnt-receiving cells paralleled an increase in β-gal/Ki67 double-positive cells (data not shown). While the majority of Ki67-positive cells remained β-gal-negative, dual β-gal and Ki67-positive cells increased approximately 3-fold (from 7.1% to 23.1%). This double-positive population may represent an actively dividing stem cell or immediate progeny from a newly divided progenitor cell.

To correlate increased Wnt responsiveness to gamma-irradiation, the mRNA expression levels of the three endogenous epithelial Wnt ligands were determined(Gregorieff et al., 2005). Crypt epithelium from 24h post-irradiation and non-irradiated TOPGAL intestines was isolated and characterized for changes in Wnt ligand expression (Figure 2.6G). Reporter *lacZ* mRNA expression was elevated in response to gamma-irradiation exposure by ~148-fold in the crypt epithelium. Consistent with this observation, increased expression of the Wnt target gene *c-Myc* was observed (34-fold). Additionally, the canonical Wnt ligands *Wnt3*, *Wnt6*, and *Wnt9b* were also elevated by 10-, 51- and 50-fold respectively. Further, the mRNA expression of the secreted frizzled protein 2 (*sFrp2*), a Wnt inhibitor, decreased from levels higher than the Wnt

ligands at steady state, to undetectable levels in response to gamma-irradiation (data not shown). This data suggests that induced injury to the epithelium results in detectable changes in Wnt signaling that can be appreciated in the Wnt-reporter mouse.

Discussion

While it is well established that Wnt signaling controls intestinal epithelial proliferation and homeostasis, the distinction between the role of Wnt as a direct regulator of both the crypt-based stem cell and TA-cell populations has not been firmly established(Kinzler and Vogelstein, 1996; Korinek et al., 1998; Bienz and Clevers, 2000; Pinto et al., 2003; Kuhnert et al., 2004). Further, aberrant Wnt signaling has been described as a proliferative stimulus in intestinal disease states such as colorectal cancer(Kinzler and Vogelstein, 1996) but a role for the pathway in epithelial regeneration after injury has not been defined. Here we examined the pattern of Wnt-activated cells in the normal mouse intestine during homeostasis and after irradiation-induced injury. Further, we characterize intestinal expression of the Wnt-reporter mouse and show that it is a useful tool in both monitoring Wnt signaling during homeostasis and in response to an epithelial-induced injury.

In both TOPGAL and BAT-Gal mouse intestines, Wnt-activated cells, as identified by Wnt-reporter expression, were primarily confined to the epithelial compartment. In the small intestine, two crypt-based patterns were observed. The majority of small intestinal crypts harbored one or two β-gal-positive cells detected by both protein and RNA localization. In a minority of crypts the entire crypt population was positive for β-gal protein expression that extended onto the adjacent villus. Additionally β-gal-positive cells were observed on villi that were associated with crypts containing single β-gal-positive cells. However, villus protein expression was not recapitulated with RNA expression profiling using *in*

situ hybridization for *lacZ* on tissue sections or by qRT-PCR for *lacZ* expression in isolated crypt and villus epithelial cell populations. Together this suggests that Wnt-reporter expression on the villus was a manifestation of the long half-life of the β-gal protein(Bachmair et al., 1986). The unique ability to track both protein and RNA expression in the Wnt-reporter mouse provides the power to analyze both lineage tracing (protein) and an identification of the Wnt-activated cell (RNA) within the same model system.

To corroborate that the Wnt-reporter provided a consistent Wnt-activated cell readout, antibody staining to detect cells harboring nuclear localized β-catenin was performed. Consistent with the frequency of β-gal-positive cells, a similar percentage of PSI crypts harbored one or two cells near the crypt base that stained positive for nuclear β-catenin. These data suggest that only a small number of cells within certain crypts were actively receiving a Wnt signal.

Interestingly, but consistent with the observed decreasing gradient of epithelial cell turnover rates down the length of the intestine, a greater number of Wnt-activated cells were observed in the PSI (15.2% of crypts harbored at least one β-gal-positive cell) as compared to the colon (0.8%). Similarly, Bmi1-positive putative stem cells also display a gradient down the length of the intestine, with greater numbers in the PSI and nearly undetectable levels in the distal small intestine(Sangiorgi and Capecchi, 2008).

While it is widely accepted that Wnt signaling influences proliferation in all crypts, the number of Wnt-activiated cells detected in Wnt-reporter mouse intestines was lower than expected. There are several possibilities to explain this

discrepancy. It is possible that the Wnt morphogen acts in a gradient highest in the base of the crypt and highest in the PSI with decreasing concentration down the length of the intestine. In this scenario, it is possible that only the highest levels of Wnt-activated cells are detected in the Wnt-reporter mice. Dilution of the protein as cells divide and migrate up the villus is therefore only detected in intestinal regions with the highest levels of Wnt activation. Presence of β-gal-positive villus cells may therefore identify regions of the intestine with robust Wnt signaling.

Some reports suggest a higher level of nuclear localized β-catenin in the crypt base than we show here(Batlle et al., 2002; van de Wetering et al., 2002). Although believed to be a gold standard, comparing nuclear β-catenin with Wnt-activated cells could be misleading. Some cancer cells display high levels of nuclear β-catenin in the absence of Wnt activity (Kiely et al., 2007). The mechanism for this in cancer is unclear, although there are known inhibitors of nuclear localized β-catenin that inhibit Wnt activation by binding to β-catenin within the nucleus, including Apc, Chibby and Duplin (Sakamoto et al., 2000; Takemaru et al., 2003; Sierra et al., 2006).

Despite the decreasing gradient of detectable Wnt signal down the length of the intestine, there remains an important physiologic role of Wnt signaling in colonic homeostasis. It was recently reported that the Wnt target gene and putative stem cell marker, Lgr5, is located in base of both small intestinal and colonic crypts (Barker et al., 2007). An alternative explanation for the proximal to distal gradient of detectable Wnt-activated cells could be that Wnt signaling in the

colonic epithelium is regulated differently than in the small intestine. There are differences in expression of the Tcf/Lef-1 family members between the two regions(Korinek et al., 1998) and therefore it is likely that other regulatory factors may convey differences in colonic Wnt activity. Due to these caveats in tracking Wnt-activated cells using other approaches, Wnt-reporter mice offer a powerful and direct approach for identifying Wnt-activated cells.

Wnt-receiving intestinal cells represent a progenitor population.

The rarity of single β-gal-positive and nuclear β-catenin-positive cells in the base of the crypt suggests that these Wnt-receiving cells may be a progenitor cell population. Therefore, to further characterize the proliferative status of the β-gal-positive cells, we surveyed intestinal sections with antibodies to Ki67 and β-gal. The majority of Ki67-positive cells were located mid-crypt in the TA-cell region and were negative for β-gal, thus not Wnt-activated. This suggests that Wnt signaling is not a general proliferative stimulant. Supportive of this observation, cells containing nuclear β-catenin were also not located within the proliferative TA-cell population, consistent with previous data from both the small intestine or colon(Batlle et al., 2002; van de Wetering et al., 2002). Further, TA-cells have been shown to lack expression of a previously described Wnt-target gene, Lgr5, that marks a columnar crypt-based proposed stem cell(Barker et al., 2007). This suggests that a second pathway may regulate proliferation of the TA-cell population. Recent evidence shows that the polycomb protein Bmi1, regulated in a Wnt-independent fashion, marks a putative intestinal stem cell

population residing at “cell position +4” within the crypt(Sangiorgi and Capecchi, 2008). Bmi1-expressing cells display a unique pattern from Lgr5-positive cells in the intestinal crypt(Barker et al., 2007). These markers identify a population of “stem cells” with different kinetics, suggesting a more complex regulation of the intestinal stem cell hierarchy(Batlle, 2008).

We observed that a portion of Ki67-positive cells were also β-gal positive. This represented 7.1% of all crypt-based β-gal positive cells and may possibly represent the stem cell or an early progenitor. We examined co-expression of β-gal with a putative stem cell marker, Msi-1. Even though the majority of β-gal-positive cells co-stained with this putative stem cell marker, Msi-1 displayed a broader pattern of expression that extended into the TA-cell region. While it is controversial whether or not Msi-1 is a true stem cell marker in the intestine, it may be expressed in a gradient including stem cells and their immediate descendents(Potten et al., 2003, Kayahara, 2003 #44; Topol et al., 2003). Despite this, co-localization of β-gal and Msi-1 supports the idea that Wnt-activated cells could represent progenitor cells. Interestingly, DCAMKL-1, a second putative stem cell marker(May et al., 2008), did not co-localize with β-gal positive cells. It is likely that DCAMKL-1 marks a lineage progenitor for enteroendocrine cells, as it is also expressed on the villus epithelium in a similar pattern with serotonin, an enteroendocrine cell marker (Figure 4F&G). Additionally, the putative stem cell marker, Lgr5, is reported to have an mRNA expression pattern encompassing a greater number of crypt cells and more total crypts(Barker et al., 2007) than the profile of Wnt-activated cells we show here.

The overt discrepancy in staining patterns of the putative stem cell markers highlights the current dearth of tools available for pinpointing the intestinal stem cell in vivo.

We also observed a population of Ki67-negative, β-gal-positive cells. These cells might represent quiescent stem cells or the differentiated progeny of a Wnt-activated progenitor cell. Therefore, we performed double staining with β-gal and select antibodies for differentiated cell lineages. β-gal-positive cells did not express differentiation markers for goblet or enteroendocrine cells. Although a majority of the Paneth cells did not express β-gal (98.7%), a small subset was β-gal-positive. The presence of these double positive cells support the previously reported role for Wnt signaling in retaining Paneth cells to the crypt base(van Es et al., 2005). Alternatively, these β-gal-positive Paneth cells could be recent descendents of an activated progenitor, as we show for differentiated epithelial cells (Figures 2.1C and 2.2D&E), highlighting the usefulness of protein detection for lineage tracing in this model system. Despite the role of Wnt signaling within the differentiated Paneth cell population, the majority of crypt-based β-gal-positive cells did not express differentiated cell markers (59.3%). Therefore, it is likely that these Wnt-activated cells represent a progenitor pool.

There is an emerging view of a more complex intestinal stem cell hierarchy with multiple pools of progenitor populations. In the absence of an intestinal reconstitution assay to validate Wnt-dependent and Wnt-independent putative stem cell pools, we cannot functionally determine the relationship of Wnt-activated cells within the hierarchy. It is likely that β-gal and nuclear β-

catenin expression may be present in only a subset of stem cells. Additionally, quiescent stem cells might not express β-gal, nuclear β-catenin, Lgr5 or Bmi1. Despite these caveats, our data suggested a limited number of Wnt-activated cells within intestinal crypts and is consistent with a role for a Wnt signal in a progenitor pool.

Wnt-reporter response to gamma-irradiation-induced injury.

To determine if a Wnt signal was elicited in response to epithelial injury, we examined intestinal Wnt activation after gamma-irradiation. Upon exposure to gamma-irradiation, analyses of Wnt-reporter mice revealed an appreciable increase in both the number of crypts harboring Wnt-activated cells, as well as an increase in the total number of Wnt-activated cells per crypt. This observation was verified at the RNA level, demonstrating that irradiation-induced injury elicited an intestinal Wnt response. To confirm this increase in intestinal Wnt signaling, we surveyed for expression of a number of Wnt pathway genes in isolated epithelial crypt cells using qRT-PCR. An increase in *lacZ* was accompanied by increases in the three canonical Wnt ligands reported to be expressed in the crypt epithelium (*Wnt3*, *Wnt6*, *Wnt9b*) and the downstream target *c-Myc*. Further, a decrease in the secreted Wnt inhibitor (*sFrp2*) was observed. This demonstrated that physiological intestinal damage can be appreciated using a Wnt-reporter mouse.

Conclusions

Our data provide a carefully detailed analysis of endogenous Wnt signaling in the intestine of Wnt-reporter mice and corroborates reporter expression with nuclear β-catenin staining. Wnt-activated cells are predominantly located in the base of the crypt where a progenitor population and differentiated Paneth cells reside. This expression pattern is consistent with reported roles for Wnt signaling in maintaining a stem cell pool and in Paneth cell differentiation.

We demonstrate that the Wnt-reporter mouse can be used for *in vivo* analyses of both lineage tracing by detection of protein expression using immunohistochemistry and identification of Wnt-activated cell populations by reporter RNA expression. Importantly, our studies validate the use of the Wnt-reporter mouse (TOPGAL and BAT-Gal) for detection of *in vivo* manipulation of Wnt signaling in response to intestinal epithelial injury.

CHAPTER 3

Lentiviral-mediated expression of WNT1 in the mouse small intestine

CHAPTER 3

Lentiviral-mediated transgene expression can potentiate intestinal mesenchymal-epithelial signaling

Adria D. Dismuke[1], Aimee D. Kohn[2], Randall T. Moon[3] and Melissa H. Wong[4]

[1]Department of Molecular and Medical Genetics, Oregon Health & Science University, Portland, OR
[2]Cascade Cancer Center, Kirkland, WA
[3]Howard Hughes Medical Institute, Division of Hematology, Department of Pharmacology, and the Center for Developmental Biology, Institute for Stem Cell and Regenerative Medicine, University of Washington School of Medicine, Seattle, WA
[4]Departments of Dermatology; Cell and Developmental Biology; Knight Cancer Institute, Oregon Health & Science University, Portland, OR.

Biological Procedures, 14 July (2009).

ADD and MHW participated in planning of all experiments within the study, as well as the writing of the manuscript. ADD performed all experiments described in this chapter. ADK and RTM created the lentiviral constructs.

ABSTRACT

Mesenchymal-epithelial signaling is essential for the development of many organs and is often disrupted in disease. In this study we demonstrate the use of lentiviral-mediated transgene delivery as an effective approach for ectopic transgene expression and an alternative to generation of transgenic animals. One benefit to this approach is that it can be used independently or in conjunction with established transgenic or knockout animals for studying modulation of mesenchymal-epithelial interactions. To display the power of this approach, we explored ectopic expression of a Wnt ligand in the mouse intestinal mesenchyme and demonstrate its functional influence on the adjacent epithelium. Our findings highlight the efficient use of lentiviral-mediated transgene expression for modulating mesenchymal-epithelial interactions *in vivo*.

INTRODUCTION

Epithelial-mesenchymal signaling networks are indispensible in vertebrates, and are essential during early organogenesis and continuing throughout adulthood. Study of these complex pathways, including the Wnt, Notch, FGF, Bmp, TGF-β, Shh, and Notch signaling pathways, is complicated by the diverse interactions that exist between their respective ligands and receptors. However, understanding these signaling pathways is important, as many are disrupted in disease states or are required for maintaining tissue homeostasis by regulating stem cell maintenance, differentiation, migration, and polarity.

The mammalian intestine critically depends upon signaling between mesenchymal and epithelial cells. Many of the key developmental signaling pathways that function in an epithelial-mesenchymal capacity are implicated in maintaining the adult intestinal homeostasis. For example, the developmentally important Wnt signaling pathway is critical for proliferation and epithelial stem cell maintenance in the adult tissue (Fevr, Robine et al. 2007). In both the developing and adult intestine, a number of Wnt ligands are expressed in the mesenchyme and signal to receptors expressed in the intestinal epithelium (Gregorieff, Pinto et al. 2005). While the importance of tightly regulated Wnt signaling in adult tissues is well-documented linking dysregulation of the pathway to hyperproliferation and cancer, our basic understanding of Wnt signaling on the ligand/receptor level is complicated by the large number of identified Wnt ligands and their receptors. In addition, ligands can bind to multiple receptor and/or co-receptor combinations to stimulate different downstream target gene expression. Therefore, due to this

contextual influence, it has been difficult to dissect such complex interactions *in vivo*. Further, although many transgenic mouse lines with modifications in the Wnt signaling pathway exist, most harbor perturbations in downstream effectors, such as Apc or β-catenin. Moreover, the limited number of ligand knockout mouse lines in existence result in developmental defects that preclude analysis in the adult (McMahon and Bradley 1990; Takada, Stark et al. 1994; Yamaguchi, Bradley et al. 1999), and tissue-specific analyses are impeded by the lack of available knockout mice with conditional alleles. Mouse models exhibiting over-expression of Wnt ligands are also not readily available. While these transgenic and knockout mice could be generated, doing so for individual Wnt ligands and receptors in different tissues or cellular compartments would be inefficient and expensive. Although the Wnt signaling pathway exemplifies the intricate nature of mesenchymal-epithelial signaling, the challenges highlighted here also apply to studies in other signaling pathways. As such, it is important to explore alternative approaches for genetic manipulation to effectively study the role of mesenchymal-epithelial signaling pathways in homeostasis and disease.

Viral delivery of transgenes to either mediate ectopic gene expression or to dampen endogenous expression represents an attractive alternative approach as it can provide a rapid functional assessment of multiple receptors and ligands, individually or in tandem. Recent advances in the biosafety of lentiviral vectors make this approach a viable option, because non-replicative, self-inactivating viruses now cause little to no adverse effects on the infected subject (Dull, Zufferey et al. 1998; Naldini 1998; Zufferey, Dull et al. 1998). Most importantly,

this approach results in stable integration of the transgene into the mouse genome (Naldini 1998). A track record for successful use of lentiviral mediated gene delivery is apparent from studies in embryonic stem cells and somatic cells from a variety of organs, including the lung, pancreas, and stomach epithelium, as well as the liver (Fassler 2004; Skarsgard, Huang et al. 2005). Additionally, *in utero* viral injection of fetal rats results in a secondary infection site in the intestinal epithelium (Seppen, van der Rijt et al. 2003). Although intriguing, this challenging technique may be an unfavorable approach for intestinal epithelial transgene expression in light of the availability of constitutive and inducible intestinal promoters that are well-established for driving intestinal epithelial transgene expression in a more uniform and robust fashion (Sweetser, Hauft et al. 1988; Madison, Dunbar et al. 2002; Ireland, Kemp et al. 2004; Sansom, Reed et al. 2004). However, few systems exist for mesenchymal transgene expression, which is required to modulate paracrine signals originating in the mesenchyme. Our studies employ such an approach, and we have used the small intestine to demonstrate its effectiveness.

It is well-documented that the small intestine displays cell signaling across its defined epithelial and mesenchymal cellular compartments (Batlle, Henderson et al. 2002; Gregorieff, Pinto et al. 2005; Rizvi and Wong 2005; Clevers and Batlle 2006), offering an ideal system to display lentiviral-mediated transgene expression to modulate mesenchymal-epithelial crosstalk. In this study, we report effective lentiviral-mediated transgene delivery to mesenchymal cells and subsequent signaling to the epithelium. Functional levels of lentiviral-mediated

WNT1 expression in the intestinal mesenchyme modulated transgene expression in the epithelium and resulted in a phenotypic readout.

MATERIALS AND METHODS

Mice. Mice were housed in a specific pathogen-free environment under strictly controlled light cycle conditions, fed a standard rodent Lab Chow (PMI Nutrition International), and provided water *ad libitum*. FVB/N and Wnt-reporter, TOPGAL mice (DasGupta and Fuchs 1999) were purchased from The Jackson Laboratory (Stock #001800, #004623). Prior to lentiviral infection, mice were housed in a specific pathogen-free barrier room. After lentiviral infection mice were moved to a standard barrier room. All procedures were performed in accordance to the OHSU Animal Care and Use Committee.

Vector production and *in vivo* transduction. Lentiviruses were produced using the 3rd generation HIV-pseudotyped system (Dull, Zufferey et al. 1998). Transducing vectors contained DsRed (pSL35=LMSCV-IRES-eGFP -DsRed) or human WNT1 (pSL35=LMSCV-IRES-eGFP -WNT1), packaging vector pSL4, envelope vector pSL3, and rev-regulatory vector pSL5. pSL35 was modified to contain the murine stem cell virus (MSCV) promoter and the IRES-eGFP and multiple cloning site from pIRES2-eGFP (Clontech). High-titer lentiviruses were produced in 293T cells by FuGene 6-mediated transient co-transfection (Roche Applied Science) of each of the four vectors. Viruses were subsequently concentrated from conditioned media harvested 48 and 72 hours after

transfection by ultracentrifugation at 25,000 rpm in a Beckman SW28 swinging bucket rotor. Viral pellet was resuspended in sterile PBS and titered by serial dilution and infection into HEK 293T/17 (ATCC # CRL-11268) cells, then expression titer determined by GFP fluorescent expression by flow-cytometry analysis (FACSCalibur, Becton Dickinson). Viral pellet was resuspended in sterile PBS and titered by serial dilution and infection of 293T cells, followed by flow-cytometry analysis (FACSCalibur, Becton Dickinson) to determine the GFP expression titer. Viral titers were on average 5×10^7 to 1×10^8 infectious units/ml. All viruses were tested for replication ability by P24 assay and found to be negative (HIV-1 P24 ELISA, PerkinElmer). For lentivirus transduction, postnatal (P) day 1 TOPGAL and FVB/N mice were administered 5×10^6 viral particles by intraperitoneal injection and analyzed 7, 14, 21, or 28 days later. Peripheral blood leukocytes were isolated at the time of sacrifice and subjected to erythrocyte depletion by sedimentation in 3% dextran (Amersham Pharmacia) and hypotonic lysis (Willenbring and Grompe 2004), followed by analyses of peripheral blood GFP expression using flow cytometry (FACSCalibur, Becton Dickinson). Dead cells were excluded by using a combination of scatter gates and propidium iodide staining.

Analyses of transgene expression. The stomach, small intestine, colon, liver, kidney, brain, lung, spleen, heart, and skin were harvested and processed for mRNA expression analyses by qRT-PCR and for protein expression by immunoblot and immunohistochemistry as described below. For a more focused

analysis of the intestine, epithelial and mesenchymal cellular compartments were independently isolated. For collection of epithelial fractions, the villus and crypt epithelium was differentially isolated using a modified Weiser preparation (Weiser 1973a,b; Davies, Dismuke et al. 2008). The remaining tissue was mechanically dissociated over a 10-mesh sieve (Bellco Tissue Sieve®, Bellco) to isolate the mesenchymal cellular compartment from the muscularis. The three individual cellular compartments (villus epithelium, crypt epithelium, and mesenchyme) were then snap frozen in liquid nitrogen for future expression analyses.

qRT-PCR and RT-PCR analyses. RNA was isolated (QIAGEN RNeasy) and cDNA generated using MMLV-RT reverse transcriptase (Invitrogen) as previously described (Wong, Saam et al. 2000). qRT-PCR analyses were performed using SYBR®-Green technology on an ABI 7900HT System (Applied Biosystems). All reactions were performed in triplicate in a reaction volume of 15µl, using 100ng of template DNA, 7.5µl of a 2X SYBR®-Green Master Mix, 0.15U UDP-N-glycosidase (Invitrogen) and 900nM forward and reverse primers. Data analysis using the $\Delta\Delta C_T$ (cycle threshold) approach was performed using the ABI Prism® SDS 2.1 software. Cycle threshold (CT) values were determined for each gene and each sample was normalized to the internal control gene, Glyceraldehyde 3-phosphate dehydrogenase (Gapdh). Primers used are listed as follows: Gapdh (F- AAATATGACAACTCACTCAAGATTGTCA, R-CCCTTCCACAATGCCAAAGT), GFP (F- TCCAGGAGCGCACCATCTT, R-CGATGCCCTTCAGCTCGAT), DsRed (F- GAGATCCACAAGGCCCTGAAG, R-

GTCCAGCTTGGAGTCCACGTA), LacZ (F- GATCTTCCTGAGGCCGATACTG, R-GGCGGATTGACCGTAATGG), c-Myc (F-AGCTTCGAAACTCTGGTGCATAA, R- GGCTTTGGCATGCATTTTAATT), EphrinB1 (F-AGGTTGGGCAAGATCCAAATG, R-AGGAGCCTGTGTGGCTGTCT), EphB2 (F-ACCTCAGTTCGCCTCTGTGAA, R-GGACCACGACAGGGTGATG), EphB3 (F-TCTGACACTCAGCTCCAACGA, R-CCAGGCATCCAAAAGTCCA).

Immunoblot analyses. Whole intestinal tissue was harvested, flushed with cold PBS, snap frozen in liquid nitrogen, lyophilized overnight and subsequently ground into a powder with a mortar and pestle. Samples were resuspended in 1X sample buffer as described (Sambrook and Russell 2001), then subjected to electrophoresis on a 4% stack/15% resolving acrylamide gel and transferred overnight at 20V, 4°C to PVDF membrane. For protein detection, the membrane was incubated with Odyssey® Blocking Buffer (LI-COR Biosciences) for 1 hour at 25°C, then probed with antibodies to GFP (1:1000; Molecular Probes), DsRed (1:1000; Clontech), WNT1 (1:1000, R&D Systems) or β-Actin (1:1000, Santa Cruz). Direct near-Infra-Red detection was performed using appropriate species-specific secondary antibodies (rabbit IRDye 800; Rockland, and mouse AlexaFluor 680; Molecular Probes), prior to being visualized on the Odyssey Infrared Imaging System (LI-COR Biosciences).

Immunohistochemical analyses. Liver, spleen, lung and the intestine were processed for frozen sectioning and antibody staining as previously described (Wong, Rubinfeld et al. 1998). GFP-expressing cells were identified in 5μm-thick sections with antibodies to GFP (1:250; Molecular Probes) and fluorescent secondary antibodies (1:500, Cy5; Jackson ImmunoResearch), or were double-labeled with antibodies to DsRed (1:200; Clontech), Ki67 (1:200, AbCam) or β-gal (1:500; Immunology Consultants Laboratory, Inc.) and visualized with Cy5- and FITC-conjugated secondary antibodies (Jackson ImmunoResearch). Slides were incubated with Hoechst 33258 (0.1 μg/ml; Sigma) nuclear stain. Sections were captured on a Leica DMR microscope with a DC500 digital camera and IM50 Image Manager Software (Leica Microsystems). Images were overlaid using Adobe Photoshop CS2 or ACD Systems Canvas.

The number of crypt-villus units containing Wnt-receiving cells was determined in WNT1-injected and DsRed-injected mice by counting positive crypt-villus units on 6x 5μm tissue sections 125μm apart (n=3 each group) and represented as a ratio relative to total crypt-villus units. Statistical significance between experimental populations was determined using a Student's two-tailed, paired t-test. A p-value <0.05 was considered statistically significant. Statistical analysis was performed using GraphPad Prism for Windows (GraphPad Software).

RESULTS AND DISCUSSION

Lentiviral-mediated transgene expression in the mouse. To demonstrate that lentiviral-mediated delivery of transgenes represents an effective approach for modulating signaling pathways dependent upon mesenchymal-epithelial interactions, we characterized *in vivo* infection and mouse tissue expression patterns of a lentivirus harboring a bicistronic message encoding DsRed sequences upstream of an internal ribosomal entry site and enhanced green fluorescent protein (DsRed-IRES-GFP). The virus was generated by co-transfecting three lentiviral packaging plasmids (Dull, Zufferey et al. 1998) with the DsRed-IRES-GFP transducing vector (Fig. 3.1A). Lentiviral particles (5×10^7) were delivered by intra-peritoneal injection into wild-type mice at postnatal day 1 (P1) that were subsequently sacrificed and analyzed at P21 (Fig. 3.1A). Multiple tissues were isolated and analyzed by quantitative reverse transcriptase polymerase chain reaction (qRT-PCR) for GFP expression (Fig. 3.1B). Expression was highest in the liver and spleen, presumably due to the high percentage of blood-derived cells in these organs, but also detectable in the kidney, lung, skin and the small intestine. As we previously noted, the small intestine has well-defined epithelial and mesenchymal cellular compartments and known pathways exhibiting signaling crosstalk between the two distinct regions, offering an ideal system in which to continue our studies.

Intestinal transgene expression is restricted to the mesenchyme. To identify the transgene-expressing cell population, we stained frozen intestinal sections from lentiviral-infected mice with antibodies to GFP and DsRed (Fig. 3.1E-G).

Co-localized expression of GFP and DsRed was restricted to the mesenchymal cells in both the crypt and villus. To confirm the mesenchyme-restricted expression pattern, cells from the mesenchyme and epithelial compartments were independently isolated by both dissociation of epithelial cells in EDTA and mechanical dispersion of mesenchymal cells (Weiser 1973a,b; Davies, Dismuke et al. 2008). Restriction of lentiviral gene expression to the mesenchymal population was confirmed by qRT-PCR using primers specific to GFP and normalized to the housekeeping gene, Glyceraldehyde phosphate dehydrogenase (Gapdh; Fig. 3.1C). This compartment-specific expression allows for manipulation of paracrine signaling from the mesenchyme to the intestinal epithelium. GFP expression was not detected in mock-injected saline-only controls for all experiments (data not shown).

Figure 3.1

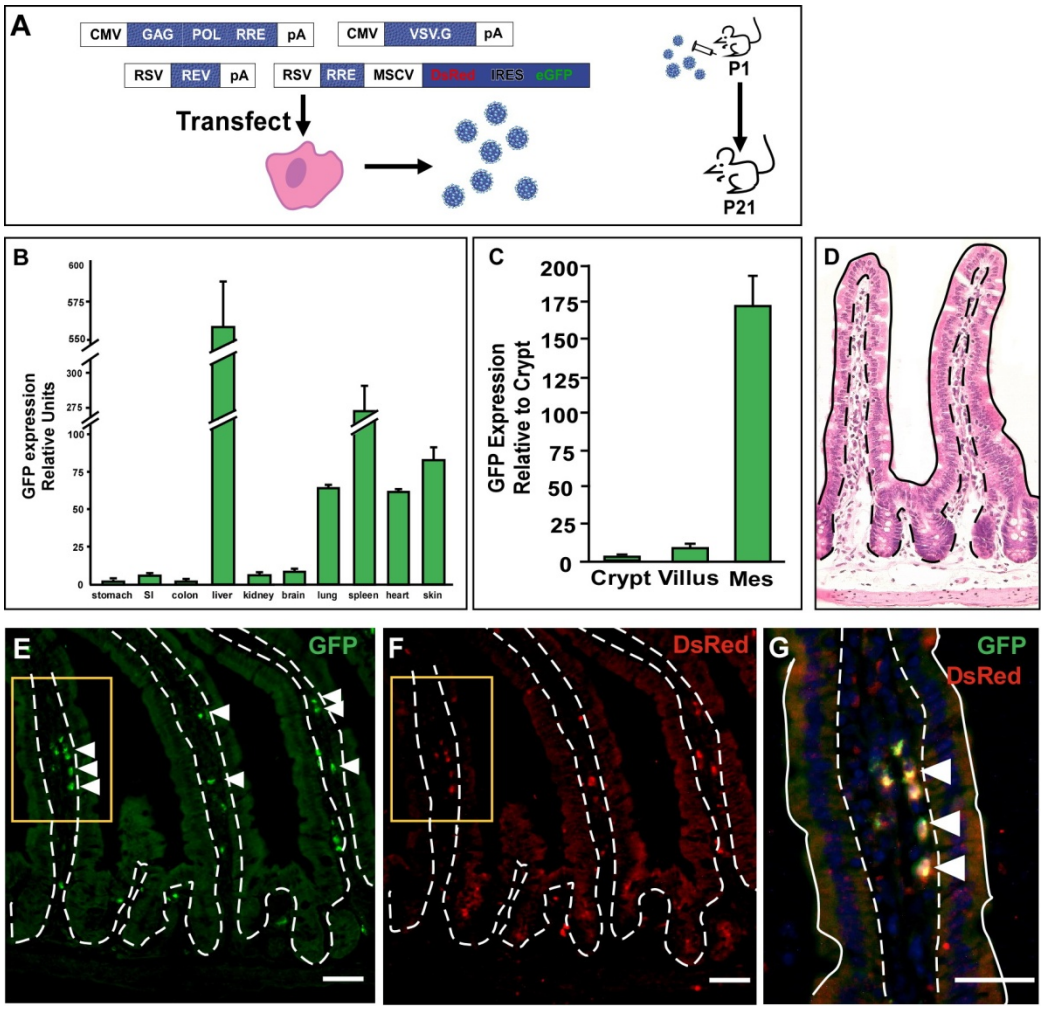
A
CMV
GAG
POL
RRE
pA
CMV
VSV.G
pA
RSV
REV
pA
RSV
RRE
MSCV
DsRed
IRES
eGFP
Transfect
P1
P21
B
GFP expression
Relative Units
600
575
550
300
275
100
75
50
25
0
stomach
SI
colon
liver
kidney
brain
lung
spleen
heart
skin
C
GFP Expression
Relative to Crypt
200
175
150
125
100
75
50
25
0
Crypt
Villus
Mes
D
E
GFP
F
DsRed
G
GFP
DsRed

Figure 3.1 Lentiviral-mediated gene delivery to the mouse small intestine. (A) Schematic of virus production in 293T cells and mouse injection. Mice were injected at postnatal (P) day 1 and sacrificed for analysis at later timepoints. (B) GFP gene expression by quantitative reverse transcriptase-polymerase chain reaction (qRT-PCR) in the gastrointestinal tract and other organs. GFP expression is normalized to Glyceraldehyde 3-phosphate dehydrogenase expression and presented relative to levels in the stomach. Graph displays triplicate samples from representative animals. Data displayed as mean±S.D. (C) GFP expression in isolated intestinal crypt and villus epithelium and mesenchymal cells by qRT-PCR. Graph displays triplicate samples from representative animal. Data displayed as mean±SD. (D) Hematoxylin and Eosin stained normal intestinal crypt-villus unit. Solid line indicates apical epithelial border, dashed line indicates epithelial-mesenchymal border. (E-G) Co-labeling of DsRed-injected intestine with antibodies to GFP (green) and DsRed (red). Yellow box in (E, F) is enlarged in (G). Arrowheads indicate dual expressing mesenchymal cells. Dashed line indicates epithelial-mesenchymal border. Solid white line in (G) marks the apical border. Bar = 25µm.

Expression of WNT1 ligand in the mouse intestinal mesenchyme. To show functional expression of a signaling molecule expressed by lentiviral infection, we chose to ectopically express the WNT1 ligand in the intestinal mesenchyme. Stimulation of the Wnt/β-catenin signaling pathway has a well-characterized effect on the epithelium, resulting in hyperproliferation (Harada, Tamai et al. 1999; Sansom, Reed et al. 2004). A WNT1-IRES-GFP lentivirus was generated and injected into mice as we described above. Similar to the DsRed lentivirus, WNT1 and GFP were expressed down the length of the intestine and were primarily restricted to the mesenchyme (Fig. 3.2A&B). Immunoblot analysis for WNT1 revealed an expected 41kD band in the proximal (PSI), mid (MSI), and distal small intestine (DSI) of infected mice (Fig. 3.2C). Further, GFP expression was detected by immunofluorescence in the mesenchyme, both near the crypts and on the villi (Fig. 3.2D&E). Thus, the expression pattern was ideal to carry out studies using overexpression of ligands of mesenchymal origin.

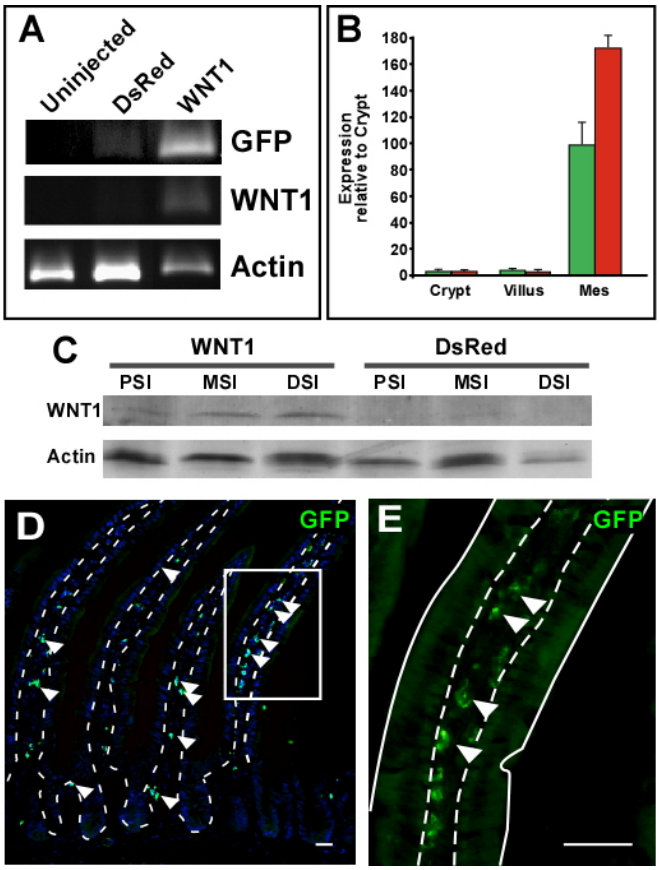

Figure 3.2 Ectopic expression of WNT1 in the mouse intestine. (A) Reverse transcriptase-polymerase chain reaction (RT-PCR) for intestinal expression of WNT1, GFP and Actin in uninjected, DsRed-injected, and WNT1-injected mice. (B) Gene expression levels of GFP (green) and WNT1 (red) in isolated crypt and villus epithelium and mesenchymal cells by qRT-PCR. Levels normalized to internal reference gene GAPDH and relative to crypt values. Samples from representative animal assayed in triplicate, data reported as mean±SD. (C) Immunoblot probed with antibodies to WNT1 and Actin from proximal, mid, and distal small intestine (PSI, MSI, DSI) of WNT1- and DsRed-infected animals. (D) Tissue section from WNT1-injected mice stained with antibodies to GFP (green) and counterstained with Hoechst dye. Arrowheads indicate GFP-expressing mesenchymal cells. White box is enlarged in (E). Dashed line represents epithelial-mesenchymal boundary, solid line represents apical epithelial border. Bar = 25μm.

Functional expression of WNT1 in the mouse intestine. Wnt-reporter mice (TOPGAL), a transgenic mouse line that expresses β-galactosidase (β-gal) in response to a canonical Wnt signal (DasGupta and Fuchs 1999), were injected with WNT1-IRES-GFP lentivirus to determine if lentiviral-mediated gene delivery could result in an increase over endogenous levels of Wnt activation within the intestinal epithelial compartment. β-gal-expressing epithelial cells were detected in juxtaposition to GFP-expressing mesenchymal cells (Fig. 3.3A). Additionally, an appreciable increase in the percentage of β-gal-positive crypt-villus units was detected in the MSI and DSI relative to control injected mouse intestines (Davies, Dismuke et al. 2008) (Fig. 3.3B). Analysis by qRT-PCR confirmed the increase in β-gal reporter expression in WNT1 infected intestines, demonstrating a >4-fold increase in the epithelial compartment of both the crypt and villus (Fig. 3.3C). Thus, lentiviral-derived ectopic expression of ligands can modulate transgene expression in the epithelium.

Epithelial response to expression of WNT1. We further validated the canonical Wnt stimulation by examining known downstream target genes. As expected, the increase in Wnt-reporter expression was accompanied by an increase in Wnt target genes c-Myc, EphB2, and EphB3, and decreased EphrinB1 (Fig. 3.3D) (Batlle, Henderson et al. 2002; Clevers and Batlle 2006). These results indicate not only that lentiviral-delivery of the WNT1 ligand stimulated the pathway as confirmed by a reporter assay, but it also resulted in an increase in endogenous Wnt targets.

Over-expression of the WNT1 ligand in other systems results in hyperproliferation and tumor formation (Huang, Chen et al. 2008). Consistent with these reports, we observed an expansion of the intestinal crypt proliferative zone (Fig. 3.3E). Ki67 antibodies recognize proliferating cells in the intestine which are confined to the crypt during normal adult intestine homeostasis (Davies, Dismuke et al. 2008). In lentiviral-mediated WNT1-expressing intestines, the proliferative zone was expanded beyond the crypt-villus junction (solid white line, Fig. 3.3E). This indicated that moderate and local influence of exogenously expressed WNT1 ligand in the mesenchyme resulted in hyperproliferation. Further, 67% of the WNT1 infected mice developed at least one polyp (Fig. 3.3F,G).

In summary, our findings show that lentiviral vectors can be used for modulation of signaling pathways that require a paracrine-expressed ligand. A single intra-peritoneal injection resulted in mesenchymal expression in the intestine, as well as other gastrointestinal and blood derived organs. Our system offers a superior approach for delivering ligand expression to the mesenchyme negating the need for technically challenging *in utero* surgeries, bone marrow transplants, or complicated mating schemes for genetic models. In addition, our approach offers the advantage of easily identifying infected cells with GFP expression driven off the bicistronic message, allowing for phenotypic changes in the epithelium to be monitored at a cellular level. The ability to track infected cells allows for comparisons of an elicited phenotype with normal adjacent regions within the local intestinal microenvironment. Recent reports using shRNA or

siRNA-containing lentiviruses (Herold, van den Brandt et al. 2008) suggest that our scheme could also be used for knock-down of ligand transcripts to extend our understanding of the factors that regulate the intestinal stem cell or other organ stem cells that are modulated by paracrine signaling. We envision that lentiviruses will become valuable tools to study Wnt and other signaling pathways, allowing us to dissect ligand-receptor interactions as we seek to further understand the intricacies of signaling within the mouse during both development and in disease.

Figure 3.3

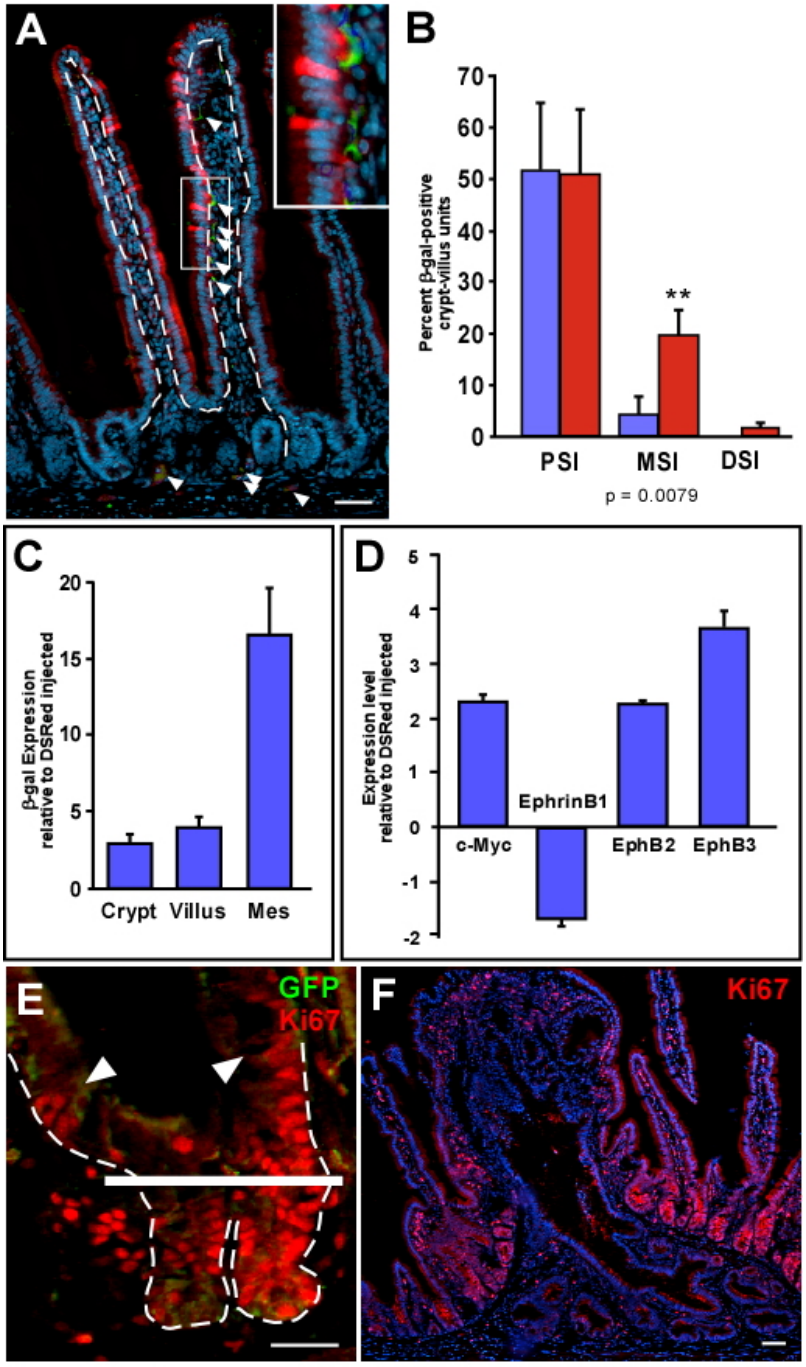

G

Virus	n	Age	Tumors
DsRed	6	3 wks	0%
WNT1	18	*3-8 wks	67%

Figure 3.3 Functional phenotype in WNT1-injected mice. (A) Intestinal section stained with antibodies to β-galactosidase (β-gal; red) and GFP (green), and counterstained with Hoechst dye (blue) in a WNT1-injected Wnt-reporter mouse. Arrowheads denote GFP-expressing WNT1-infected cells. Higher magnification of white box in inset. Dashed line represents epithelial-mesenchymal boundary. (B) Quantitation of intestinal Wnt-receiving cells in the proximal, mid, and distal small intestine (PSI, MSI, DSI) by immunostaining with antibodies to β-gal. The number of crypt-villus units containing Wnt-receiving cells was counted in DsRed-injected (blue bars) and WNT1-injected (red bars) Wnt-reporter mice and represented as a ratio to total crypt-villus units counted (n=3 for all three regions; MSI, $p = 0.0079$). (C) Quantitative reverse transcriptase-polymerase chain reaction (qRT-PCR) assay for LacZ expression in isolated intestinal crypt, villus and mesenchymal cells from WNT1- and DsRed-infected Wnt-reporter mice. Graph displays triplicate samples from representative animals. Data displayed as mean±SD. (D) qRT-PCR for gene expression of canonical Wnt target genes: c-Myc, EphrinB1, EphB2, and EphB3. All qRT-PCR samples normalized to internal reference gene, represented relative to DsRed-infected cells and run in triplicate. (E) Intestinal crypt section from WNT1-injected mouse stained with antibodies to Ki67 (red) and GFP (green). Solid white bar indicates crypt-villus junction. Arrowheads denote Ki67-positive epithelial cells outside of normal proliferative zone. Dashed line indicates epithelial-mesenchymal boundary. (F) Polyp from PSI of WNT1-infected mouse stained with antibodies to Ki67 (red) and Hoechst (blue). Bar = 25μm. (G) Quantitation of intestinal tumors from DsRed- and WNT1-injected mice.

CHAPTER 4

Wnt5a in the mouse intestine

CHAPTER 4

Wnt5a is a negative regulator of the canonical Wnt pathway in the mouse small intestine

Adria D. Dismuke[1], Aimee D. Kohn[2], Randall T. Moon[3] and Melissa H. Wong[4]

[1]Department of Molecular and Medical Genetics, Oregon Health & Science University, Portland, OR;
[2]Cascade Cancer Center, Kirkland, WA;
[3]Howard Hughes Medical Institute, Division of Hematology, Department of Pharmacology, and the Center for Developmental Biology, Institute for Stem Cell and Regenerative Medicine, University of Washington School of Medicine, Seattle, WA;
[4]Departments of Dermatology; Cell and Developmental Biology; Knight Cancer Institute, Oregon Health & Science University, Portland, OR.

ADD and MHW participated in planning of all experiments within the study, as well as the writing of the manuscript. ADD performed all experiments described in this chapter. ADK and RTM created the lentiviral constructs.

Abstract

The Wnt signaling pathway is essential for regulation of epithelial homeostasis in the mouse small intestine. However, not all Wnt ligands always stimulate the β-catenin dependent canonical Wnt pathway and may signal through an alternative pathway. Both types of ligands co-exist within the intestine and it is unclear if they play a coordinate role in regulating epithelial homeostasis. Here we show that Wnt5a, a ligand that signals independently of β-catenin and is normally expressed in the mouse small intestinal mesenchyme, negatively regulates the canonical Wnt pathway. Using the TOPGAL Wnt reporter mouse, we show that Wnt activation is inhibited when Wnt5a is ectopically expressed in the intestine, both by changes in reporter gene expression and by the aberrant localization of differentiated Paneth cells. However, this ectopic expression did not affect overall rates of migration or PCP pathway effectors. Furthermore, evaluations of damage and disease models that activate the canonical Wnt pathway suggest that Wnt5a may exist in a negative feedback loop. Our studies have important implications as to how different intestinally expressed Wnt ligands interact to regulate intestinal homeostasis and response to injury.

Introduction

The mammalian intestine is a complex organ with highly specified architecture that relies on the Wnt signaling pathway for proper development and maintenance throughout adulthood. In the intestinal crypts, Wnt stimulation drives a proliferation gene program and is essential for establishment and maintenance of the intestinal stem cell (Korinek et al., 1998; Fevr et al., 2007), and also controls differentiation and migration of Paneth cells (Batlle et al., 2002). Alternatively, suppressed or absent Wnt signals on the villus allow for differentiation and cell cycle arrest. Furthermore, Wnt signaling directly controls expression of the EphB/ephrinB receptors and ligands. The Eph/ephrins control Paneth cell positioning in the small intestine (Batlle et al., 2002) and the establishment of the crypt/villus boundary. Tight regulation of Wnt signaling along the crypt-villus axis is thereby essential to its maintenance, explaining the complex expression patterns of Wnt ligands, Fz and LRP receptors, and Wnt inhibitory factors in the epithelium and the adjacent mesenchyme (Gregorieff et al., 2005). The balance of these factors is of utmost importance in maintaining the proper gradient of Wnt activation.

One ligand normally expressed in the mesenchyme of both developing and adult mouse intestine is Wnt5a, a ligand that is the subject of much controversy. Even though its first characterization as a Wnt ligand established that it does not stimulate β-catenin signaling, the actual *in vivo* function of this ligand remains unclear. In frog and zebrafish development, Wnt5a regulates convergence and extension movements during gastrulation in a process likely

mediated by Ror2, RhoA GTPase, Jun kinase (JNK), and Ca2+ release (Slusarski et al., 1997; Slusarski et al., 1997; Kuhl et al., 2000; Yamanaka et al., 2002; Zhu et al., 2006; Schambony and Wedlich, 2007). In a mammalian system, mice deficient in Wnt5a are embryonically lethal. They exhibit a profound defect in elongation along the anterior-posterior axis, in addition to morphogenesis and outgrowth of limb buds and other structures, without affecting specific cell fate (Cervantes et al., 2009).

Recent studies of the $Wnt5a^{-/-}$ embryonic intestine show that this ligand is essential for proper intestinal development (Cervantes et al., 2009). $Wnt5a^{-/-}$ mice display dramatic shortening of the small intestine and defective closure of the primitive gut tube at E10 resulting in an aberrant bifurcation of the midgut. Interestingly, all of the differentiated cell lineages normally present by E18.5 still exist in the $Wnt5a^{-/-}$ mice, suggesting that this signaling pathway is not required for cell fate decision. Intriguingly, Wnt5a remains expressed in the intestinal mesenchyme through adulthood (Gregorieff et al., 2005), suggesting it continues to play a role in regulation of a Wnt-associated pathway there.

The highly conserved Wnt signaling pathway modulates transcriptional programs that control many crucial developmental and adult processes (Logan and Nusse, 2004), and Wnt mutations can result in severe developmental defects including early gastrulation defects, neural tube defects, axis formation, and structural outgrowth (Liu et al., 1999; Barrow et al., 2003). However, tight regulation of this signaling pathway is also essential, as misregulated Wnt transduction is implicated in tumorigenesis and disease (Clevers, 2006).

Furthermore, it is also known that Wnt signaling is essential in a number of stem and progenitor cell populations and is key regulator of cell fate decisions. Thus far, since the first description of Wnt1, a total of 19 mammalian Wnt ligand-encoding genes have been identified (Nusse, 2008).

In the canonical β-catenin-mediated Wnt pathway, the absence of a Wnt ligand causes the downstream effector β-catenin to be bound and phosphorylated by a protein complex including Axin, the adenomatous polyposis coli (Apc) protein, and glycogen synthase kinase-3β (GSK-3β), targeting it for subsequent ubiquitination by the beta-transducin repeat–containing homologue protein (βTrCP) and degradation by the proteasome (Clevers, 2006). Binding of a Frizzled (Fz) receptor and low-density lipoprotein receptor-related protein (Lrp5/6) co-receptor by a Wnt ligand inhibits this complex, allowing β-catenin to accumulate in the cytoplasm. β-catenin then translocates to the nucleus, where it activates the Tcf/LEF transcription factors, stimulating transcription of target genes.

While these Wnt homologs have a high degree of sequence similarity (Nusse, 2008), their specific expression patterns within different tissue and cell types and disparate knock out phenotypes suggest that their functional activities may also differ (Logan and Nusse, 2004). Further, misexpression in developmental systems can have largely different outcomes. Early on in the discovery of Wnt family genes, Wnt proteins were categorized in one of two functional groups based on the observation that injection of mRNA from some Wnt genes, such as Wnt1 and Wnt3a, resulted in induction of duplication of the

dorsal-ventral axis in Xenopus embryos, whereas expression of ‘‘Wnt5a class’’ Wnts, including Wnts 4, 5a, and 11, did not (Du et al., 1995). Furthermore, Wnts that resulted in axis duplication, which became known as “canonical Wnts”, can morphologically transform C57MG mouse mammary epithelial cells (Wong et al., 1994). Subsequently, it was proposed that “Wnt5a class” Wnts must signal through an alternate intracellular pathway, one that does not activate the canonical target genes. Interestingly, in Xenopus embryo assays, expression of Wnt5a mRNA was found to abrogate the ability of other Wnts to induce axis duplication, suggesting that it is capable of inhibiting canonical Wnt ligand activity (Torres et al., 1996). However, more recent evidence suggests that signaling either through the canonical pathway or alternate pathways is dictated by Wnt receptors expression context on receiving cells, and that Wnt5a can in fact stimulate the canonical pathway in the presence of certain receptors (Gordon and Nusse, 2006; Mikels and Nusse, 2006). While the importance of Wnt5a expression has been established in intestinal development, its function in the adult intestine remains unclear.

MATERIALS AND METHODS

Mice. Mice were housed in Oregon Health and Science University animal facility under strictly controlled light cycle conditions and fed a standard rodent Lab Chow (PMI Nutrition International), and provided with water *ad libitum*. FVB/N and the Wnt-reporter TOPGAL mice (DasGupta and Fuchs, 1999) were

purchased from The Jackson Laboratory (Stock #001800, #004623). Before infection with lentivirus, mice were housed in a specific pathogen-free barrier room. After lentiviral infection mice were moved to a standard barrier room. AhCre mice(Sansom et al., 2004) and Apc^{580S} mice (designated as $Apc^{fl/fl}$ in the unrecombined state and $Apc^{-/-}$ after recombination)(Shibata et al., 1997) were kindly provided by Dr. Douglas Winton (University of Cambridge). $Apc^{Min/+}$ mice were purchased from The Jackson Laboratory. All procedures were performed in accordance to the OHSU Animal Care and Use Committee.

Vector production and *in vivo* transduction. Lentiviral vectors were generated using the 3rd generation HIV-pseudotyped system (Dull et al., 1998). Transducing vectors contained DsRed (pSL35=LMSCV-IRES-eGFP -DsRed) or human WNT5A (pSL35=LMSCV-IRES-eGFP –WNT5A), packaging vector pSL4, envelope vector pSL3, and rev-regulatory vector pSL5. pSL35 was altered to utilize the murine stem cell virus (MSCV) promoter as well as the IRES-eGFP and multiple cloning site from pIRES2-eGFP (Clontech). High-titer lentiviruses were produced in HEK 293T/17 (ATCC # CRL-11268) cells by co-transfecting each of the four vectors using FuGene 6-mediated transient co-transfection (Roche Applied Science). Viruses were subsequently collected from harvested conditioned media at 48 and 72 hours after transfection by ultracentrifugation at 25,000 rpm in a Beckman SW28 swinging bucket rotor. Viral pellet was resuspended in sterile PBS, titered by serial dilution and infection into HEK 293T/17 (ATCC # CRL-11268) cells, then infectious units determined by GFP

fluorescent expression by flow-cytometry analysis (FACSCalibur, Becton Dickinson). Viral titers were on average 5 x 10^7 to 1 x 10^8 infectious units/ml. All viruses were tested for negative replication ability by P24 assay (HIV-1 P24 ELISA, PerkinElmer). Lentivirus transduction was achieved by administering 5 x 10^6 viral particles to TOPGAL and FVB/N mice by intraperitoneal injection at postnatal (P) day 1, which were then analyzed 21 days later. Mock-injected control mice received only sterile PBS injections.

Analyses of gene expression. Epithelial and mesenchymal cellular compartments were independently isolated for gene expression analysis. The villus and crypt epithelium were isolated differentially using a modified Weiser preparation (Weiser, 1973; Davies et al., 2008). To isolate the mesenchymal cellular compartment from the muscularis, the remaining tissue was mechanically dissociated over a 10-mesh sieve (Bellco Tissue Sieve®, Bellco). The three individual cellular compartments (villus epithelium, crypt epithelium, and mesenchyme) were then snap frozen in liquid nitrogen for future expression analyses. Samples of the intestinal tissue were taken at each stage of isolation and fixed, blocked, and stained with H&E to ensure proper fractionation.

qRT-PCR and RT-PCR analyses. RNA was isolated (5 Prime Perfect Pure^{TM}) and cDNA generated using MMLV-RT reverse transcriptase (Invitrogen) as previously described (Wong et al., 2000). SYBR®-Green qRT-PCR analyses were performed on an ABI 7900HT System (Applied Biosystems). Each reaction

was performed in triplicate in a reaction volume of 15µl, using 100ng of template DNA, 7.5µl of a 2X SYBR®-Green Master Mix, 0.15U UDP-N-glycosidase (Invitrogen) and 900nM forward and reverse primers. Data was analyzed using the standard $\Delta\Delta C_T$ (cycle threshold) approach using the ABI Prism® SDS 2.1 software. Cycle threshold (CT) values were determined for each gene and normalized to the internal control gene, Glyceraldehyde 3-phosphate dehydrogenase (Gapdh). Primers used are listed as follows: Gapdh (F-AAATATGACAACTCACTCAAGATTGTCA, R- CCCTTCCACAATGCCAAAGT), GFP (F- TCCAGGAGCGCACCATCTT, R- CGATGCCCTTCAGCTCGAT), LacZ (F- GATCTTCCTGAGGCCGATACTG, R-GGCGGATTGACCGTAATGG), EphrinB1 (F-AGGTTGGGCAAGATCCAAATG, R-AGGAGCCTGTGTGGCTGTCT), EphB2 (F-ACCTCAGTTCGCCTCTGTGAA, R-GGACCACGACAGGGTGATG), EphB3 (F-TCTGACACTCAGCTCCAACGA, R-CCAGGCATCCAAAAGTCCA), WNT5A (F- CGCTAGAGAAAGGGAACGAATC, R- TTACAGGCTACATCTGCCAGGTT).

Immunoblot analyses. Whole intestinal tissue was removed, divided into thirds by length, flushed with ice cold PBS, snap frozen in liquid nitrogen, lyophilized overnight and ground into a powder using a mortar and pestle. Samples were resuspended in 1X sample buffer as described (Sambrook and Russell, 2001) with the addition of a Complete Protease Inhibitor tablet (Roche), then subjected to electrophoresis on a 4% stack/15% resolving acrylamide gel and transferred overnight at 20V, 4°C to PVDF membrane. For protein detection, the membrane

was incubated with Odyssey® Blocking Buffer (LI-COR Biosciences) for 1 hour at 25°C, then probed with antibodies to GFP (1:1000; Molecular Probes), WNT5A (1:1000, R&D Systems), β-Actin (1:1000, Santa Cruz), Phospho-Jnk (1:1000, R&D Systems), or Pan-Jnk (1:1000, R&D Systems). Direct near-Infra-Red detection was performed using appropriate species-specific secondary antibodies (rabbit IRDye 800; Rockland, and mouse AlexaFluor 680; Molecular Probes), prior to visualization on the Odyssey Infrared Imaging System (LI-COR Biosciences).

Histochemical and Immunohistochemical analyses. The intestine was processed for frozen sectioning and antibody staining as previously described (Wong et al., 1998). Briefly, whole intestine was removed from the mouse abdomen, divided into thirds, and flushed with cold PBS and 4% paraformaldehyde. Each tube was cut down the length and pinned open onto a wax plate, then fixed for 1 hour in 4% paraformaldehyde, then washed in PBS and stored in PBS with 30% glucose overnight. Gut strips were then blocked in Tissue-Tek® Optimal Cutting Temperature (OCT) compound and frozen at -80°C and subsequently cut in 5µm sections.

GFP-expressing cells were identified in 5µm-thick sections with antibodies to GFP (1:250; Molecular Probes) and fluorescent secondary antibodies (1:500, Cy5; Jackson ImmunoResearch), or were double-labeled with antibodies to DsRed (1:200; Clontech), Ki67 (1:200, AbCam), Lysozyme (1:500, The Binding Site), Phospho-Jnk (1:100; R&D Systems), Rac (1:100; AbCam), β-actin (1:500;

Sigma Biosciences) or β-gal (1:500; Immunology Consultants Laboratory, Inc.) and visualized with Cy5- and FITC-conjugated secondary antibodies (Jackson ImmunoResearch). Slides were incubated with Hoechst 33258 (0.1 μg/ml; Sigma) nuclear stain.

Lendrum's Phloxine-Tartrazine staining was performed as previously described (Lendrum, 1947). Briefly, frozen sections were washed in water and incubated for 15 minutes in a solution of 50 mg/mL Phloxine B and 50 mg/mL calcium chloride, then rinsed in water, blotted, and incubated in a saturated solution of Tartrazine in 2-ethoxy ethanol for 30-60 seconds until tissue was cleared of phloxine except for Paneth cells, then rinsed briefly in ethanol and coverslipped.

Photos of all histochemical and immunofluorescent stained sections were captured on a Leica DMR microscope with a DC500 digital camera and IM50 Image Manager Software (Leica Microsystems). Images were overlaid using Adobe Photoshop CS2 or ACD Systems Canvas.

The number of crypt-villus units with aberrant Paneth cells was determined in WNT5A-injected and DsRed-injected mice by counting crypts containing Paneth cells above the +6 position on 6x 5μm tissue sections 125μm apart (n=3 each group) and represented as a percentage of total crypts counted. Statistical significance between experimental populations was determined using a Student's two-tailed, paired t-test. A p-value <0.05 was considered statistically significant. Statistical analysis was performed using GraphPad Prism for Windows (GraphPad Software).

Migrational Assay

5-bromo-2-deoxyuridine (BrdU) migrational assays were performed by injecting WNT5A-infected and DsRed-infected mice with 30mg/kg BrdU (Sigma) 48 hours prior to sacrifice. Intestinal tissues were prepared as described and then stained with antibodies to BrdU as follows: slides were rinsed in PBS, then incubated in 1N HCL for 10 minutes on ice, followed by 2N HCL for 10 minutes at room temperature, then 2N HCL for 20 minutes at 37°C. Slides were then incubated for 15 minutes at room temperature in 0.1M Boric acid buffered to pH 8.5 with NaOH. Slides were washed in PBS and followed by antibody staining as previously described with goat anti-BrdU (a kind gift from Dr. Jeffery Gordon) diluted 1:1000. The tissues were then imaged and the distances between the crypt base, leading edge, and lagging edge of the BrdU labeled zone were measured using the ImageJ program (http://rsbweb.nih.gov/ij/) and the “Measure and Label” plugin.

Irradiation- and ischemia-induced epithelial damage.

For the temporal analysis of irradiation, TOPGAL mice were exposed to 12Gy and sacrificed at 1, 6, 12, 24, 48, 72, and 168h post-irradiation. For the ischemic time course in TOPGAL mice, the cranial mesenteric artery was occluded with a veterinary microaneurism clip (Roboz #5420) for 20 minutes and sacrificed 1, 6, 12, 18, 24, 36, and 48h post-ischemia. Intestinal tissue was harvested and processed and stained with Hematoxylin & Eosin (H&E) and RNA was isolated as described above for qRT-PCR.

Results and Discussion

Lentiviral mediated expression of WNT5A in the intestinal mesenchyme.

Ectopic expression of WNT5A in the mouse intestine was mediated by *in vivo* lentiviral-mediated delivery as described in Chapter 3. Using an approach that we have previously demonstrated to result in successful transgene expression in the intestinal mesenchyme, post-natal day 1 (P1) mice were injected with 5×10^7 viral particles that harbored the WNT5A or DsRed transgene (control). mRNA levels of WNT5A were determined by quantitative reverse transcriptase-PCR (qRT-PCR). Because endogenous levels of Wnt5a are confined to the intestinal mesenchyme, we divided the intestine into three fractions: villus epithelium, crypt epithelium and mesenchyme. Confirming previously published *in situ* hybridization data, we showed that endogenous Wnt5a was present in the DsRed, control, injected intestines (Figure 4.1A) and excluded from the villus and crypt epithelium. qRT-PCR also demonstrated that effective compartmental expression of WNT5A in the WNT5A-injected mice was also confined to the mesenchymal region, but at 6.7-fold greater levels than endogenous expression (Figure 4.1A). To show that increased levels of WNT5A translated to increased protein levels, immunoblot analysis was performed. A specific ~52kDa band was robustly identified in the intestinal mesenchyme of the WNT5A-injected mice (Figure 4.1B) at a 10.5-fold higher level than the control infected animal, as determined by band density quantification. Protein competition experiments revealed high antibody specificity for this band (Supplemental Figure 4.S1). Interestingly a larger sized band was identified in

both the control DsRed and WNT5A mesenchyme lanes that was absent from the epithelial fractions. Presumably this ~70kDa band represents the endogenous mouse Wnt5a protein that is differentially post-translationally modified when compared to the lentiviral-mediated expression of WNT5A. Ectopic expression of WNT5A was confirmed by immunohistochemical analyses of the injected intestine with antibodies to Wnt5a and GFP, the bi-cistronic reporter that is co-expressed with both DsRed and WNT5A (Figure 4.1C-E). WNT5A-injected mice harbored mesenchymal cells that co-expressed both Wnt5a and GFP (Figure 4.1D, white arrow), whereas DsRed-injected intestines contained mesenchymal cells that either expressed Wnt5a or GFP, but not both (Figure 4.1E, white arrow, yellow arrowhead).

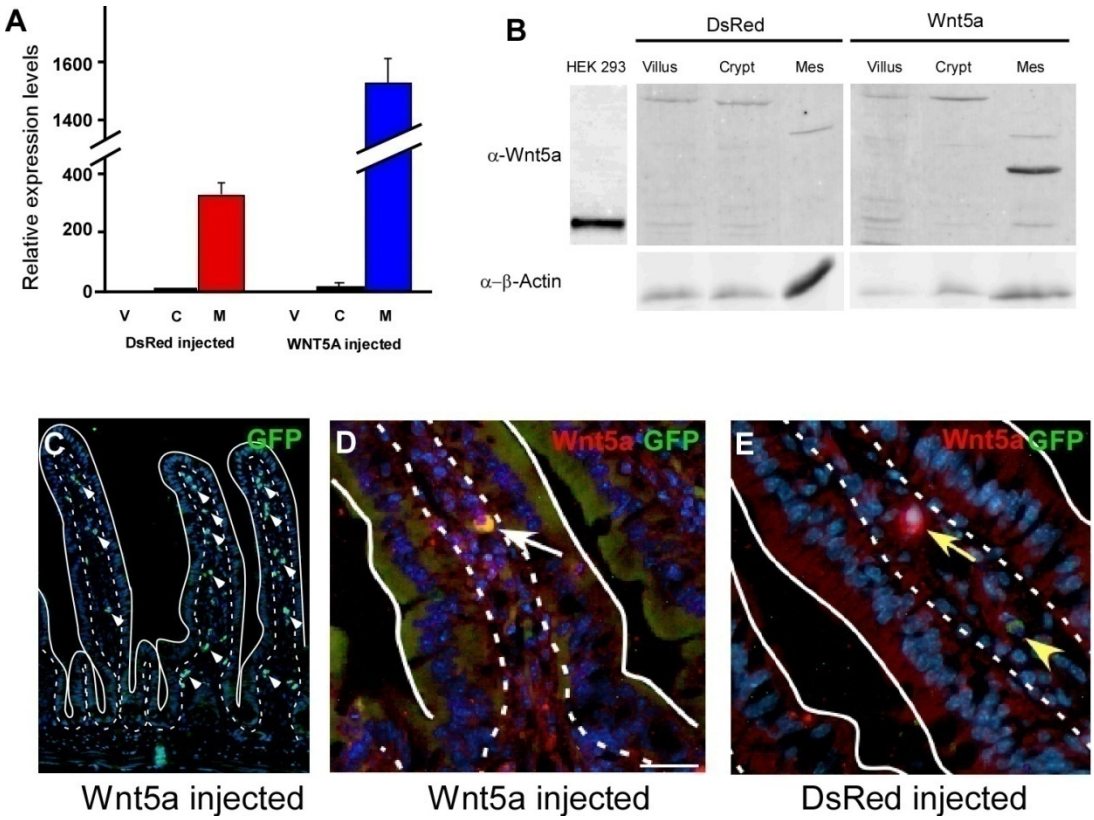

Figure 4.1. Lentiviral-mediated expression of WNT5A in the intestinal mesenchyme. (**A**) Quantitative reverse transcriptase-polymerase chain reaction (qRT-PCR) analysis of Wnt5a expression in the mouse small intestinal villus epithelium (V), cryptal epithelium (C), and mesenchyme (M) in control DsRed (red bars) and WNT5A (blue bars) infected intestines. WNT5A expression is normalized to Glyceraldehyde phosphate dehydrogenase (Gapdh) expression and presented relative to levels in the DsRed infected villus. Graph displays triplicate samples from representative animals. Data displayed as mean±std. (**B**) Immunoblot probed with antibodies to WNT5A and Actin with small intestinal protein from isolated villus epithelium, crypt epithelium, and mesenchyme of WNT5A- and DsRed-infected mice, as well as WNT5A-infected HEK 293 cells. (**C**) Tissue section from WNT5A-injected mouse stained with antibodies to GFP (green) and counterstained with Hoechst dye (gray). Solid white line = apical border. Dashed white line = epithelial-mesenchymal boundary. (**D, E**) Higher magnification images from WNT5A-injected (D) and DsRed-injected (E) intestines co-stained with antibodies to GFP (green) and Wnt5a (red) and counterstained with Hoechst dye (blue). Solid white line = epithelial brush border, dashed white line = epithelial-mesenchymal border, white arrow = double stained cell. White arrow = Wnt5a expressing cell, yellow arrowhead = GFP expressing cell. Bar = 25 μm.

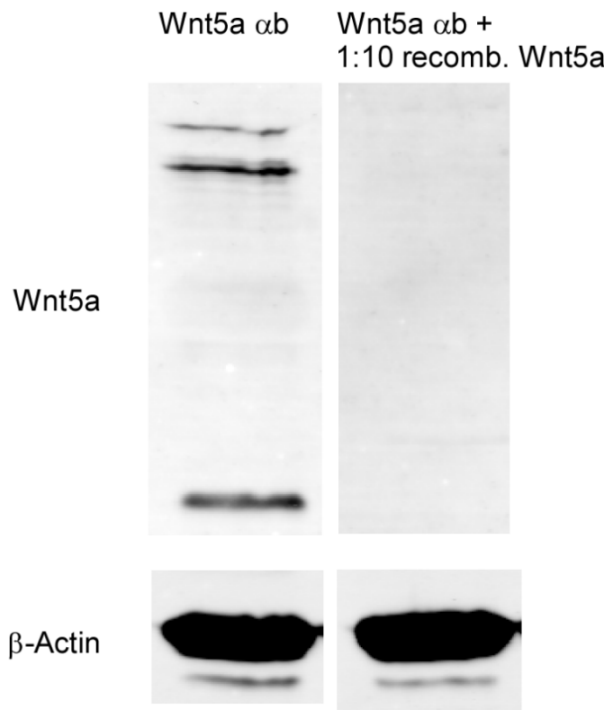

Supplemental Figure 4.S1. Bands from Wnt5a immunoblots of WNT5A-infected intestinal tissue are competed away by pre-incubation with recombinant Wnt5a.

Overexpression of WNT5A does not elicit an overt alteration in epithelial migration or Jnk-mediated defect in cellular polarity.

The Wnt5a ligand has previously been shown to have an important role in cell migration in mammalian development (Roarty and Serra, ; He et al.), and can induce migration in cell culture (Nishita et al., ; Cheng et al.). To determine if ectopic expression of WNT5A elicits changes in the rate of epithelial migration up the intestinal villus, we utilized a BrdU-labeled “pulse-chase” assay to track cell migration over time. Mice injected with either DsRed or WNT5A lentiviral particles were injected with BrdU 48h prior to sacrifice. BrdU incorporates into the DNA of actively cycling cells, labeling these cells and their immediate progeny. Epithelial cells rapidly migrate up the villus in a linear band, allowing for analysis of this migratory population. BrdU-labeled cells were visualized with antibodies to BrdU to mark the leading edge and lagging edge of labeled cells (Figure 4.2A) and the distance migrated was quantified. Comparison of the distance between the leading and lagging edge provides information regarding proliferative rates. Surprisingly, we did not detect any differences among migratory epithelial cells in DsRed- and WNT5A-injected mice (Figure 4.2B). This may be due to the fact that migrational cues in differentiated tissues like the intestine and those of developing tissues differ. Further, if Wnt5a acts in a gradient as a chemoattractant, simple overexpression evenly within the villus core may not be sufficient to elicit a phenotype.

Wnt5a has also been described to be a mediator of the Planar Cell Polarity (PCP) pathway. In this capacity, it is thought to mediate cytoskeletal

changes through phosphorylation of Jun kinase (Jnk) (Yamanaka et al., 2002). Although we were unable to detect gross phenotypic changes in the actin cytoskeleton morphologically or by immunohistochemical analysis of actin (data not shown), it is possible that the levels of ectopic WNT5A was not sufficient to dramatically alter cell polarity on a grossly detectible level. Therefore we examined the phosphorylation state of Jnk in WNT5A and DsRed infected intestinal protein extracts by immunoblot using antibodies for pan-Jnk as well as antibodies specific to phosphorylated Jnk. Again, because we suspected specific alterations would be manifested in the epithelial fraction, we isolated crypt and villus epithelium separately from intestinal mesenchymal cells for the analysis. We found no significant changes in the relative levels of phosphorylated Jnk (p54) in comparison to overall expression of Jnk in DsRed- and WNT5A-infected intestinal cell fractions (Fig. 4.2C). Gross expression levels of Jnk were also unchanged (data not shown). Further, immunostaining with phospho-specific antibodies to Jnk showed no changes in sub-cellular localization or altered levels of phosphorylated Jnk in epithelial cells in close proximity to WNT5A-expressing mesenchymal cells (Fig. 4.2D). Similar immunofluorescent studies using antibodies to Rac and β-Actin also showed no changes (data not shown). Subsequently, we did not further pursue effects on cell migration or the PCP pathway using this system. Interaction with the PCP pathway cannot be ruled out, but may result in a very subtle phenotype, or perhaps it is not affected by WNT5A overexpression. This may be clarified with an inducible, tissue-specific Wnt5a knockout mouse.

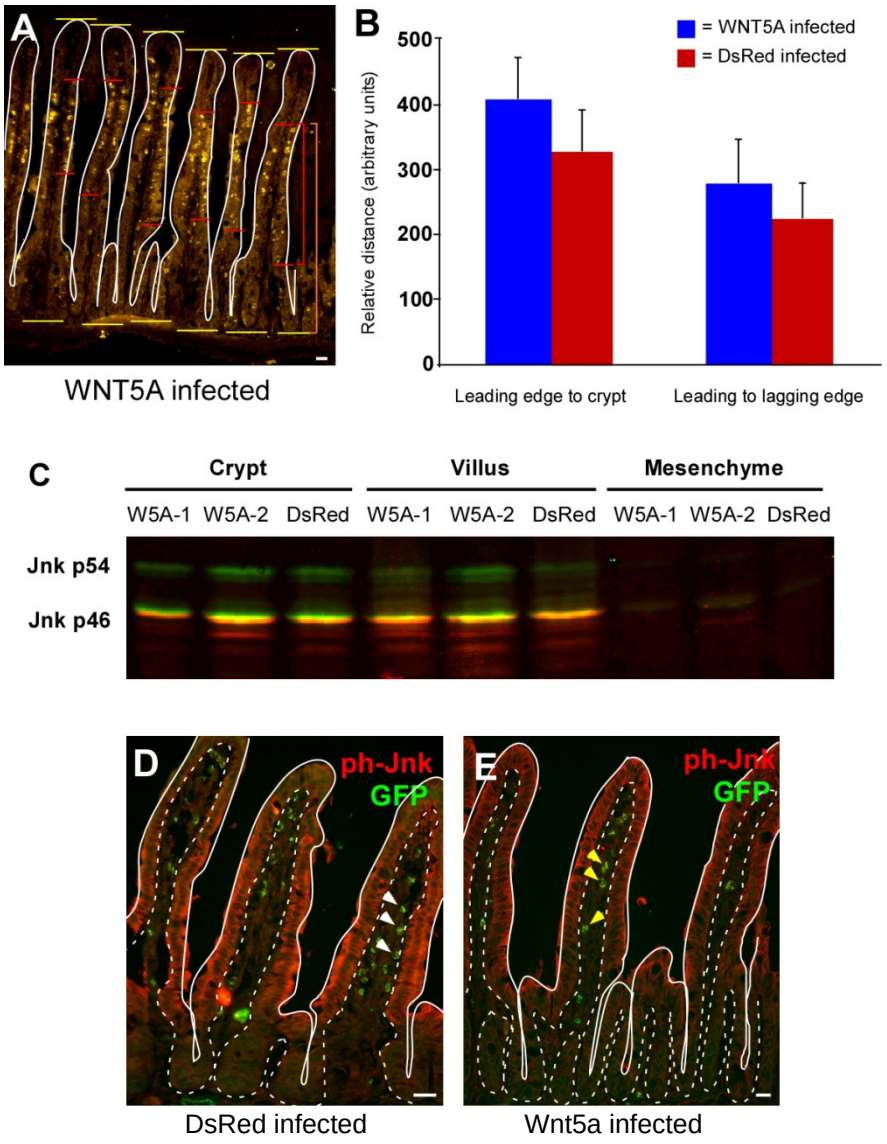

Figure 4.2. WNT5A injected mice do not display a detectable difference in cell migration or Jnk phosphorylation status. (**A**) Tissue section from WNT5A-injected mouse labeled with BrdU (orange). Yellow lines = base of the crypt and tip of the villus. White lines = leading and lagging edge of BrdU labeled zone. (**B**) Quantification of distances from leading edge of BrdU zone to base of the crypt and leading edge of BrdU zone to lagging edge of BrdU zone in DsRed and WNT5A infected mice (n=6 mice). Data displayed as mean±std. (**C**) Two-color immunoblot probed with antibodies to phosphorylated-Jnk (green) and pan-Jnk (red) with protein from crypt, villus, and mesenchyme of the proximal small intestine from two WNT5A-infected mice (W5A-1 and W5A-2) and one DsRed-infected mouse. (**D-E**) Tissue sections from WNT5A-injected mouse and DsRed control mouse stained with antibodies to GFP (green) and phospho-Jnk (red). Bar = 25 μm.

Ectopic expression of WNT5A suppresses the canonical Wnt pathway in the mouse intestine.

It is possible that WNT5A expression in the adult intestine does not maintain its developmental function of participating in conversion extension, cellular polarity and cell migration. However, its existence within the intestinal mesenchyme suggests that it may retain a physiologic relevance in directing epithelial homeostasis. One potential role for Wnt5a is as a regulator of the canonical Wnt signaling pathway. The relationship between Wnt5a and the β-catenin-dependent canonical Wnt pathway remains controversial, as Wnt5a has been described both as an inhibitor and a suppressor in cell culture systems (Mikels and Nusse, 2006). Therefore, to clarify an in vivo relationship between the two pathways, we examined its influence on canonical Wnt activation. To do this we utilized canonical Wnt reporter mice (TOPGAL) (DasGupta and Fuchs, 1999) that activate the *LacZ* reporter gene and produce β-galactosidase when canonical Wnt signaling is endogenously stimulated. This mouse model has been successfully used to assay the cell types within the intestine in which Wnt signaling is active (Davies et al., 2008). TOPGAL mice were infected with WNT5A and DsRed control lentiviral particles, and the intestine analyzed for activation of the β-gal reporter gene. We confined our analysis to the cryptal epithelium, where the majority of canonical Wnt activation is restricted (Davies et al., 2008). Interestingly, ectopic expression of WNT5A suppressed the canonical pathway, as determined by a 7-fold decrease in Wnt-reporter expression by qRT-PCR in the WNT5A infected proximal small intestine relative to DsRed-infected

intestines (Figure 4.3A). Uninfected mock-injected control mice expressed approximately the same amount of LacZ as the DsRed-infected animals (data not shown).

Morphologically, WNT5A-infected intestines did not appear to have defects in proliferation, as one might expect with modulating the canonical Wnt signaling pathway. This is not particularly surprising, since the intestine has the great capacity to overcome challenges and compensate in order to maintain epithelial homeostasis. Therefore, to further explore how WNT5A suppression of the canonical pathway may occur, we investigated the positioning and differentiation of the intestinal Paneth cell. The canonical Wnt signaling pathway has a well-described role in maintaining Paneth cell position by modulation expression of the downstream Wnt target genes, the Eph receptors (Batlle et al., 2002; Clevers and Batlle, 2006). To examine the Paneth cell population we identified these cells by Phloxine-Tartrazine histochemical staining (Lendrum, 1947) (Figure 4.3B&C) and immunofluorescent staining of the Paneth cell-specific marker lysozyme (Figure 4.3D&E). Although Paneth cells are normally confined to the base of the intestinal crypts, WNT5A infected intestines exhibited aberrant Paneth cells located near the crypt-villus junction (Figure 4.3B&D). When quantified by counting the number of aberrant crypts out of 1500 total crypts WNT5A-infected intestines (n=3), we found that 6.4% of total crypts exhibited aberrant Paneth cells (Fig. 4.3H) as compared to 0.9% in DsRed-infected intestines. To further confirm that these mislocalized Paneth cells were the result of aberrant canonical Wnt signaling, we examined expression levels of

the Eph2 and Eph3 receptors, direct Wnt target genes (Batlle et al., 2002; Clevers and Batlle, 2006), and found that they were suppressed approximately two fold (data not shown) in WNT5A-expressing isolated crypt epithelium relative to DsRed infected cells. Our WNT5A-mediated phenotype of mislocalized Paneth cells is consistent with that in mice in which the EphB2 and EphB3 receptors have been knocked out (Batlle et al., 2002).

To determine if aberrantly located Paneth cells were in crypts with epithelial cells that were actively receiving a Wnt signal, we correlated Paneth cell position with Wnt-reporter expression in WNT5A-expressing and DsRed-expressing intestines. Our lab has previously shown that crypts visualized in 5μm sections of TOPGAL adult mouse intestines contain β-galactosidase expressing cells in 15% of total crypts (Fig. 4.3G). When we co-stained control and WNT5A-infected intestines for β-galactosidase and lysozyme, we found that, out of 150 crypts exhibiting an aberrant Paneth cell, none also contained a Wnt-activated, β-galactosidase-expressing epithelial cell (Figure 4.3F), suggesting that the aberrant Paneth cell localization was a result of suppression of the canonical Wnt pathway by WNT5A. Though we cannot ascertain under these conditions whether or not the aberrant Paneth cells migrated to the crypt-villus junction or differentiated there, it is known that the Eph receptors are important guidance molecules (Batlle et al., 2002), suggesting that migrational cues may play at least a partial role.

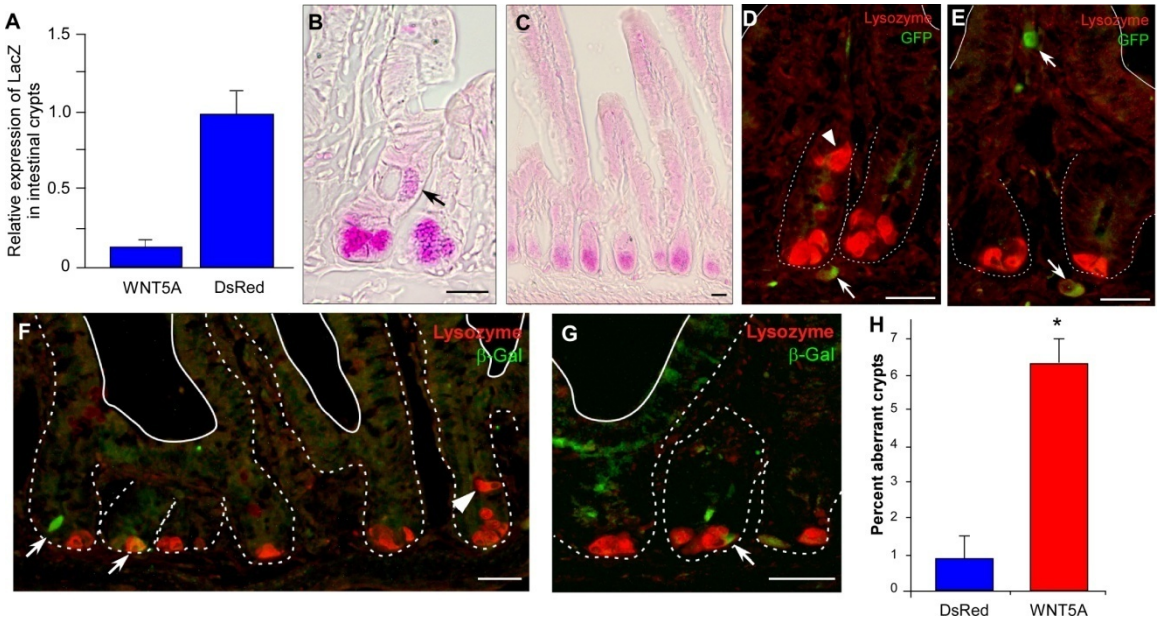

Figure 4.3. Ectopic WNT5A expression suppresses canonical Wnt activation. (**A**) qRT-PCR analysis of expression of the *LacZ* Wnt reporter in the crypts of WNT5A infected and control DsRed infected mice. *LacZ* expression is normalized to Gapdh expression and presented relative to levels in the DsRed infected crypt. Graph displays triplicate samples from representative animals. Data displayed as mean±std. (**B&C**) Tissue sections from WNT5A-infected (**B**) and DsRed-infected (**C**) proximal small intestines stained with Phloxine-tartrazine for Paneth cell granules (pink). Black arrow = mislocalized Paneth cell. (**D-E**) Tissue sections from WNT5A infected (**D**) and DsRed infected (**E**) proximal small intestines stained with antibodies to GFP (green) and Lysozyme (red). (**D**) White arrow = WNT5A infected mesenchymal cell. White arrowhead = mislocalized Paneth cell. (**E**) White arrows = DsRed infected mesenchymal cells. (**F&G**) Tissue sections from WNT5A infected (**F**) and DsRed infected (**G**) proximal small intestines stained with antibodies to β-galactosidase (β-gal) (green) and Lysozyme (red). White arrows = β-gal-positive Wnt-activated cells. White arrowhead = mislocalized Paneth cells. (H) Quantification of crypts containing mislocalized Paneth cells in DsRed and WNT5A-infected intestines. n=6 each group, data displayed as mean±std. P=0.043. Bar = 25μm.

Endogenous Wnt5a expression in disease and damage models.

Our findings suggest that Wnt5a expression within the intestine may act to dampen the canonical Wnt signaling pathway. Therefore to determine if Wnt5a may be coordinately regulated with alterations in the canonical pathway, we evaluated expression of both pathways in environments where the canonical pathway is known to be perturbed. The canonical Wnt signaling pathway is dysregulated in >90% of all human colorectal cancers (Reya and Clevers, 2005), and Wnt5a has been shown by *in situ* hybridization to be elevated in intestinal polyps (Gregorieff et al., 2005). Therefore, to confirm this relationship, we evaluated the endogenous expression levels of Wnt5a in the mouse model for colon cancer, the $Apc^{MIN/+}$ mouse (Su et al., 1992) (Figure 4.4A). qRT-PCR analysis on the mesenchyme from intestines from $Apc^{MIN/+}$ mice revealed elevated Wnt5a mRNA expression 10-fold over that of wild type C57B/6 (Figure 4.4B). Consistent with this finding, Wnt5a was also induced >800 fold in mice with induced ablation of Apc (Figure 4.4E), using the transgenic mouse model $Apc^{fl/fl}$/AhCre (Sansom et al., 2004; Sansom et al., 2005). Induced ablation of Apc resulted in a widespread increase of proliferation in the intestinal crypts (Figure 4.4D). Because the stimulation of the canonical Wnt pathway in both of these mouse models is genetically downstream of the receptor/ligand level, it stands to reason that Wnt5a expression is activated by over-stimulation of the canonical Wnt pathway, perhaps as a cellular compensatory mechanism to down-regulate elevated canonical Wnt signaling.

To determine if a coordinated relationship between Wnt5a and canonical Wnt activation exists in response to intestinal damage, we evaluated two different intestinal damage models. First, we used γ-irradiation-induced epithelial damage based upon our previous studies that demonstrated the canonical Wnt signaling pathway was upregulated in response to injury (Davies et al., 2008). We analyzed the temporal response to γ-irradiation-mediated injury of *LacZ* and Wnt5a mRNA levels after 1, 2, 6, 12, 24, 48, 72, and 168 hours (Figure 4.4F). Canonical Wnt activation peaked 24 hours post-irradiation, then declined to near-baseline levels by 48 hours. Interestingly, Wnt5a expression levels decreased immediately after irradiation, but began to increase above baseline as canonical Wnt levels peaked. This relationship was evaluated in a second model of intestinal injury, intestinal ischemia. A similar pattern was observed in the ischemic intestine analyzed 1, 2, 6, 12, 18, 24, 36, 48, and 72 hours post-injury, with activation of the canonical Wnt signaling pathway peaking at 12 hours (Figure 4.4G). It is possible that Wnt5a and the canonical Wnt signaling pathway are regulated in a signaling feedback loop, in which Wnt5a is initially suppressed by intestinal damage to allow activation of the canonical Wnt pathway. High levels of canonical Wnt activation then stimulates Wnt5a expression, causing Wnt5a to then inhibit canonical Wnt signaling, allowing levels to return to a pre-damage state. In support of this notion, it has been reported that other Wnt effectors including Fz, Lrp, and Dkk are known to be canonical Wnt targets (Nusse, 2008), allowing for rapid and discrete regulation of the pathway.

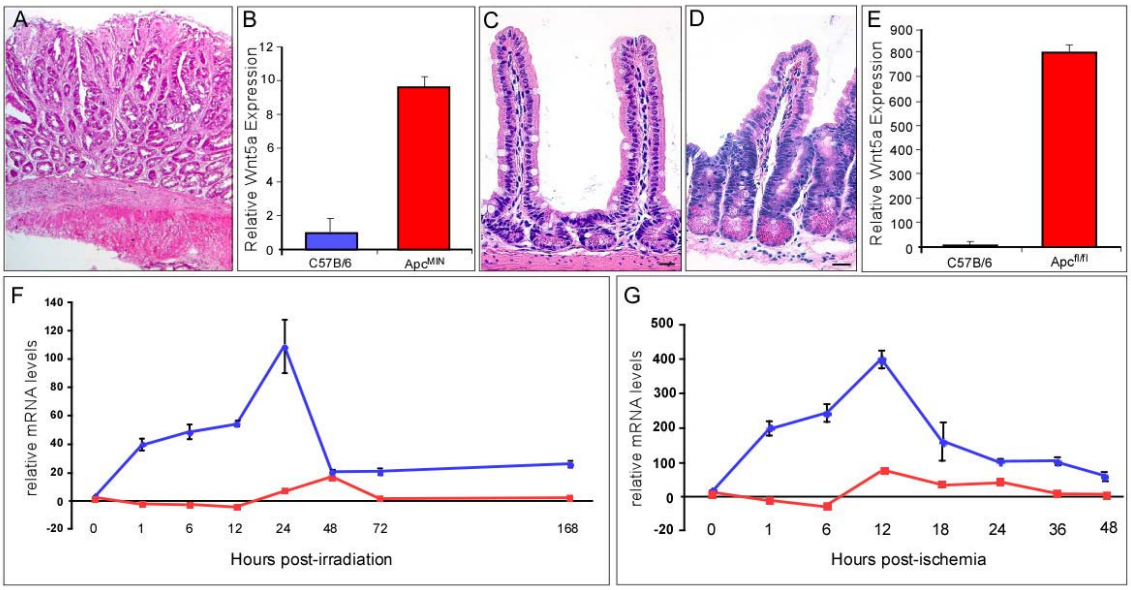

Figure 4.4. Endogenous expression of Wnt5a and canonical Wnt activation in disease and damage models. (**A**) Tissue section of an intestinal polyp from an $Apc^{MIN+/-}$ mouse stained with hematoxylin and eosin (**H&E**). (**B**) qRT-PCR analysis of Wnt5a expression in the intestinal mesenchyme from wild type C57 B/6 mice and $Apc^{MIN+/-}$ mice. Wnt5a expression is normalized to Gapdh expression and presented relative to levels in the wild-type animal. Graph displays triplicate samples from representative animals. Data displayed as mean±std. (**C**) H&E stained tissue section of wt medial small intestine. (**D**) H&E stained tissue section of medial small intestine from an induced $Apc^{fl/fl}$ mouse. Black bars = 25µm. (**E**) qRT-PCR analysis of Wnt5a expression in intestinal mesenchyme from wild type C57 B/6 mice and induced $Apc^{fl/fl}$ mice. Wnt5a expression is normalized to Gapdh expression and presented relative to levels in the wt animal. Graph displays triplicate samples from representative animals. Data displayed as mean±std. (**F**) Timecourse of qRT-PCR analysis of Wnt5a (red) and *LacZ* (blue) expression in whole intestines from TOPGAL mice subjected to 12gy irradiation at t=0. Wnt5a expression is normalized to Gapdh expression and presented relative to levels in an untreated animal. Graph displays triplicate samples from two animals. Data displayed as mean±std. (**G**) Timecourse of qRT-PCR analysis of Wnt5a (red) and *LacZ* (blue) expression in whole intestines from TOPGAL mice subjected to 20 minutes of intestinal ischemia t=0. Wnt5a expression is normalized to Gapdh expression and presented relative to levels in an untreated animal. Graph displays triplicate samples from two animals. Data displayed as mean±std.

These studies show, for the first time *in vivo*, that Wnt5a inhibits the canonical pathway in adult intestinal epithelial cells and suggest a role for endogenous Wnt5a there in adulthood. While it remains to be seen if Wnt5a is an important PCP effector in adulthood, it is important to note that in vivo studies such as these are essential to clarify possible outcomes from cell culture models. Furthermore, these studies offer insight in to how canonical Wnt signaling is regulated in the intestine during homeostasis, as well as in neoplastic and damaged states.

CHAPTER 5

CONCLUSIONS AND FUTURE DIRECTIONS

Conclusions

The small intestinal epithelium is subject to tight regulation by the Wnt signaling pathway during embryonic organ development and during adult homeostasis in epithelial maintenance along the crypt-villus axis. While the impact of the canonical Wnt ligands has been widely studied, a number of β-catenin-independent Wnt ligands are expressed in the adult intestine. The functional relevance of these β-catenin-independent Wnt ligands and how they interplay with the canonical Wnt signaling pathway is largely unknown. A better understanding of how the various Wnt ligands interact to regulate intestinal epithelial homeostasis will provide greater insight into the tight regulation of epithelial proliferation and has the potential to contribute to the development of treatments and therapies for intestinal disease. In this dissertation, I have addressed the dynamic relationship between Wnt5a and the canonical Wnt signaling pathway in response to intestinal damage and disease using mouse models and a novel ligand delivery system. In my studies, I have reached the following conclusions:

1. Canonical Wnt-activated epithelial cells are restricted to the base of the intestinal crypt or stem cell niche. Canonical Wnt activation is stimulated in response to γ-irradiation-mediated injury.

We identified rare Wnt-activated cells that are restricted to the base of the small intestinal crypts, using TOPGAL Wnt-reporter mice. This was the first report to identify cells within the adult intestinal epithelium that were actively receiving a canonical Wnt signal. Interestingly, Wnt-activated cells were highest in numbers in the proximal small intestine, perhaps reflecting the difference in epithelial turnover down the length of the small intestine. Intriguingly, the majority of the reporter-positive cells did not express markers of the rapidly proliferating transient-amplifying cell population. While Wnt-activated cells stained positively for the putative stem cell marker Musashi-1, they did not co-express markers of cell differentiation, suggesting that Wnt-activated cells in the base of the crypt were likely stem cells. Finally, γ-irradiation stimulated an increase in Wnt-activated intestinal crypt cells, peaking at 24 hours post-irradiation.

This study identifies a discrete epithelial cell population within the stem cell niche that actively receives a Wnt signal. The significance of this finding is that it contradicts previous studies that suggested that all intestinal epithelial proliferation is regulated in a Wnt-dependent fashion. Our data supports the concept that activation of Wnt signaling may only occur in a stem cell population and is not activated in proliferating transient-amplifying cells. The rare number of Wnt-activated crypt-based cells is consistent with the idea that Wnt signals are required for entry of a stem cell into the cell cycle. Furthermore, γ-irradiation-

mediated epithelial injury elicits an increase in the number of Wnt-activated crypt-based cells. This finding is important because it suggests that certain types of epithelial injury rely on a Wnt-mediated increase in stem cell numbers for tissue regeneration. Understanding the signals that regulate epithelial repair processes has an important impact on further defining the mechanism that drives intestinal regeneration after injury or disease. Because the Wnt signal was not present in the greater transient-amplifying population, this suggests that there are different pathways that mediate rapid proliferation and expansion as opposed to the more slowly cycling stem cells. These studies offer insight into the regulation of the intestinal stem cell hierarchy during homeostasis and in disease states.

Furthermore, a more recent paper from Hans Clever's lab both supports our findings and adds additional fodder for speculation on the role of Wnt in intestinal stem cells. In their studies, ablation of the APC gene in intestinal stem cells resulted in long-lived microadenomas and cell transformation, while ablation of the APC gene in the transit-amplifying population only produced short-lived, smaller adenomas (Barker, 2009). This suggests that intestinal stem cells are particularly receptive of a Wnt signal, and that increased Wnt signaling alone is not capable of conferring longevity on TA-cells.

2. Lentiviral-mediated transgene expression can potentiate intestinal mesenchymal-epithelial signaling. Ectopic WNT1 expression in the mesenchyme by lentiviral delivery methods induces a proliferative phenotype in the adult mouse intestinal epithelium.

My findings show, for the first time, that lentiviral vectors can be used for modulation of signaling pathways that require a paracrine-expressed ligand. Lentivirus introduced by a single intra-peritoneal injection at postnatal day (P)1 resulted in effective and functional mesenchymal transgene expression in the intestine and in other gastrointestinal and blood-derived organs, sustained at least 6 weeks post-injection. Further, infection of the intestinal mesenchyme with human WNT1 resulted in expansion of the proliferative epithelial compartment and initiated intestinal polyp formation.

My studies illustrate that lentiviral vectors are a powerful vehicle for the delivery of mesenchymally expressed ligands to facilitate the study of signaling pathways in the intestine. While this system is a valuable tool for the study of Wnt ligand effects in the mouse small intestine, it can be broadly applied to other signaling pathways that rely upon paracrine influences. Further, constitutive expression of the canonical Wnt ligand WNT1 induced a proliferative epithelial phenotype in the intestine. This is significant, in light of our previous studies showing rare Wnt-activated putative stem cell populations are restricted to the crypt base, suggesting that effective ligand expression may be confined to this region. Thus, our ectopic expression studies support the notion that expansion of Wnt ligand expression is capable of driving over-proliferation in the intestinal epithelium and that it is possible that a larger zone of epithelial cells (including transient-amplifying cells) are competent to respond to a Wnt signal.

3. The Wnt5a ligand functions to suppress the canonical Wnt signaling pathway in the mouse small intestine.

Wnt5a is an essential ligand that plays an important role in intestinal development, but is also retained in the adult. Interestingly, over-expression of human WNT5A in the mouse intestinal mesenchyme using lentiviral-mediated delivery did not result in overt effects on cellular migration or polarity, even though it has previously been described to result in Planar Cell Polarity (PCP) pathway phenotypes when modulated. Importantly, over-expression of WNT5A resulted in suppression of the canonical Wnt pathway. We established a dynamic relationship between the expression of Wnt5a and the canonical pathway in disease and injury models, suggesting that they interact in a compensatory mechanism to try to reign in out-of-control Wnt signaling (Figure 5.1).

These findings are important because, while the role of Wnt5a has been established in embryonic development and organogenesis, its role in the adult intestine has not yet been identified amidst the controversy of its function and interactions with the canonical pathway. My research suggests that Wnt5a may play an important role in the regulation of Wnt signaling during intestinal homeostasis and damage response. As my previous research has shown, Wnt signaling is under very tight control in the small intestine and is important for epithelial regeneration. Only by understanding the mechanisms by which Wnt is regulated will we gain the necessary insight to develop potential therapeutic agents for intestinal disease.

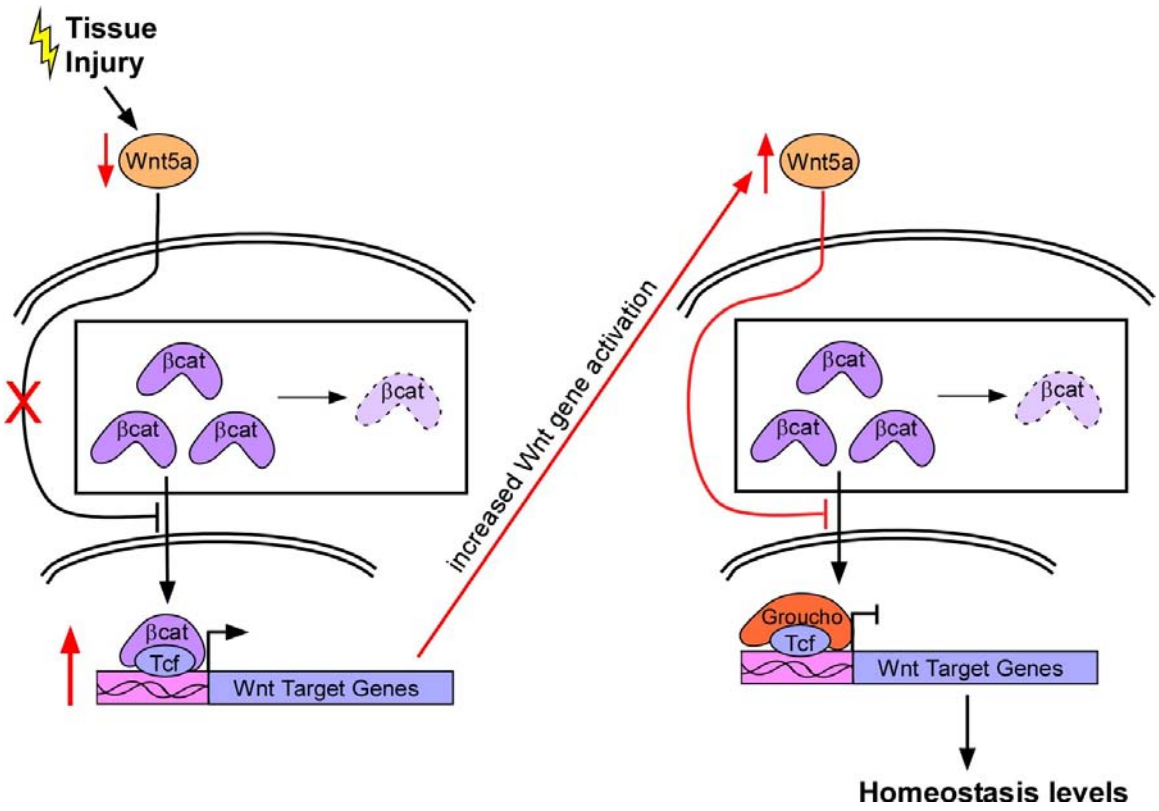

Figure 5.1. A model for a Wnt5a and canonical Wnt regulatory feedback relationship in response to epithelial injury. Tissue injury by irradiation or ischemia results in depressed levels of Wnt5a relieving its inhibitory effect on the canonical Wnt signaling pathway by an unknown mechanism. This results in activation of canonical Wnt signaling (represented by an increase in nuclear β-catenin) and an increase in expression of Wnt target genes. The stimulation of the canonical Wnt signaling pathway has previously been shown to stimulate Wnt5a expression levels (Ch. 4), reinstating its inhibitory effect of the canonical Wnt signaling pathway. In this manner, canonical Wnt activation decreases. This model suggests that Wnt5a and the canonical Wnt signaling pathway are regulated by a feedback mechanism.

Future Directions

Although the canonical Wnt signaling pathway has been well studied in the intestine, many questions remain. The intestinal stem cell is established during embryonic development and it is thought that Wnt signaling plays a major role in this process. However, the exact temporal regulation of Wnt and whether or not it directs selection and maintenance of the intestinal stem cell during morphogenesis of the stem cell niche has not been established. This question can be approached using the mouse lines and lentiviral techniques I established during my thesis research.

Further, although my studies using lentivirus-derived overexpression of Wnt5a did not result in a PCP pathway-related phenotype, both grossly nor on the cellular level, it is still possible that a specific role for this ligand exists related to PCP signaling, migration, and cytoskeletal changes that could not be elucidated by simple overexpression. Tissue-specific and temporally controlled Wnt5a ablation models must be developed to further investigate this question.

Although my temporal studies illustrate the relationship of Wnt5a expression and canonical Wnt activation in damage and disease in a correlative manner, more studies must be done to concretely establish a causal relationship. It would be most expedient to first carry out these studies in a tissue culture model, in which a TOPFLASH assay could be used in conjunction with co-transfection of Wnt5a under irradiation or hypoxic conditions to determine if abrogation of canonical Wnt signaling occurs. Further studies could be carried out in the intestine with lentiviral vectors, but increased levels of infection of

Wnt5a or stronger promoters within the lentiviral construct may be necessary to potentiate an effect on the large levels of canonical Wnt induction in these damage models.

In conclusion, my studies have contributed towards the understanding of how Wnt signaling is regulated in maintaining epithelial homeostasis. I have contributed towards the characterization of the canonical Wnt signaling pattern in adult mouse intestines using a Wnt-reporter mouse, pioneered a method by which Wnt ligands can be functionally over-expressed in the mouse intestinal mesenchyme, and utilized this method to clarify how Wnt signaling is regulated in the intestine by its ligands to elucidate the role of such a controversial ligand in the mouse intestine. These studies give novel insight into the importance of Wnt signaling in the intestine, its essential role in stem cell regulation, and a mechanism of canonical Wnt regulation in response to damage and disease.

APPENDIX 1

A broadly applicable quantitative PCR-based assay for identifying transgene copy number

Adria D. Decker[1], and Melissa H. Wong[2]

[1]Department of Molecular and Medical Genetics
[2]Department of Dermatology and Cell and Developmental Biology,
Oregon Health and Science University, Portland OR.

ABSTRACT

The ability to determine transgene copy number is essential for studies in transgenic animals. Here we describe an application of quantitative PCR technology in transgenic mice using a plasmid-based standard curve to identify transgene copy number. Quantitative PCR methods have emerged as a viable and efficient approach for determining transgene copy number over traditional methods. Our technique allows for rapid, efficient, quantitative and inexpensive screening of a large number of transformed ES cell clones prior to generation of transgenic animals. The use of this transgene-specific, plasmid-based standard curve approach can be applied to a variety of systems where determination of transgene copy number is required and is therefore broadly applicable.

INTRODUCTION

The ability to temporally induce or suppress transgene expression in mouse model systems represents a valuable approach for the study of development and disease. The ability to achieve successful Cre recombinase-mediated temporal control of transgene expression depends heavily upon the ability to identify founder mouse lines carrying a single-copy transgene insert. Due to the nature of transgene integration into the genome, multiple transgene copies in head to tail or head to head orientations can insert as concatemers Thus, for effective Cre recombinase-mediated excision of the desired sequences, a single transgene insertion is required. Further, studies in traditional transgenic animals are aided by the knowledge of transgene copy number because large concatemer transgene insertions have been linked to low and sometimes unstable transgene expression (Flavell, 1994; Vaucheret et al., 1998).

Transgenic mouse generation by electroporation, pronuclear microinjection, or lentiviral-mediated gene delivery can result in multiple transgene copy insertions (Nagy, 2003; Kosaka et al., 2004). Currently, the standard approach to determine transgene copy number is Southern blot analysis. This method is labor intensive and requires substantial quantities of DNA. Furthermore, low hybridization efficiency can yield ambiguous results. It is not uncommon for single transgene copy clones to be overlooked due to low signal using Southern blot.

Previous reports have described quantitative polymerase chain reaction (qPCR) as an alternative to Southern blot analysis for determining transgene

copy number (Ingham et al., 2001; Ballester et al., 2004; Bubner and Baldwin, 2004). This technique has been used to determine transgene copy number in transformed plants by comparing amplification of the gene of interest to that of a previously determined single-copy gene control sample (Ingham et al., 2001; Bubner and Baldwin, 2004). This approach does not eliminate the need for Southern blot analysis, as a single-copy control must first be identified before qPCR analysis can be performed. More recently, Ballester and colleagues adapted this approach to transgenic mice (Ballester et al., 2004). In their study, goat genomic DNA (gDNA) was used as a source of a known single-copy gene control to identify a single-copy goat transgene in their generated transgenic mouse (Ballester et al., 2004). Although these PCR-based approaches simplify the ability to screen for transgene copy number in organisms, they rely upon the comparison of the target gene with a known endogenous or previously identified single-copy gene, and therefore, are not applicable in all situations. Availability of a single-copy gene control becomes a limiting factor in the ease of using these previously published assays.

To generate a more widely applicable qPCR-based approach to determine transgene copy number, we designed an assay that utilizes a plasmid-based standard curve to bypass the limitations of previous methods. In addition, our approach includes a high-throughput semi-quantitative PCR pre-screen to be utilized in the event that large numbers of candidate clones need to be assessed for transgene copy number. This pre-screen has the advantage of rapidly eliminating clones with high transgene copy numbers. Therefore, this pre-screen

reduces the number of clones that need to be screened by qPCR, thus reducing cost of qPCR reagents. Our method uses detection of SYBR-Green incorporation into the amplified region of gDNA and relative comparison using the $2^{-\Delta\Delta C_T}$ equation to establish fold differences between samples (Livak and Schmittgen, 2001).

Our plasmid-based standard curve is generated in a wild-type mouse gDNA background and includes samples representing 1, 2, 4, 8 and 16 transgene copies. This method uses a single primer set to directly compare the transgene copy number in candidate clones with the standard curve. Additionally, an endogenous control gene such as Glyceraldehyde-phosphate dehydrogenase (Gapdh) is used to normalize samples for gDNA concentration variation. We have validated our standard curve approach using a transgenic embryonic stem (ES) cell line with a known single-copy transgene copy that was generated by targeted recombination. Our report establishes a method for efficient screening of gene copy number in transgenic animals that is broadly applicable to many other models.

MATERIALS AND METHODS

Transgenic ES cells

Mouse ES cell clones were generated by electroporating a linearized inducible Wnt/β-catenin signaling transgene plasmid (pβ-catAD2) into wild-type ES cells. Our transgene contains a Phosphoglycerine kinase-Neomycin resistance cassette (Tn5) that was used for selection of transgene-containing ES

cell clones. A total of 64 ES clones were isolated. gDNA was harvested from these clones using a standard phenol-chloroform extraction-based method (Sambrook and Russell, 2001). All clones were subjected to our pre-screen and qPCR protocol to determine transgene copy number. A subset of these clones was used to compare copy number using Southern blotting and a probe specific to Tn5. Concurrently, we generated ES cell lines harboring our inducible Wnt/β-catenin signaling gene by targeted recombination into the ROSA locus (Soriano, 1999) for a separate study. Targeted insertion ensures that a single-copy of the transgene is integrated into the genome. This clone (AD1) was used in our assay to validate our plasmid-based approach for determining transgene copy number.

Generation of plasmid-based standard curve

Plasmid DNA was isolated using the HiSpeed® Plasmid Maxi kit (Qiagen, Valencia, CA). It was then diluted to 5ng/μl and quantified by spectroscopy, then two 1:10 serial dilutions performed to acquire a 0.05ng/μl working stock of DNA. The copy number standard curve was generated by adding the appropriate mass of non-linearized pβ-catAD2 plasmid DNA calculated to represent 1, 2, 4, 8, and 16 transgene copies to gDNA from wild-type ES cells. The haploid content of the mouse genome is $3x10^9$ base pairs (bp), and transgenic mouse founders are hemizygous. Therefore, the calculated mass of a single copy of our 12,050 bp pβ-catAD2 plasmid is 4.02pg per 1μg of mouse gDNA, when expressed as a ratio of plasmid size to genome size. To generate our standard curve, we first

made a 16-copy sample by adding 321.6pg of plasmid DNA to 5μg of a 50ng/μl wild-type gDNA stock. This was determined by calculating the ratio of plasmid size in base pairs to that of the entire mouse genome (Silver, 1995). Then, serial 1:1 dilutions were performed with 50ng/μl wild-type ES cell genomic DNA to generate the 8-, 4-, 2-, and 1-copy standard curve samples.

Modified semi-quantitative PCR

To reduce the number of candidates for qPCR analysis, we performed a modified semi-quantitative PCR pre-screen. Standard PCR conditions were employed (Sambrook and Russell, 2001) to assay 100ng of each sample. PCR primers were designed with Primer Express™ (Applied Biosystems, Foster City, CA) software to amplify an 85 bp amplicon from the endogenous mouse Gapdh gene (F-5'-AAATATGACAACTCACTCAAGATTGTCA-3', R-5'-CCCTTCCACAATGCCAAAGT-3') and a 174 bp amplicon from Tn5 present in the plasmid and transgenic mice (F-5'-GCTCCCGATTCGCAGC-3', R-5'-AGGTACTCTGTTCTCACCCTTCTTAA-3'). Each primer set was used in individual reaction tubes with a 55°C annealing temperature for 25 cycles. These conditions allowed for analysis of amplification levels within the linear range of the reaction. Amplicons were subjected to gel electrophoresis and analyzed for ethidium bromide incorporation. The band intensities of our candidate clones were subjectively evaluated relative to those of the standard curve (Fig. A1.1). Gapdh amplicons were evaluated as a loading control. As our objective was to identify ES cell clones harboring a single-copy transgene, only clones that

exhibited band intensity lower than the 8-copy standard were carried further as candidate clones.

SYBR-Green quantitative PCR analysis

qPCR analysis was performed using SYBR®-Green technology. All reactions were performed in triplicate in a reaction volume of 15μl, using 100ng of template DNA, 7.5μl of a 2X SYBR®-Green Master Mix, 0.15U UDP-N-glycosidase (Invitrogen) and 900nM forward and reverse primers. All primers (sequences listed above) were screened for optimal melting temperatures, linear amplification, and gene specificity prior to use as previously described (Stappenbeck et al., 2002). Further, due to the nature of SYBR®-Green, all assays contained a single primer set (monoplex). qPCR analysis was performed on an ABI 7900HT Fast Real-Time PCR System and subsequent data analysis with the ABI Prism™ SDS 2.1 software. Cycle threshold (C_T) data was collected below the amplicon melting temperature at 76°C for both primer sets. A C_T value within the linear range of amplification was established for each data set. Independent threshold values were established for each primer set, as the 7900HT allows for use of separate fluorescent detectors for each gene set within a single assay.

RESULTS AND DISCUSSION

qPCR has been embraced as an accurate method for mRNA level analysis. Its use as a viable method for determining genomic copy number is

growing in popularity. As early as 1998, Ringel and colleagues used competitive PCR and denaturing gel electrophoresis to determine low copy number transgenic mice (Ringel et al., 1998). Recently, Bruce et al. report a method similar to that of Ballester et al. to determine specific viral load in macaques and baboons using a known single-copy gene as a calibrator (Bruce et al., 2005). However, these reports highlight that use of qPCR as a broadly applicable approach to determine transgene copy number is hindered by the absence of an easily obtainable single-copy control. Our assay utilizes a plasmid-based standard curve method to provide a single-copy calibrator. Furthermore, in experimental settings where a large number of individual clones will be screened, a semi-quantitative PCR pre-screen can be employed to reduce the cost of qPCR reagents.

Plasmid standard curve validation

We generated a standard curve to represent five different transgene copy numbers. Because our objective was to identify single-copy transgene clones, not to define absolute transgene copy number, we limited our standard curve to a 16 copy range. As transgenic inserts often concatemerize leading to insertions of greater than 16 copies, the standard curve can be expanded to the desired range.

Our standard curve was generated by adding non-linearized transgene-containing plasmid DNA into wild-type mouse gDNA at concentrations simulating hemizygous copy numbers. This calculation has been previously described

(http://www.med.umich.edu/tamc/spike.html, ; Camper, 1987). Calculation of wild-type ES cell gDNA concentration used for the curve is critical, as the validity of the copy number simulation is dependent upon the proper ratio of plasmid copies to genomic background. If the concentration of either is too low or too high, this will alter the calculated relative copy number once normalized to the calibrator gene.

Previous reports state that SYBR-Green® in qRT-PCR or qPCR allows reliable detection of at least two-fold differences in amplification within the limits of triplicate assays and as low as 20% differences with six replicates (Martinez and Walker, 2004). Thus, we created a plasmid-based standard curve representing incremental two-fold increases in gene copy number; 1, 2, 4, 8, and 16 copies. qPCR quantification of our standard curve revealed the expected linear incremental increase in amplification (Fig. A1.2). Furthermore, when we compared transgene amplification of our known single-copy number ES cell clone to our standard curve, the C_T values were comparable to the 1X standard.

The $\Delta\Delta C_T$ method was used as previously described (Livak and Schmittgen, 2001) to establish relative copy number values. Briefly, for each sample the ΔC_T represents the difference between the C_T of the gene of interest (in our case, Tn5) minus the C_T of the normalizer gene, Gapdh (usually an endogenous, statically expressed gene). The $\Delta\Delta C_T$ represents the ΔC_T of each sample minus the ΔC_T of a calibrator sample (the sample to which all data are relative). In this case, we used the 1X standard curve sample as our calibrator. The fold change is calculated using the $2^{-\Delta\Delta C_T}$ method as previously described

(Stappenbeck et al., 2002). As our calibrator sample represents a single-copy, the fold change can be expressed as copy number.

We validated our standard curve approach using a known single-copy transgene clone. Amplification of this single-copy clone reproducibly resulted in amplification levels equivalent to the 1X copy standard (n=4; Fig. A1.2). Our standard curve approach does not rely upon the comparison of transgene copy number to endogenous single-copy transgene control genes and therefore represents a broadly applicable method for the identification of single and multiple transgene copies in transgenic animals and plants.

Semi-quantitative PCR Pre-Screen

To reduce the cost of our assay by minimizing the use of qPCR reagents, we implemented a high-throughput, semi-quantitative PCR pre-screening process to reduce the number of clones assayed by qPCR. Starting with 64 clones, we employed conventional PCR using primers specific to the Tn5 gene along with primers specific to the endogenous Gapdh gene as a DNA loading control. We compared transgene amplification in our candidate ES cell clones of unknown copy number to that of our plasmid-based standard curve and the known single-copy clone AD1 (Fig. A1.1). The relative band intensities of the standard curve samples were consistent and reproducible, and the differences in amplification were readily detectable by gel electrophoresis when subjectively evaluated. Of our 64 original clones, we identified two clones with band intensities closest to the 1X controls (samples 1.1 and 1.5) as well as several

clones that amplified at higher levels (2.3 and 2.9). Clone 2.3 also showed multiple bands by Southern blot analysis (Fig. A1.3), and we chose it as our multiple copy control in our qPCR assay. Of our single-copy candidate clones, most did not have robust or clear bands by Southern blot, exemplifying one of the difficulties of using this method. While only 64 ES cell clones were screened in this assay, the generation of some transgenic animal lines requires screens of even larger numbers of individual clones. The potential to eliminate 90% or more of multiple-copy number clones makes this pre-screen a relatively inexpensive and efficient way to decrease the number of clones to be screened using SYBR-Green®.

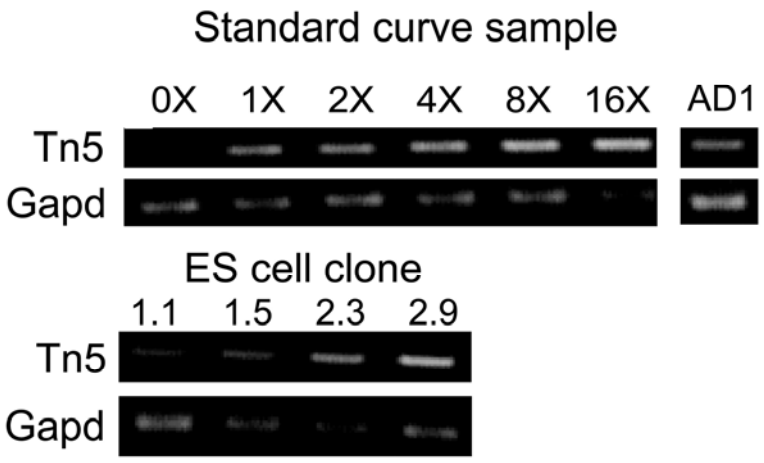

Figure A1.1 Semi-quantitative PCR pre-screen
Comparison of candidate clones and plasmid standard curve by semi-quantitative PCR. Regions of the Tn5 gene and the endogenous Gapdh gene were amplified with 25 cycles. Amplicons were resolved by gel electrophoresis and visualized for the incorporation of ethidium bromide using UV light. Samples 1X-16X represent our standard curve. The single copy ES cell control AD1 was generated by targeted insertion. Candidate ES cell clones 1.1, 1.5, 2.3, and 2.9 were among the original 64 clones assayed. Candidate clones 1.1 and 1.5 have band intensity similar to the 1X standard. Candidate clones 2.3 and 2.9 have band intensity similar to the 8X and 16X standards.

SYBR-Green® copy number assay

To determine which of our identified clones carried a single-copy of our transgene, we analyzed our 6 pre-screened ES cell clones and used the $2^{-\Delta\Delta C_T}$ method to determine relative copy number to our standard curve. All of our determined values are statistically significant at a 95% confidence level. We identified two clones (1.1 and 1.5) within 0.2 copies of the 1X control (Fig. A1.2). These two clones were identified and subsequently used to generate transgenic mice. The ES cell clones that had 8X or greater band intensity as detected by our pre-screen (2.3) were also subjected to qPCR analysis and were found to have transgene copy numbers consistent with that estimated by our pre-screen and our Southern blot results.

Figure 2

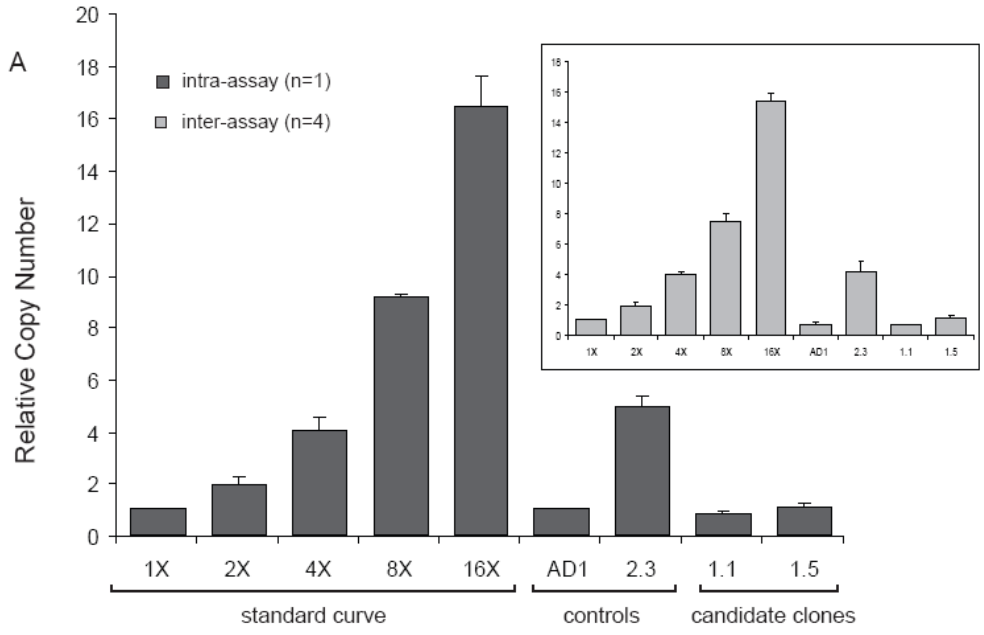

B

Relative copy number (±SEM)		
Sample	intra-assay (n=1)	inter-assay (n=4)
1X	1.0 ±0.0	1.0 ±0.0
2X	1.9 ±0.3	1.9 ±0.3
4X	4.0 ±0.5	4.0 ±0.1
8X	9.1 ±0.1	7.5 ±0.5
16X	16.4 ±1.1	15.4 ±0.5
AD1	1.0 ±0.0	0.8 ±0.2
2.3	4.9 ±0.4	4.2 ±0.7
1.1	0.8 ±0.1	0.7 ±0.1
1.5	1.1 ±0.1	1.2 ±0.1

Figure A1.2 Relative copy number as determined by qPCR

(A) Graphical representation of relative copy number as determined by SYBR Green Analysis and the $2^{-\Delta\Delta CT}$ method. Dark gray bars correspond to a single representative triplicate assay. Error bars represent the standard error of the mean of the replicates. Inset, light gray bars correspond to average mean values of 4 independent triplicate assays. Error bars represent the standard error of the mean for each run. Single copy control obtained by targeted insertion. Multiple copy control (clone 2.3) identified by Southern blot and semi-quantitative pre-screen. **(B)** Data represented by panel A in tabular form.

In conclusion, we present a reliable and universal method for the determination of copy number, based on qPCR methodology. Our approach builds upon previous qPCR methods and offers the advantage of being very widely applicable. For example, it eliminates the need for an endogenous single-copy gene control (Ingham et al., 2001; Bubner and Baldwin, 2004) by using a plasmid-based standard curve. This method is not limited to mice and can be generated for any transgenic animal. By designing primers that span promoter/transgene or insertion site/transgene junctions, this application can be used for mis-expression transgenics in which the transgene itself is present endogenously. This application is extremely useful for screening copy number in transfected or infected ES cells prior to generation of transgenic animals, allowing for rapid screening of hundreds of clones to quickly identify those with the desired copy number. Further, by screening ES cells prior to generation of the transgenic animal, the risk of the need to regenerate is reduced. Additional applications for this concept could be developed, such as ploidy determination in non-metaphase cells. We also describe a semi-quantitative pre-screening process that utilizes traditional PCR technology to reduce the cost of further screening. Temporally inducible transgenic models are indispensable for the study of development and disease. A number of these models depend upon single-copy transgene insertions. Our qPCR copy number assay is designed to reduce the time between the conception and generation of these models without increasing the cost.

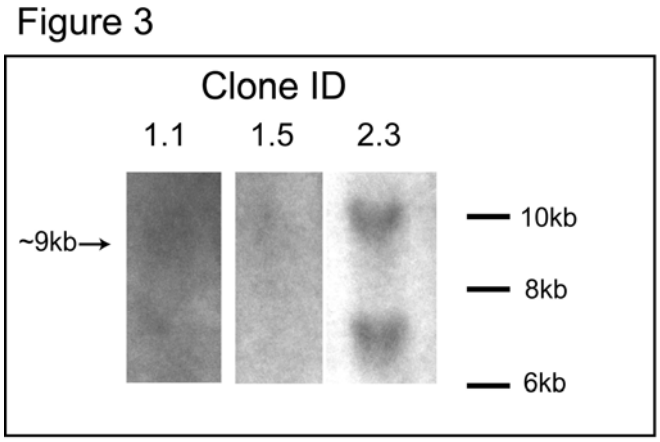

Figure A1.3 Southern blot

Determination of single copy clones by Southern blot. Ten μg of gDNA isolated from transgenic ES cells clones was digested with the restriction enzyme BclI and resolved by agarose gel electrophoresis and visualized under UV light for the incorporation of ethidium bromide. DNA was transferred to a nylon membrane and then hybridized with a ^{32}P dCTP-labeled probe to Tn5 and detected radiographically. Clones with multiple or concatemerized insertions are identified by multiple bands. Single copy clones should display a single band greater than 6500kb.

APPENDIX 2

Bone marrow-derived cells fuse with normal and transformed intestinal stem cells

Adnan Z. Rizvi[1], John R. Swain[2], Alexis Bailey[&], Paige S. Davies[2], Adria D. Decker Dismuke[2], Holger Willenbring[3,5], Markus Grompe[3,5], William H. Fleming[4,5], and Melissa H. Wong[2,5]

[1] Department of Surgery
[2]Departments of Dermatology and of Cell and Developmental Biology,
[3]Department of Molecular and Medical Genetics
[4]Center for Hematologic Malignancies, Division of Hematology and Medical Oncology, Oregon Cancer Institute
[5]Oregon Stem Cell Center, Oregon Health & Science University, Portland, OR.

***PNAS*, 103(6), 6321–6325 (2006).**

ADD contributed to the planning and execution of the experiments represented in figures 1 and 2. ADD executed the bone marrow transplants and tissue processing for Figure 1 and captured the wholemount images in Figure 1 panels a and b.

Abstract

Transplanted adult bone marrow-derived cells (BMDCs) have been shown to adopt the phenotype and function of several nonhematopoietic cell lineages and promote tumorigenesis. Beyond its cancer enhancing potential, cell fusion has recently emerged as an explanation of how BMDCs regenerate diseased heptocytes, contribute to Purkinje neurons, skeletal and cardiac muscle cells, and participate in skin and heart regeneration. While bone marrow-derived epithelial cells have also been observed in the intestine, their fusion origin has not been investigated. Here, we show that transplanted BMDCs fuse with both normal and neoplastic intestinal epithelium. Long-term repopulation by donor-derived cells was detected in all principal intestinal epithelial lineages including enterocytes, goblet cells, Paneth cells and enteroendocrine cells, suggesting that the fusion partners of the BMDCs are long-lived intestinal progenitors or stem cells. Fusion of BMDCs with neoplastic epithelium did not result in tumor initiation. Our findings suggest an unexpected role for BMDCs in both regeneration and tumorigenesis of the intestine.

Introduction

The use of adult stem cells for therapeutic treatment of human disease has great potential. Recently, adult stem cells were successfully used for gene therapy in a mouse model of Type 1 tyrosinema (Lagasse et al., 2000) and demonstrated to accelerate wound healing in a human burn patient (Rasulov et

al., 2005). Although the biological significance and potential clinical applications of the incorporation of bone marrow-derived cells (BMDCs) are unquestionably important (Laflamme et al., 2002; Alvarez-Dolado et al., 2003; Nygren et al., 2004; Rasulov et al., 2005), the underlying mechanism of cell incorporation into other organs remains unclear. The mechanism of cellular fusion of BMDCs with host cells in organs such as the liver has been elegantly illustrated using serially transplanted cells and extensive karyotyping of engrafted cells (Vassilopoulos et al., 2003; Wang et al., 2003). Other studies, however, suggest that BMDCs incorporate into organs through mechanisms whereby the transplanted cells transdifferentiate into tissue-specific stem cells (Ferrari et al., 1998; Wagers et al., 2002; Ianus et al., 2003).The means of BMDC incorporation in the intestine, however, have not fully been defined. Recent reports illustrate that BMDCs incorporate into the pericryptal fibroblast region of the small intestine (Brittan et al., 2002), and contribute to the intestinal epithelium of human gender-mismatched bone marrow transplants (Matsumoto et al., 2005). However, neither of these observations have been attributed to a cellular fusion mechanism. In order to understand the role of BMDC contribution in the progression of disease or the regeneration of damaged tissue, the underlying mechanism and cellular participants must be identified.

While it may be possible that BMDCs participate in intestinal epithelial regeneration or repair through a variety of different mechanisms, it has been hypothesized that circulating BMDCs could fuse with transformed intestinal epithelium to confer phenotypic and genotypic diversity to the tumor (Duelli and

Lazebnik, 2003) and participate in tumorigenesis (Lyden et al., 2001; Houghton et al., 2004; Peters et al., 2005). It is intriguing to hypothesize that these rare fusion events may lead to a cell type that possesses greater metastatic characteristics. Currently, in vitro studies support this hypothesis (Kerbel et al., 1983), although in vivo occurrences of this phenomenon have been difficult to prove. In this study, we show that transplanted BMDCs can incorporate into the intestinal epithelium of gamma-irradiated mice through a fusion mechanism, and provide evidence that the intestinal stem cell is the fusion partner. Finally, we provide in vivo evidence that strongly supports the hypothesis that fusion between circulating hematopoietic cells and transformed intestinal epithelium is involved in intestinal tumorigenesis.

Materials and Methods

Bone marrow transplantation. Bone marrow-derived cells were harvested from 5-12 week old female donor mice harboring β-galactosidase [ROSA26,(Soriano, 1999)] or enhanced Green Fluorescent Protein (GFP) transgenes (Okabe et al., 1997) using standard procedures (Battaile et al., 1999). Harvested bone marrow was filtered to obtain a single cell suspension, and resuspended in modified Hank's Balanced Salt Solution (HBSS). Hematopoietic stem cells (HSCs) were isolated as previously described (Bailey et al., 2004). An aliquot was diluted in Turk's reagent (Merck, Darmstadt, Germany) to perform a cell count. To prepare recipient mice for transplantation, eight week old recipient male C57Bl/6 mice or 5 week old recipient male Min mice (Jackson Laboratories, Bar Harbor, ME) were enterally administered acidified water (pH 2.2) for one week prior to whole body

gamma irradiation (12 Gy) in two equal doses, four hours apart. The early intestinal epithelial response to 12 Gy is crypt cell apoptotic death, however clonogenic regeneration of the crypt is observed over the first four days post-irradiation and complete healing of the epithelium is apparent by 7 days post-irradiation (Potten, 1990). A total of $5x10^6$ unfractionated donor bone marrow cells (or 500 HSCs) were then injected into the retro-orbital plexus of the recipient mouse. All recipient mice were administered antibiotic drinking water (neomycin sulfate at 1.1 g/L and polymixin B sulfate at 167 mg/L) for one month post-transplantation to reduce infection. All procedures were performed in accordance to the OHSU Animal Care and Use Committee.

Analysis of transplanted intestine. BMDC-transplanted mice were sacrificed at various times between 2 weeks and 14 months post-transplant. Wholemount analysis was conducted as previously described(Wong et al., 1998), except that intestines were fixed with 4% paraformaldehyde and visualized with fluorescence (GFP bandpass filter 470/40 nm) for GFP-incorporated or with X-gal and light microscopy for ROSA26-incorporated intestines, and images digitally captured. The number of donor-derived intestinal crypts were quantified in mice transplanted with ROSA26-BM by counting the number of X-gal positive crypts in the distal third of the small intestine and was reported as LacZ-positive crypts per cm^2. Standard error of the mean and significance was calculated.

After gross analysis of the intestine, frozen blocks were prepared and sectioned as previously described(Wong et al., 1998). Five μm thick sections

were analyzed for GFP-expressing cells using polyclonal antibodies (1:250; Molecular Probes, Eugene, OR) and fluroescent secondary antibodies (indocarbo-cyanine [Cy3]-labeled donkey anti-rabbit antibody; 1:500, Jackson ImmunoResearch, West Grove, PA), or for brightfield detection using biotin-avidin secondary antibodies and visualizaiton with 3-3'-Diaminobenzidine (DAB) according to maufacturer's guidelines (Vector Laboratories, Burlingame, CA). GFP-expressing cells were double labeled with antibodies to hematopoietic lineage markers (CD45 and c-kit, eBioscience, San Diego, CA), or intestinal epithelial-specific markers (Fabpl, a kind gift from Dr. JI Gordon, St Louis, MO; cytokeratin, Research Diagnostics Inc, Flanders, NJ; and 5α-HT, lysozyme, Peninsula Labs, San Carlos, CA). Sections were examined using a Leica DMR microscope and standard epifluorescence filters for FITC (470/40) and Cy3 (535/50). Digital images were captured.

Analysis of cell fusion. Y-chromosome Fluorescence *In Situ* Hybridization (FISH) was performed on GFP-transplanted intestinal paraffin sections. GFP-expressing cells were first identified using antigen retrieval (5 mM sodium citrate buffer; pH 6.0), polyclonal GFP antibodies and brightfield development with DAB (Vector Laboratories). FISH was subsequently performed as previously reported using cy3-conjugated-Y-chromosome paint (Cambio, Cambridge, UK) followed by incubation with 2'-(4-Hydroxyphenyl)-5-(4-methyl-1-piperazinyl)-2,5'-bi(1H-benzimidazole) trihydrochloride (Hoechst 33258; 0.1μg/ml in PBS, for 10 min). The presence of the Y-chromosome was localized to the nucleus using overlay of

Hoechst-stained and cy3-stained digital images, and confirmed by confocal microscopy. Tissue sections of GFP-expressing female or male mice were used as controls.

Analysis of GFP-transplanted ROSA26 intestines was performed as described above. Intestinal sections of transplanted mice were stained with antibodies for β-gal (1:100; Eppendorf). Secondary antibodies conjugated to cy-5 were used for β-gal detection because the excitation spectrum for cy-5 (590-650 nm) is spectrally separate from the fluorescence emission of GFP (450-570 nm). Regions co-expressing GFP and β-gal were identified using a MRC-1024 confocal laser scanning imaging system (Bio-Rad).

Results and Discussion

To determine the fate of BMDCs in intestinal epithelium, we transplanted whole bone marrow or hematopoietic stem cells (HSCs) from female Green Fluorescent Protein (GFP)-expressing or ROSA26 mice into lethally irradiated male recipients. As early as 2 weeks and for as long as 14 months post-transplant, donor-derived cells were detected in both crypt and villus epithelium, and lamina propria of the small intestine (Figure 1a-c). Moreover, donor-derived cells were readily detected in the pericryptal mesenchyme as previously reported (Brittan et al., 2002). Similar results were observed following transplantation of highly purified HSCs (Figure 1d-f). The architecture of crypt-villus units containing GFP-expressing cells was morphologically indistinguishable from regions devoid of epithelial-derived donor cells. GFP-expressing cells were present in discontinuous regions throughout the epithelium; a finding that is likely due to

variegation of GFP transgene expression that is also observed within the intestinal epithelium of the transgenic donor mouse (data not shown). In contrast, β-galactosidase (β-gal) is ubiquitously expressed in the intestinal epithelium of ROSA26 mice (Soriano, 1999), which prompted us to use it as a marker to determine the efficiency of donor cell incorporation. For this, we counted the number of donor-derived intestinal crypts in wholemount prepared intestines from transplanted mice (Figure 1b). While donor-derived intestinal crypts were present throughout the length of the intestine, they were most frequent in the distal region of the small intestine, and represented $0.25 \pm 0.05\%$ of total crypts (n=4 animals). This percentage of donor-derived intestinal cells is consistent with levels reported in other tissues (Daley et al., 2003).

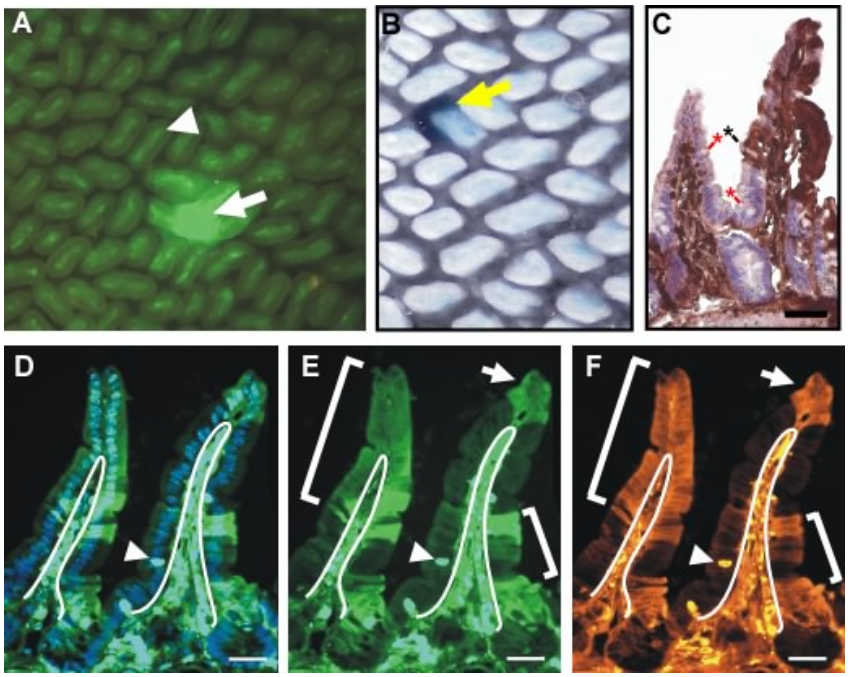

Figure A2.1. Bone marrow-derived cells incorporate into intestinal epithelium. (a) Wholemount preparation of the distal small intestine of a lethally irradiated (12 Gy) recipient mouse transplanted with $1x10^6$ Green Fluorescent Protein (GFP)-expressing BMDCs, 6 months post-transplantation. Arrow indicates GFP-positive epithelial cells populating a crypt and an adjacent villus. Arrowhead indicates GFP-positive non-epithelial cells that populate the villus core of all villi. (b) Wholemount intestine from a β-galactosidase (β-gal) expressing bone marrow transplanted recipient. Yellow arrow indicates β-gal-positive crypt and villus. (c) Tissue section from a transplanted distal small intestine stained with antibodies to GFP, detected with 3-3'-Diaminobenzidine (DAB, brown), and counterstained with Hematoxylin. The brown staining represents GFP-positive epithelium, while the GFP-negative epithelium appears pink/purple. GFP-positive cells populate the epithelium of the right villus. The left villus is negative for GFP expression. The black asterisk marks a differentiated goblet cell that is GFP-positive and the red asterisks denote GFP-negative goblet cells. (d-f) Tissue section of the distal small intestine of a recipient mouse transplanted with 500 GFP-positive hematopoietic stem cells. Section in (d) is stained with Hoechst dye (blue) and visualized for GFP expression (green) by direct fluorescence. (e) GFP detected by direct fluorescence. GFP-positive cells populate the villus-associated epithelium and are designated with white brackets and arrow. White lines designate the boundary between the epithelium and lamina propria. Arrowhead indicates an intraepithelial lymphocyte. (f) Identical tissue section in 'd&e' stained with antibodies to GFP and detected with cy3 conjugated secondary antibodies. Bar = 25 μm.

To determine if cell fusion is the mechanism that facilitates BMDC integration, we assayed for presence of the Y-chromosome in donor-derived cells in the intestines of transplanted male mice (Figure 2a-c). Co-localization of donor-derived GFP expression and recipient-specific Y-chromosome labeling within the same cell indicated that these two cell populations had undergone fusion (Figure 2a-c). An average of 51% of the donor-derived cells were positive for both markers in a total of 200 epithelial nuclei analyzed from six mice. Since the villus epithelial compartment is anatomically distinct from the hematopoietic cells that reside within the lamina propria, it is unlikely that cells positive for both the Y-chromosome and GFP represent contaminating lymphocytes or macrophages. This was confirmed by using antibodies to the panhematopoietic marker CD45 (data not shown). Wild-type male intestinal sections probed with whole Y-chromosome paint produced a detectable signal in ~85% of cells (data not shown). Implementing this as a correction factor, approximately 60% of donor-derived epithelial cells were positive for both donor and recipient cell markers. A second independent approach for examining fusion in the intestine supported these initial observations. In β-gal-expressing recipient male mice transplanted with female GFP-expressing BMDCs, both β-gal and GFP were detected in the same epithelial cell using confocal microscopy (Figure 2d-f). We were unable to identify intestinal regions containing cells expressing GFP but not β-gal, suggesting that the use the Y-chromosome approach as a host-specific marker may under-estimate the extent of cellular fusion.

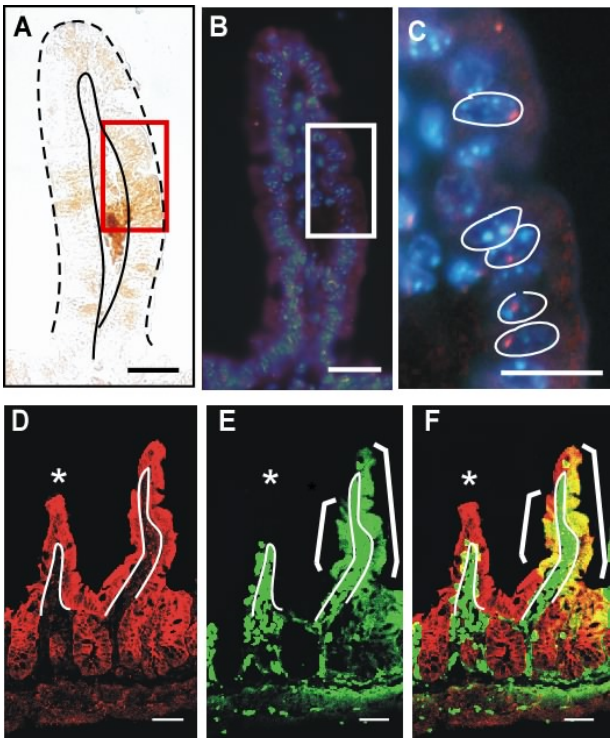

Figure A2.2. Fusion between BMDCs and intestinal epithelium. Intestine from a male recipient transplanted with female donor GFP-expressing BMDCs analyzed for GFP expression and Y-chromosome. (a) GFP-stained intestinal epithelium detected with GFP antibodies and DAB-staining (brown). Red rectangle represents a region containing GFP-positive cells. Epithelium is demarcated with solid and dashed black lines. (b) Y-chromosome probe (red) and Hoechst-stained nuclei (blue) detected on the same tissue section in panel 'a'. GFP-expressing region is denoted by a white rectangle. Boxed region is magnified in (c). Nuclei are outlined in white. (d-f) Intestinal tissue section from a β-gal expressing recipient transplanted with GFP-positive BMDC was analyzed for co-expression of β-gal and GFP by confocal microscopy. White line indicates boundary between the epithelium and lamina propria. White asterisk denotes a villus lacking GFP epithelial expression. (d) β-gal (red) is uniformly expressed in the intestinal epithelium as detected with antibodies to β-gal and cy5 conjugated secondary antibodies. (e) GFP expression (green) on the same tissue section as in panel 'd' detected by direct fluorescence. (f) Merge of β-gal- and GFP-stained tissue showing co-localization of markers for both donor and recipient populations (yellow). Epithelial cells expressing β-gal only appear red and GFP-positive lamina propria cells are green. Bar = 25 μm.

Importantly, fusion between BMDCs and intestinal epithelial cells resulted in a morphologically normal epithelial population. To address the fate of the initial fusion product, we surveyed hematopoietic gene expression within the donor-derived cells in the intestinal epithelium. Expression of CD45, c-kit or Sca-1 was present in cells residing in the lamina propria but was absent from all intestinal epithelial cells (data not shown). These results suggest that the nuclei of the fused cells have been reprogrammed and no longer express these hematopoietic markers. We found BMDCs expressing markers for all four principal intestinal epithelial lineages for up to 6-14 months post transplantation. Donor-derived absorptive enterocytes were identified by double labeling of intestinal sections with antibodies to GFP and to cytokeratin (Figure 3b-d). There was no apparent difference in enterocytic cytokeratin expression between GFP^+ or wild-type cells, indicating that GFP-expressing enterocytes possessed normal differentiation profiles. The three secretory lineages were also represented among the donor-derived population. Differentiation of donor-derived cells into enteroendocrine cells was demonstrated with antibodies to serotonin (Figure 3e-g). Donor-derived goblet cells were morphologically identified by brightfield detection for GFP-expressing cells (Figure 3a, black asterisk). Moreover, both donor-derived goblet cells and Paneth cells were also identified by lectin staining (data not shown).

The presence of donor-derived cells in all four principal epithelial lineages and even more so, the presence of multiple differentiated epithelial lineages in a single villus indicate that BMDCs fuse with a multipotent intestinal progenitor or stem cell. For example, GFP-expression detected with brightfield methods allow

for morphologic identification of mucous secreting goblet cells interspersed among absorptive enterocytes (Figure 3a, Figure 1c). Furthermore, long-term detection of GFP-expressing cells suggests that a long-lived progenitor/stem cell population propagates the GFP signal, because the differentiated intestinal epithelium is rapidly renewing and turns over every 3-5 days (Wright, 2000). Therefore, if the BMDCs fuse with differentiated cells, donor-derived markers would be absent at the later time points post-transplantation. Lineage committed progenitor cells are retained in the intestine for approximately 100 days (Bjerknes and Cheng, 1999), while long-lived progenitors and stem cells reside for longer periods. Although the persistence of donor-derived epithelium in transplanted mice suggests BMDC fusion with a long-lived progenitor or intestinal stem cell, this does not rule out fusion with lineage progenitor cells or even differentiated cells. It is unlikely that donor-derived intestinal cells of various differentiated lineages are derived from continuously occurring direct fusion events, since GFP-expressing BMDCs failed to incorporate into the intestinal epithelium of non-irradiated mice (data not shown). This observation suggests that local injury is important for BMDCs fusion and that this fusion mechanism participates in epithelial regeneration.

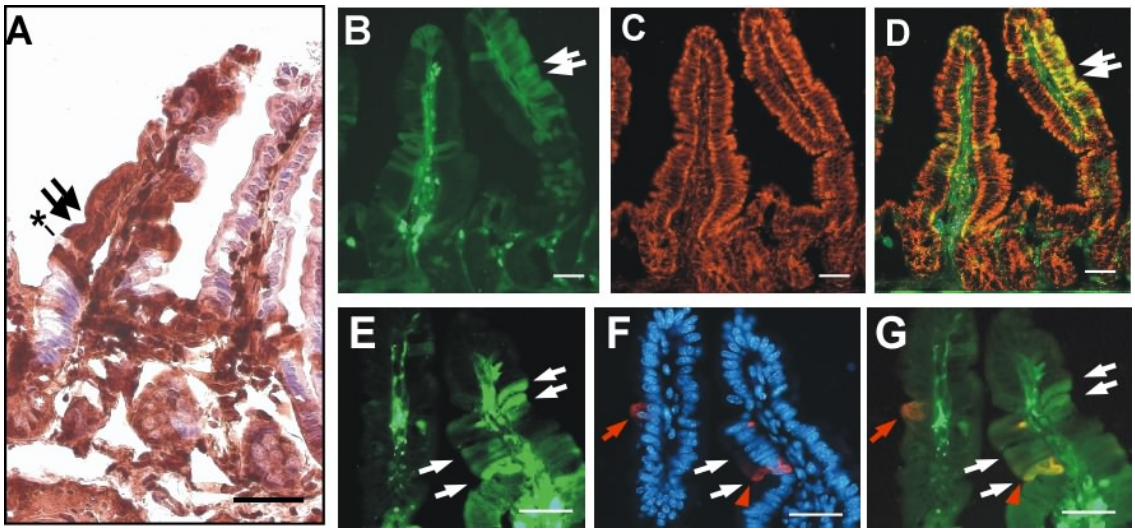

Figure A2.3. GFP expression is detected in all four principal intestinal epithelial lineages. The intestines from GFP-expressing BMDC transplanted recipients were analyzed with markers for intestinal lineages at 6 months post-transplantation. (a) Intestine stained with antibodies to GFP, detected with DAB (brown), and hematoxylin counterstained. GFP-negative epithelium on the right villus appears pink/purple, while GFP-positive epithelium on the left villus is dark brown. Black asterisk denotes a GFP-positive goblet cell adjacent to enterocytes (arrows) on the same villus. (b-d) Intestine stained with the enterocyte marker, Cytokeratin. (c) Cytokeratin staining (orange) is uniformly distributed in villus-associated epithelium, and is unaltered in GFP-expressing cells (green; b). (d) Merged image from ‘b&d’ showing co-localization of GFP and Cytokeratin (yellow). Arrows point to GFP-expressing epithelium. (e-g) Intestine stained with an enteroendocrine cell marker. (e) GFP-expressing cells (green). White arrows point to four of the GFP-expressing cells on the right villus. (f) Enteroendocrine cells identified with antibodies to serotonin (red) in the nuclear Hoechst dye-stained tissue (blue). Red arrow/arrowhead indicate the serotonin positive cells. (g) Merged image; serotonin expression in GFP-expressing enteroendocrine cells (orange, red arrowhead) is similar to expression in wild-type enteroendocrine cells (red, red arrow). Bar = 25 μm.

Our data suggests that fusion of BMDCs with wild-type intestinal epithelial cells occurs in the stem cell niche of the small intestine. This led us to ask if transplanted BMDCs have an increased propensity to incorporate into the highly proliferative epithelium of intestinal tumors or if they act as tumor stem cells, as has been recently reported in gastric carcinoma (Houghton et al., 2004). Remarkably, we found that GFP-expressing BMDCs incorporate into tumor intestinal epithelium of mice harboring intestinal adenomas (Moser et al., 1990) (Min mice) at a higher frequency when compared to wild-type intestinal epithelium (Figure 4a). While GFP-expressing cells were observed in the majority of intestinal adenomas screened, we did not detect any ubiquitously GFP-expressing adenomas. This finding, along with the observation that BMDC transplant did not alter overall polyp number (data not shown), suggests that BMDCs are not involved in tumor initiation in the small intestine. Donor-derived tumor epithelium possessed a normal expression pattern of cytokeratin, a widely expressed epithelial marker (Figure 4b-c), but failed to express the intestinal epithelial differentiation marker Fatty acid binding protein (Fabpl (Carroll et al., 1990); Figure 4d-e). This suggests that GFP-expressing tumor epithelium had lost epithelial differentiation markers, possibly due to an undifferentiated tumor environment that is more conducive to incorporation of GFP-expressing hematopoietic cells. Alternatively, integrated donor cells may fail to efficiently express tissue-specific differentiation markers. Similar to donor-derived epithelium in wild-type recipients, GFP-expressing tumor epithelium did not express hematopoietic differentiation markers (data not shown).

To determine if transplanted BMDCs incorporate into tumor epithelium by cell fusion, we analyzed GFP-expressing regions of intestinal adenomas for presence of the host-specific Y-chromosome. Donor-derived cells expressed both GFP and the Y-chromosome, indicating that cell fusion had occurred (Figure 4f-h). As the transplanted BMDCs contain wild-type copies of the Apc gene, it is unlikely that these cells could acquire mutations in both alleles and give rise to intestinal adenomas within two weeks post-transplantation. In contrast, our data strongly supports the notion that BMDCs fuse with tumor epithelium rather than function as a tumor stem cell as previously reported in gastric cancer (Houghton et al., 2004). However, the previous study did not use a dual marker system for detecting donor and recipient populations, but rather relied upon the absence of multiple nuclei to exclude the absence of fusion. Therefore, it is possible that unrecognized cell fusion may also underlie BMDC incorporation into tumors of the gastric epithelium.

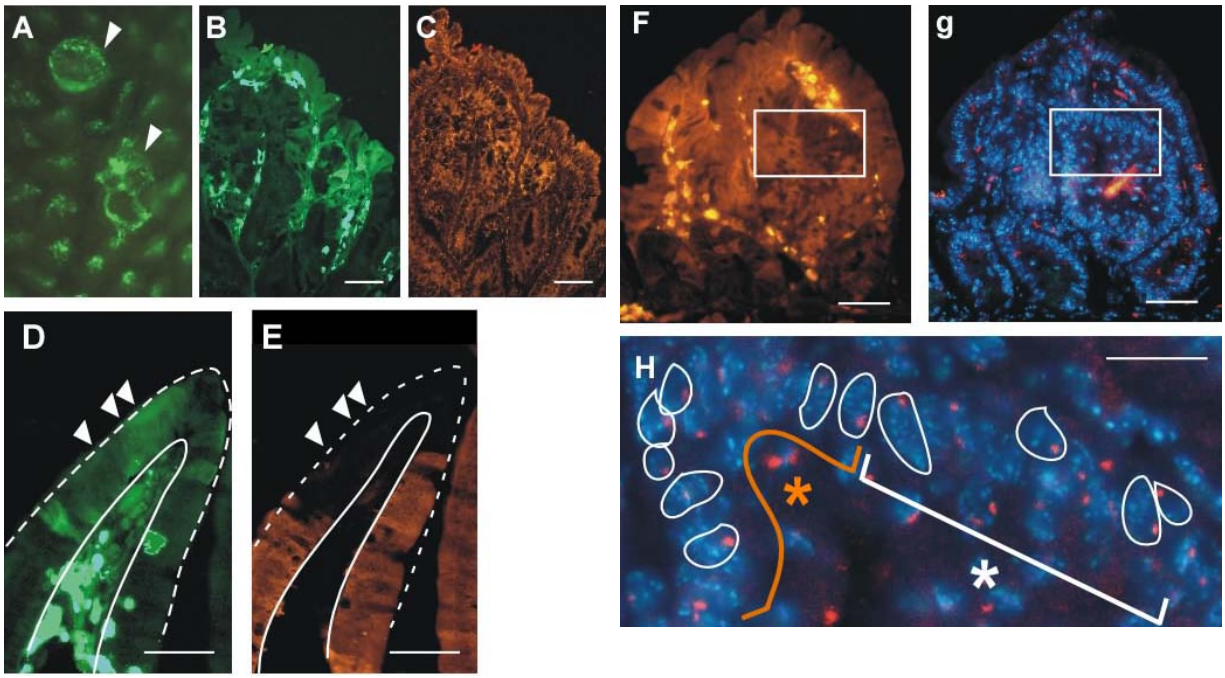

Figure A2.4. BMDCs fuse with tumor epithelium. GFP-expressing BMDCs incorporate into intestinal adenomas (arrowhead) observed by (a) intestinal wholemount and (b) tissue sections. (b-c) GFP-expressing regions (green) have a normal expression pattern of the epithelial marker, Cytokeratin (orange), when compared to adjacent non donor-derived areas. (d-e) However, donor-derived regions (green) do not express the intestinal epithelial differentiation marker, Fabpl (orange). White arrowheads mark several GFP-expressing tumor epithelial cells. Villus epithelium is demarcated with white lines. (f-h) BMDCs fuse with tumor epithelium. (f) Adenoma stained with antibodies for GFP and cy3-conjugated secondary antibodies (orange). White box contains both GFP-positive and wild-type cells. (g) Adjacent tissue section in 'f' stained with Hoechst nuclear dye (blue) and Y-chromosome probe (red). (h) Higher magnification of boxed region. Orange asterisk represents donor-derived population while white asterisk represents the recipient population. Nuclei are outlined in white. Bar = 25 μm.

While our data directly demonstrates that BMDCs fuse with the intestinal epithelium, we cannot rule out additional mechanisms for BMDC incorporation into the intestinal epithelium (Pomerantz and Blau, 2004) because the Y-chromosome was undetected in up to 40% of donor-derived epithelial cells. However, using the Y-chromosome as a host-specific marker leads to underestimation of fusion events, which suggests that alternative mechanisms such as transdifferentiation are rare.

Importantly, our findings show that BMDCs can fuse with a long-lived progenitor or intestinal stem cell population of gamma-irradiated damaged intestinal epithelium. Fusion of BMDCs with progenitors or stem cells serves to overcome the inefficiency of the rare intestinal fusion events and may play an important role in regeneration of damaged tissue. Currently, the role of BMDC fusion with tumor epithelium is less clear. Although it is apparent that incorporation of these cells into intestinal adenomas does not initiate cancer of the small intestine as was reported in gastric epithelium of BMDC transplanted mice (Houghton et al., 2004), Min mice do not survive long enough to evaluate the impact on tumor progression. While our data does not support the notion that BMDCs act as tumor-stem cells, the high frequency of fusion between BMDCs and tumor cells may indicate that fusion is a common but late event in intestinal tumorigenesis. There is precedence for the involvement of BMDCs in tumorigenesis as demonstrated by the contribution of these cells to tumor vasculature (Peters et al., 2005) and in initiation of the angiogenic switch that is critical for tumor progression (Lyden et al., 2001). Further, there is *in vitro* evidence that fusion

between blood-derived cells and tumor cell lines results in a more metastatic cellular product (Duelli and Lazebnik, 2003). Thus the *in vivo* fate of these fusogenic cells is clearly important. Whether this fusion event allows cells to acquire metastatic potential or if they become less genetically stable remains to be investigated. The observation that BMDCs can fuse with tumor epithelium is an important finding, and further examination of this event will enhance our understanding of the biology of tumorigenesis, and may provide a novel strategy for the development of anticancer therapies.

APPENDIX 3

Characterization of the intestinal cancer stem cell marker, CD166/ALCAM, in the human and mouse gastrointestinal tract

Trevor G. Levin[1], Anne E. Powell[1], Adria D. Dismuke[2], Paige S. Davies[3], Eric C. Anderson[4], John R. Swain[3], Christine Glynn[3] and Melissa H. Wong[3]

[1]Department of Cell and Developmental Biology

[2]Department of Molecular and Medical Genetics

[3]Department of Dermatology, Knight Cancer Center, Oregon Stem Cell Center

[4]Department of Internal Medicine, Division of Hematology and Medical Oncology, Oregon Health & Science University, Portland, OR.

ADD contributed to planning of all experiments, editing of manuscript, and staining and imaging in Figure 3.

Abstract

CD166 or Activated Leukocyte Cell Adhesion Molecule (ALCAM/memD) expression in a variety of cancers is emerging as a marker for aggressive disease and an exciting potential therapeutic target. Although cell surface expression of CD166 has been correlated with a shortened patient survival for colorectal cancer, little is known about the molecule's function and expression pattern in normal intestinal epithelia. In this study, we characterized the protein expression of CD166 in normal and diseased human and mouse intestines. Our data show that the CD166 expression pattern was conserved across species. In both the small and large intestine, CD166 was expressed on the cell surface of epithelial cells residing in the stem cell niche. Interestingly, in the small intestine, CD166 was expressed on both crypt-based Paneth cells and putative stem cells, the neighboring intervening crypt-based columnar cells. Further, a subset of CD166-positive crypt-based columnar cells co-expressed the putative stem cell markers Lgr-5 or Musashi-1. Examination of CD166 expression within human intestinal tumors and metastatic disease confirmed both cytoplasmic and cell surface expression patterns. Interestingly, CD166-positive cells were also detected in mouse benign adenomas, as were a very rare population of double-positive CD166 and CD44 or ESA cells. Significantly, our studies illustrate a robust expression pattern for CD166 within the endogenous intestinal stem cell niche. We further show that CD166-positive cells are expressed in multiple stages of intestinal

carcinoma including benign tumors and metastatic disease. Our findings provide the foundation for investigating the function of CD166 within the stem cell niche, and more importantly has implications on targeting CD166 for disease therapy.

Introduction

Colorectal cancer (CRC) is the third most prevalent cancer in the United States, with nearly 150,000 new cases recorded each year. Despite efforts to improve early detection and treatment, over one-third of patients die annually from this disease(2008). The focus on cancer initiation and progression has predominated the effort to better understand disease pathology and guide therapeutic approaches. As such, the cancer stem cell theory, suggesting that cancer is driven by cells harboring stem cell-like qualities, offers one explanation for why many current therapeutic approaches result in relapse of disease. In this model, some cancer stem cells (CSC) or cancer-initiating cells (CIC) may be quiescent and evade eradication by standard therapies that target proliferating cells. These surviving cells can then proceed to reseed the tumor and therefore may hold the potential to initiate metastatic disease(Pardal et al., 2003; Cho and Clarke, 2008; Dylla et al., 2008). The reinvigoration of the cancer stem cell theory(Nowell, 1976; Weiss, 2000; Vermeulen et al., 2008) has led to identification, isolation and characterization of subsets of intestinal cancer cells that can recapitulate tumorigenesis when transplanted into immune-deficient mice(Al-Hajj et al., 2003; Dalerba et al., 2007; Li et al., 2007; O'Brien et al., 2007; Hong et al., 2008). Although some cell surface molecules, such as CD133 and

CD44, have been shown to mark CICs in multiple organs, in colorectal cancer, a number of markers have shown promising CIC expression including DCAMKL-1, CD133, ESA, CD44 and CD166(Dalerba et al., 2007; O'Brien et al., 2007; May et al., 2008).

CD166 or Activated Leukocyte Cell Adhesion Molecule (ALCAM/memD) expression is pathologically correlated with aggressive disease in a variety of cancers including melanoma, prostate, breast, ovarian, esophageal, and bladder cancers(van Kempen et al., 2000; Kristiansen et al., 2003; Tomita et al., 2003; Weichert et al., 2004; Verma et al., 2005; Burkhardt et al., 2006; Doane et al., 2006; Klein et al., 2007; Mezzanzanica et al., 2008). In human CRC, aberrant cell surface CD166 expression is strongly correlated with a 15 month shortened patient survival(Weichert et al., 2004). Subsequent isolation of CD166-positive cells from human CRCs confirmed that these cells could recapitulate tumorigenesis when injected at low numbers into immune-deficient mice(Dalerba et al., 2007), a hallmark of the CSC population. Although these findings suggest that CD166 may have a role in the progression of colorectal cancer, little is known about its endogenous function and cellular localization within the intestine.

In other systems, CD166 has been described to have a myriad of functions. This conserved protein participates in physiologic processes including leukocyte intravisation across the blood brain barrier, monocyte migration across endothelial junctions, angiogenesis, capillary formation, protection against apoptosis in breast cancer cells, and T-cell activation by antigen presenting and tumor cells(Ohneda et al., 2001; Hassan et al., 2004; Ikeda and Quertermous,

2004; Jezierska et al., 2006; Kato et al., 2006; Masedunskas et al., 2006; Cayrol et al., 2008). Further, CD166 has been described as a ligand that binds to CD6 on thymic epithelium(Kanki et al., 1994; Bowen et al., 1995; Patel et al., 1995), and as a cell surface marker for a subset of hematopoietic progenitor cells(Corbel et al., 1992; Uchida et al., 1997) and multipotent mesenchymal stem cells(Bruder et al., 1998; Arai et al., 2002). Based upon the intriguing CD166 expression pattern in multiple stem cell populations it has a potential role in maintaining a stem cell state in both normal and disease states. However, the potential overlap between CD166 normal and tumorigenic physiologic function have not been elucidated. Further, based upon its multiple roles in tumor-related processes, CD166 could play an important role in tumor pathology.

Correlation of CD166 expression pattern with aggressive disease has led to efforts targeting this molecule as a cancer therapeutic. Treatment of cancer cells with a CD166-internalizing antibody conjugated to chemotherapy filled lipid vesicles was shown to effectively target and kill CD166-expressing ovarian cancer cells and prostate cancer cells *in vitro*(Piazza et al., 2005; Roth et al., 2007). While early results from these types of targeted cancer therapies appear promising, it necessitates an even more careful understanding of the endogenous expression pattern and function of CD166. In this study, we analyze CD166 expression in normal human and mouse intestine. We identified enriched cell surfaced CD166 expression in the colon and small intestine crypt base, marking both the differentiated Paneth cell population and the intervening crypt-based columnar cells. We also confirmed observations for both elevated cell

surface and cytoplasmic CD166 expression in human colorectal cancer(Weichert et al., 2004). Interestingly, both normal and tumor CD166 expression patterns were conserved in mice, highlighting the value of using the mouse as a model for studying regulation of CD166 in cancer. Further, we show that a subset of CD166-expressing cells residing in the stem cell niche co-express other putative stem cell markers including Musashi-1 and Lgr-5(Potten et al., 2003; Barker et al., 2007; Sato et al., 2009). We propose that CD166 marks both a subpopulation of progenitor cells and differentiated cells within the normal intestinal stem cell niche, and that a possible function for CD166 is in maintaining the epithelial microenvironment of the stem cell niche. Therefore, targeting this cell surface antigen in cancer therapy requires careful consideration of potential effects in normal tissues.

Material and Methods

Mice

Mice were housed in a specific pathogen-free environment under strictly controlled light cycle conditions, fed a standard rodent Lab Chow (#5001 PMI Nutrition International, Brentwood, MO), and provided water ad libitum. All procedures were performed in accordance to the OHSU Animal Care and Use Committee. The C57Bl/6 and MIN mice were purchased from The Jackson Laboratory (Bar Harbor, ME). (Moser et al., 1990)

Immunohistochemical and histochemical analyses of intestinal tissue

Adult (6 weeks) and embryonic [(E) 14.5, 15.5, 16.5, 17.5, 18.5] mouse intestines were dissected and prepared for paraffin and frozen tissue analyses as we have previously described(Wong et al., 1998). Human small intestine and colonic tissue was fixed in 10% buffered formalin prior to being embedded in paraffin or OCT. Human tissues were acquired from the OHSU Histopathology Shared Resource. Tissue sections were cut to a 5 μm thickness, then stained with antibodies to CD166 (15ug/mL; R&D Systems), Msi-1 (1:100; Chemicon International), Lgr-5 (dilution, GeneTex), Ki67 (1:250; Abcam), seratonin (1:500; Incstar), E-cadherin (1:1000; Decma), or the lectin UEA-1 (1:1000; Sigma). For paraffin embedded tissues, antigen retrieval was performed for a subset of antibodies. Briefly, slides were incubated in 10mM citrate buffer, pH=6 or in 10mM Tris, 1mM EDTA, pH=9 for 20 minutes at 100˚C. Antigens were visualized using either species-specific secondary antibodies [Indocarbocyanine3 (Cy3), Indocarbocyanine5 (Cy5), Fluorescein isothiocyanate (FITC)] (1:500; Jackson ImmunoResearch), or brightfield diaminobenzidine (DAB) detection (Vectastain ABC kit; Vector, Burlingame, CA) and Methyl green counter staining (Vector, Burlingame, CA). Nuclear counterstaining with Hoechst dye (33258; Sigma; St. Louis, MO; 0.1 μg/ml) was performed. For detection of CD166-positive Paneth cells, human small intestinal tissue sections were first incubated with antibodies to CD166 and visualized with secondary antibodies conjugated to Cy3. Images were captured using a Leica DMR fluorescent microscope (Leica Microsystems, Bannockburn, IL), then the tissue was re-stained with Lendrum’s Phloxine-

Tartrazine according to standard procedures(Luna, 1968), and superimposed images recaptured.

Analyses of isolated intestinal epithelial cells

The crypt and villus/colonic cuff epithelial cells of the mouse small intestine (SI) and colon were independently isolated using a modified Weiser preparation(Davies et al., 2008), stained with antibodies to CD166, then sorted using a Cytopeia Influx to collect $CD166^{+}$ differentiated cells (SI villus or colonic cuff epithelia) and the $CD166^{+}$ undifferentiated cells (SI and colonic crypt epithelia). Briefly, intestines were cut longitudinally, rinsed with modified Hanks Buffered Saline solution (HBSS; $-Ca^{++}$, $-Mg^{++}$), then incubated in HBSS with EDTA (for SI differentiated cells: 1 mM EDTA, for colonic differentiated cells: 10mM EDTA) for two rounds at 4°C, 15 minutes. This was followed by two additional incubations for isolation of the undifferentiated fractions (for SI undifferentiated cells: 5mM EDTA, for colonic undifferentiated cells: 15mM EDTA). Small intestinal cells were subsequently incubated in 15U/ml Type II collagenase at 25°C for 10 min, followed by 0.3U/ml dispase at 25°C for 10 min. Cells were resuspended in modified HBSS and gently filtered through a 0.45μm filter. Cells were then incubated with a combination of antibodies to CD45 conjugated to Allophycocyanin (APC; 1:100; BD Pharmingen), CD166 (1:100; R&D Systems) and Lgr-5 (1:100) on ice for 20 min, followed by incubation with secondary antibodies conjugated to FITC for CD166 (1:500; Jackson Immunoresearch) or PE for Lgr-5 (1:500; Molecular Probes). Cells were

resuspended in modified HBSS/ 5μg/ml propidium iodide/1% bovine serum albumin and sorted using a Cytopeia Influx (150 μm nozzle, 4.5 psi) and Spigot software. FACS data was analyzed using FCS Express Version 3 Research Edition (DeNovo Software). 100,000 $CD166^+$, $CD45^-$, PI^- cells were collected and spun onto glass slides using a Shandon Cytospin 4 (Thermo Electron) then subsequently analyzed for expression of Paneth cell markers or expression of Lgr-5 as described in the previous section.

Results

CD166 protein expression is enhanced in the base of the human and mouse small intestinal and colonic crypt epithelium.

Human colonic expression patterns of CD166 have been previously reported to localize to the cytoplasm of cells within the crypt base(Weichert et al., 2004). To confirm this finding and extend the analysis to the human small intestine, we stained normal human small intestine and colon tissue sections with antibodies to CD166. Detection with both fluorescent and brightfield immunohistochemisty revealed enriched expression of CD166 protein in cells at the base of the crypts in both the small intestine (Fig. A3.1A-C) and colon (Fig. A3.1D-F). In the small intestine, CD166 expression appeared strongest on the cell surface. In the colon CD166 was expressed in a more pronounced gradient which increased in intensity towards the base of the crypt.

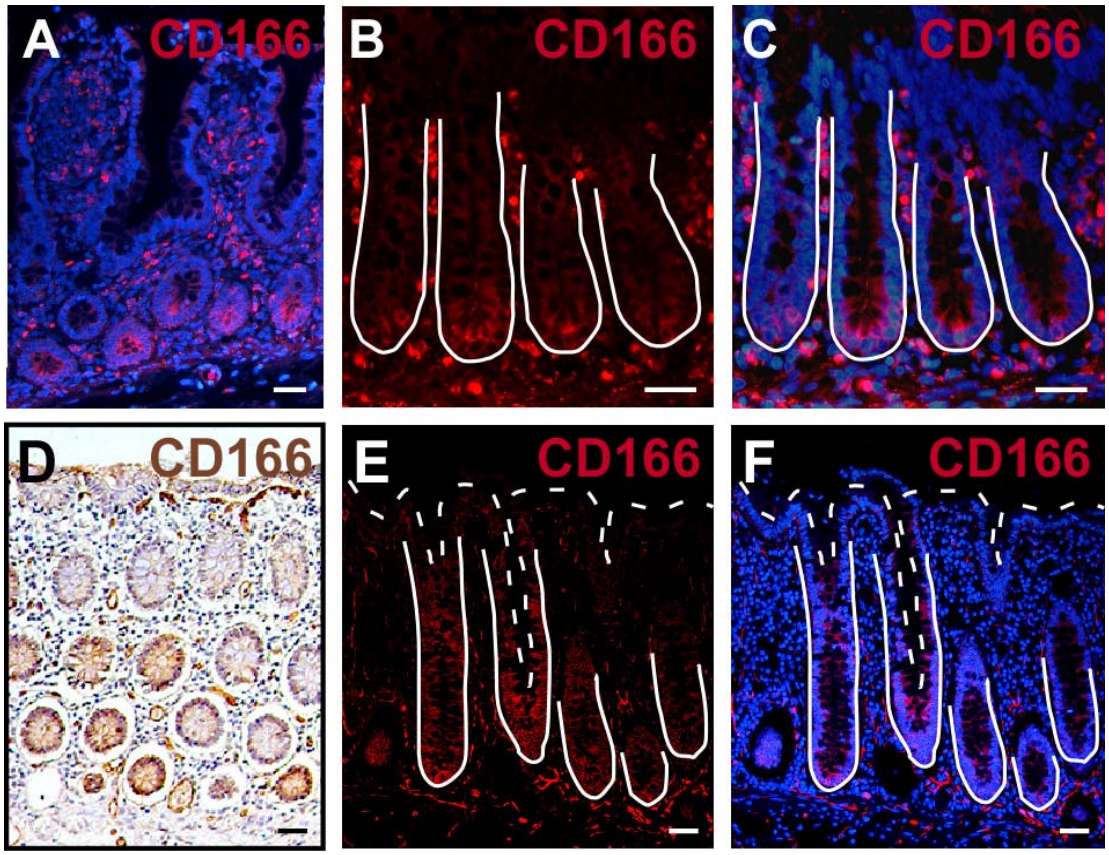

Figure A3.1 CD166 expression pattern in the human small intestine and colon. (A-C) Human small intestine stained with antibodies to CD166 (red) and counterstained with Hoechst (blue). (D-F) Human colon stained with antibodies to CD166, visualized by DAB (brown) in (D) and by fluorescence (red) with Hoechst counterstain (blue) in (E,F). Solid lines demark epithelial-mesenchymal boundary and dashed lines mark the apical epithelial surface. Bars = 25 μm.

Next, we characterized CD166 expression patterns in the mouse small intestine in order to validate it as a model organism for future studies dissecting the role of CD166 in normal intestinal physiology and tumorigenesis. Crypt-based expression did not vary down the small intestinal length. Recapitulating the human expression pattern, CD166 was detected on the epithelial plasma membrane with increasing gradients of expression toward the small intestinal and colonic crypt base or stem cell niche (Fig. A3.2A-E). However, strikingly, protein expression was more readily detectable and robust, allowing resolution of a distinct expression domain in the crypt of the small intestine (Fig. A3.2B). Low levels of cell surface CD166 were apparent on the small intestinal villus when sectioned on a tangential plane (Fig. A3.2C, arrowheads).

To further define the expression pattern within the crypt and villus epithelial fractions, we isolated the intestinal epithelium using a method that disrupts cell adhesion complexes(Davies et al., 2008). Enriched populations of differentiated, villus epithelium and undifferentiated, crypt-base epithelium were isolated and stained with antibodies to CD166. FACS analyses revealed a CD166-positive subset in both the differentiated and undifferentiated fractions of the small intestine (Fig. A3.2F). The $CD166^{hi}$ population was represented by a low number of positive villus cells (0.8%) and a larger subset of crypt cells (8.1%), recapitulating the staining patterned observed in Fig. A3.2A-C.

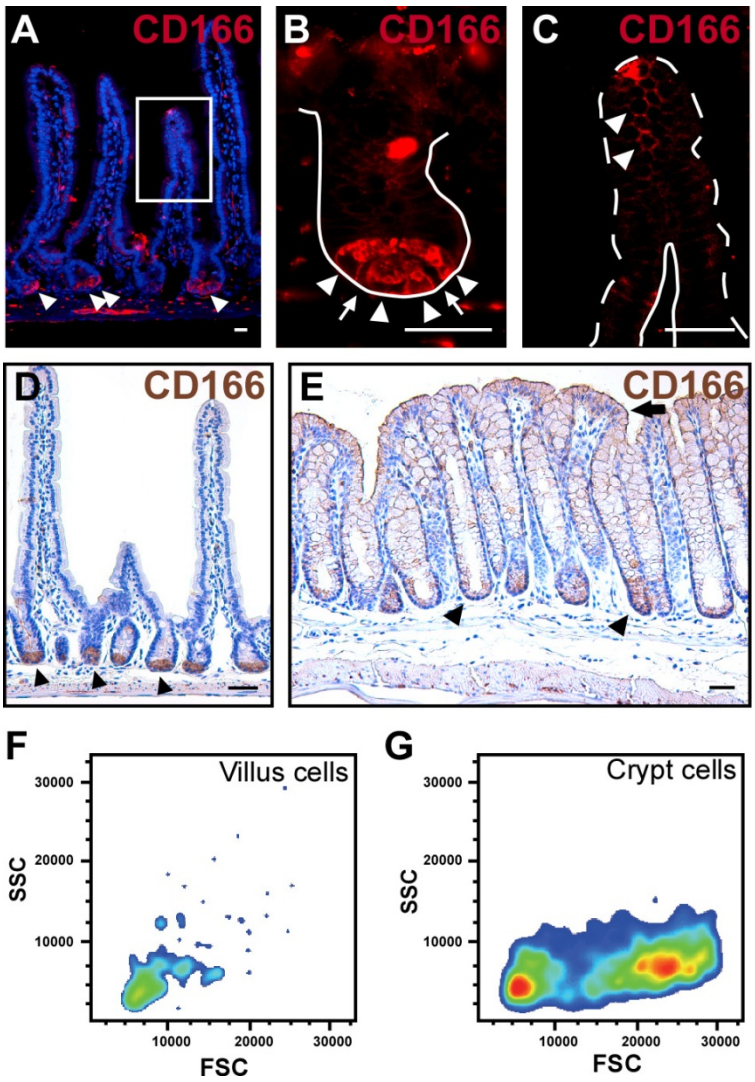

Figure A3.2 CD166 expression pattern in the mouse small intestine and colon. (A-C) Mouse small intestine stained with antibodies to CD166 (red) and counterstained with Hoechst (blue). Arrows mark CD166 expressing cells, box marks a tangential section through a villus, magnified in panel (C). (B) Higher magnification of CD166expression in the small intestine crypt. Arrow heads mark differentiated Paneth cells, arrows mark intervening crypt base columnar cells. Solid line denotes the epithelial-mesenchymal boundary. (D, E) Mouse small intestine and colon stained with antibodies to CD166 (brown), demonstrating enhanced expression in crypt base of both organs. (F, G) Flow cytometry analysis of independently isolated villus and crypt epithelial cell fractions stained with PE-conjugated CD166 antibodies. Forward and side scatter of CD166 expressing cells in villus population (F) shows a very small single population of cells. Crypt epithelial cells in (G) display two distinct populations of cells (orange) of varying size. Bar = 25 μm.

Surprisingly, two distinct population of crypt-based cells expressed CD166: Paneth cells (Fig. A3.2B, arrowheads), as well as the intervening crypt-based columnar cells (Fig. A3.2B, arrows). In the Paneth cell population, both granules and the junctional cell membranes stained positive for CD166 (Fig. A3.2B, arrowheads). Paneth cells contain granules that are known to non-specifically cross-react with antibodies resulting in false-positives. Therefore, FACS was performed to collect CD166-positive cells, by which cells remain fully intact allowing for isolation of a population based only on cell surface expression. To confirm our immunohistochemical observations, we subsequently stained FACS-isolated CD166-expressing cells with markers for Paneth cells. Phloxine Tartrazine, an established Paneth cell histochemical stain, identified a subset of CD166 sorted cells (Fig. A3.3B; arrowheads). Interestingly there was a population of CD166-positive cells that did not stain for UEA1 or Phloxine Tartrazine (Fig. A3.3A&B, arrows).

While only a subset of FACS-isolated CD166-expressing cells were Paneth cells, we sought to characterize the CD166-positive crypt-base columnar cells. To determine if these cells co-expressed additional putative stem cell markers, we performed flow analysis on Lgr-5, CD166 double-labeled small intestinal crypt cells. Lgr5-positive cells represented a small fraction of CD166-positive crypt-based cells (Fig. A3.3C-E). A second putative stem cell marker, Musashi1(Potten et al., 2003), also shared overlapping expression with a subset of CD166-expressing cells (Fig. A3.4G).

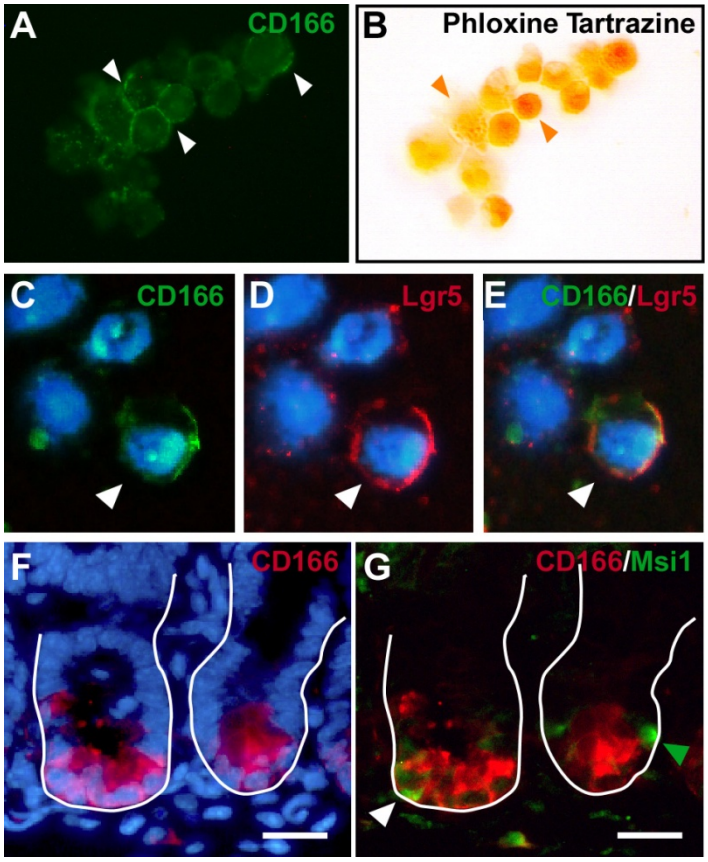

Figure A3.3 CD166 is expressed in crypt-based Paneth cells. (A-E) CD166^{+} mouse cytospun crypt cells (green). (B) Phloxine Tartrazine (orange) where white arrows designate CD166+ cells, orange arrows designate Phloxine Tartrazine positive cells, or (D) antibodies to Lgr5, a putative stem cell marker (red). (E) Mouse intestinal tissue co-stained with antibodies to CD166 (green) and a second putative stem cell marker, Lgr5 (red). (F&G) Mouse intestinal tissue co-stained with antibodies to CD166 (red) and another putative stem cell marker, Msi1 (green). Arrow designated co-expressing cell. White line marks epithelial-mesenchymal boundary. Bar = 25 μm.

CD166 is highly expressed in human colon adenocarcinoma and liver metastases

To further characterize the expression patterns of CD166 during intestinal tumorigenesis, we stained human adenocarcinoma and liver metastases with antibodies to CD166. We identified both cell surface and cytoplasmic expression in primary tumors and metastases (Fig. A3.4A-D). Human tumors were decidedly heterogeneous in their CD166 expression. While some tumor samples exhibited only cell surface patterns, others exhibited both cell surface and cytoplasmic expression. CD166-positive cells generally appeared within clustered regions of epithelium. Interestingly, for one matched primary tumor and liver metastasis, the expression pattern was identical (data not shown).

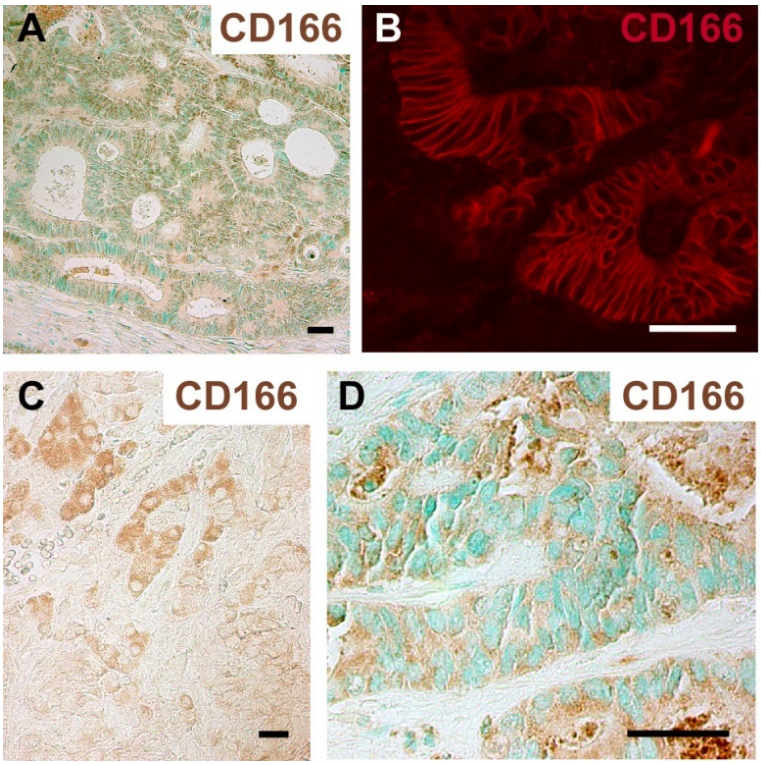

Figure A3.4 CD166 expression in human colorectal cancer. (A,B) Human primary colorectal adenomas stained with antibodies to CD166 for brightfield detection (brown) with methylgreen or (B) fluorescent detection (red). (C,D) CD166 is expressed in both the cytoplasm and on the cell surface of human liver metastatic colorectal cancer lesions. Bar = 25 μm.

Tumors in a mouse model for intestinal tumorigenesis, the $Apc^{MIN/+}$ mouse(Moser et al., 1990), displayed a strikingly similar CD166 expression pattern compared to human colorectal tumors (Fig. A3.5A&B). Both predominant cell surface staining and diffuse cytoplasmic expression was detected. Interestingly, only a subset of the CD166-expressing tumor cells were actively in the cell cycle, as determined by co-expression of the proliferative marker Ki67 (data not shown). This might reflect the possibility that at any one time only a subset of CSC are actively cycling.

To further characterize the expression domain of CD166 in the normal intestine and in intestinal tumors, we performed double staining with CD166 and either CD44 or ESA on $Apc^{MIN/+}$ mouse intestinal sections. CD44 and ESA were previously used in combination with CD166 to identify and isolate a cancer stem cell population in human colorectal cancer(Dalerba et al., 2007). We found that in the normal intestine, CD44 was undetectable, while in nearby adenomas, CD44 expression was primarily restricted to aberrant crypts within the tumor structure (Fig. A3.4C). Interestingly CD166 expression was generally lost in the aberrant crypt structures and therefore CD166 and CD44 were primarily expressed in a mutually exclusive cell populations. However, there was a small subset of dual-expressing cells. In contrast, ESA was expressed on all epithelial cells in the normal intestine (Fig. A3.5D), but its expression was lost on large clusters of tumor cells (Fig. A3.5E). Again, CD166 and ESA were generally expressed in mutually exclusive cell populations, although a small subset of cell expressed both antigens (Fig. A3.5E).

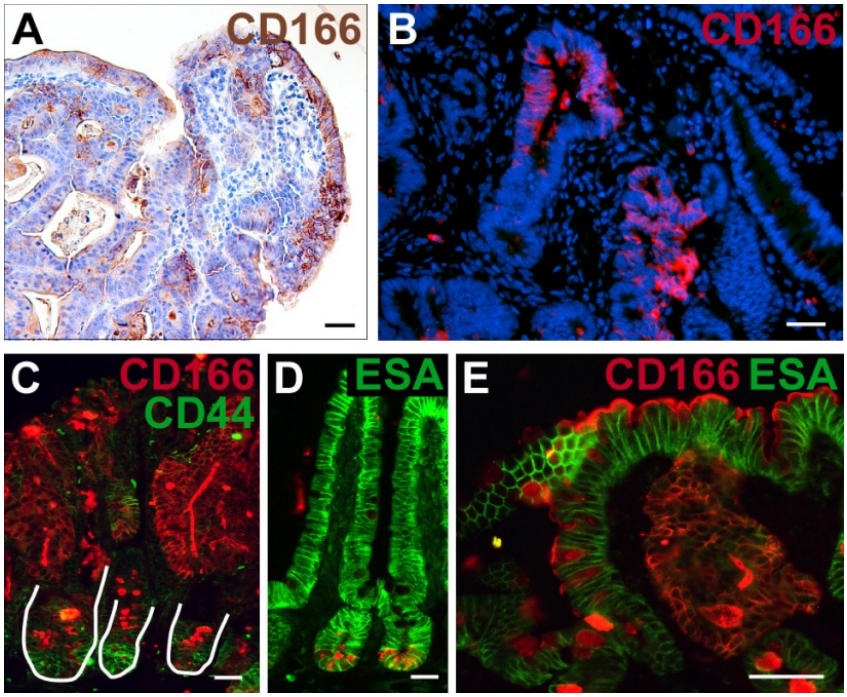

Figure A3.5 A subset of CD166-expressing mouse tumor cells are proliferating. (A&B) CD166 staining in mouse intestinal tumors recapitulates staining patterns in human colorectal cancer adenomas. (C& D) CD166 is generally expressed in cells that do not express CD44 or ESA, CD166 (red), CD44 or ESA (green). Bar = 25 μm.

Discussion

Our findings suggest that CD166 is an important molecule in the intestinal stem cell niche in both the human and mouse intestine. We show that CD166 was expressed at low levels in the differentiated cell population of the small intestine and colon, but at high levels within the stem cell niche at the base of the crypt. In the small intestine, CD166 was distinctly present on both putative stem cells, the crypt-based columnar epithelial cells and the differentiated Paneth cells. In light of the previously described role in cell adhesion and its capacity to form dimmers across adjacent cell membranes, it is intriguing to postulate that CD166 may have an important function in anchoring the stem cell within the intestinal stem cell niche. Further, a precedence for adhesion molecules participating in establishing cellular polarity and stem cell asymmetric division exists (Picco et al., 2007).

The stem cell marker Lgr-5(Haegebarth and Clevers, 2009) is substantially enriched in a subset of CD166-expressing crypt cells. In contrast, the putative stem cell marker Musashi-1 is often expressed in a single crypt cell surrounded by CD166 positive cells. Interestingly, Musashi-1 is also expressed in cells at the +6 position where they are not surrounded by CD166 positive cells. While the current understanding of the relationship between these potential discrete intestinal progenitor populations is lacking, it is clear that development of a multi-marker stem cell signature will be required to gain a deeper understanding for the implication of CD166-expressing cells in disease.

CD166 may possess multiple functions within the intestinal epithelium. This is suggested by its multi-faceted expression pattern in subsets of fully differentiated Paneth and enteroendocrine cells juxtaposed its expression in a putative stem population. Interestingly, this type of expression pattern has also been displayed for other putative intestinal stem cell markers including DCAMKL-1(May et al., 2008) and Musashi-1 (data not shown). Future exploration of CD166 differential function and regulation in intestinal epithelium will help to better understand its misregulation and contribution to disease in intestinal cancers.

Consistent CD166 expression in both human and mouse tumors demonstrates that the mouse provides a viable model for studying the function and expression of CD166 in tumorigenesis. Interestingly, CD166 was highly expressed in early adenoma formation in the $Apc^{MIN/+}$ mouse. Further, we confirmed that CD166 expression is retained within human CRC and metastatic disease, and that both a cell surface and cytoplasmic expression pattern is apparent. These findings, in particular an alteration in cellular localization of CD166, support a potential functional role for this molecule in tumorigenesis. Our analysis extends these initial findings and shows that these expression patterns are also retained in metastatic lesions.

CD166 expression relative to other CSC and proliferative markers in the $Apc^{MIN/+}$ mouse recapitulated previous findings which showed that cells positive for both CD166, CD44 and ESA constitute a small subpopulation of total tumor mass. By analyzing the expression pattern of these markers in the $Apc^{MIN/+}$

mouse, our finding suggest that co-expression of these markers is not sufficient to promote invasive tumorigenesis. Analysis of CD166 expression in $Apc^{MIN/+}$ polyps found that crypt-like structures near the muscularis tend to be low or lack expression of CD166 while they are high in CD44 and Ki67 expression.

Our data is the first to describe normal expression of CD166 in human and mouse intestine and to characterize its expression in Lgr-5 positive crypt cells and paneth cells. This initial characterization of expression suggests that the mouse is a valid model for understanding CD166 function and its role in tumorigenesis. Before CD166 can be targeted therapeutically in cancer we must first better understand its normal function.

References

Aberle, H., A. Bauer, J. Stappert, A. Kispert and R. Kemler (1997). beta-catenin is a target for the ubiquitin-proteasome pathway. *EMBO J* **16**(13): 3797-804.

Al-Hajj, M., M. S. Wicha, A. Benito-Hernandez, S. J. Morrison and M. F. Clarke (2003). Prospective identification of tumorigenic breast cancer cells. *Proc Natl Acad Sci U S A* **100**(7): 3983-8.

Alvarez-Dolado, M., R. Pardal, J. M. Garcia-Verdugo, J. R. Fike, H. O. Lee, K. Pfeffer, C. Lois, S. J. Morrison and A. Alvarez-Buylla (2003). Fusion of bone-marrow-derived cells with Purkinje neurons, cardiomyocytes and hepatocytes. *Nature* **425**(6961): 968-73.

American Cancer Society (2008). Cancer Facts & Figures 2008. *Atlanta*, American Cancer Society.

Amit, S., A. Hatzubai, Y. Birman, J. S. Andersen, E. Ben-Shushan, M. Mann, Y. Ben-Neriah and I. Alkalay (2002). Axin-mediated CKI phosphorylation of beta-catenin at Ser 45: a molecular switch for the Wnt pathway. *Genes Dev* **16**(9): 1066-76.

Arai, F., O. Ohneda, T. Miyamoto, X. Q. Zhang and T. Suda (2002). Mesenchymal stem cells in perichondrium express activated leukocyte cell adhesion molecule and participate in bone marrow formation. *J Exp Med* **195**(12): 1549-63.

Asai, R., H. Okano and S. Yasugi (2005). Correlation between Musashi-1 and c-hairy-1 expression and cell proliferation activity in the developing intestine and stomach of both chicken and mouse. *Dev Growth Differ* **47**(8): 501-10.

Bachmair, A., D. Finley and A. Varshavsky (1986). In vivo half-life of a protein is a function of its amino-terminal residue. *Science* **234**(4773): 179-86.

Ballester, M., A. Castello, E. Ibanez, A. Sanchez and J. M. Folch (2004). Real-time quantitative PCR-based system for determining transgene copy number in transgenic animals. *Biotechniques* **37**(4): 610-3.

Barker, N., J. H. van Es, J. Kuipers, P. Kujala, M. van den Born, M. Cozijnsen, A. Haegebarth, J. Korving, H. Begthel, P. J. Peters and H. Clevers (2007). Identification of stem cells in small intestine and colon by marker gene Lgr5. *Nature* **449**(7165): 1003-7.

Barker, N. (2008). The canonical Wnt/beta-catenin signalling pathway. *Methods Mol Biol* **468**: 5-15.

Barker, N., R. Ridgway, J. van Es, M. van de Wetering, H. Begthel, M. van den Born, E. Danenberg, A.R. Clark, O.J. Sansom, and H. Clevers (2009). Crypt stem cells as the cells-of-origin of intestinal cancer. *Nature* **457**: 607-612.

Barrow, J. R., K. R. Thomas, O. Boussadia-Zahui, R. Moore, R. Kemler, M. R. Capecchi and A. P. McMahon (2003). Ectodermal Wnt3/beta-catenin signaling is required for the establishment and maintenance of the apical ectodermal ridge. *Genes Dev* **17**(3): 394-409.

Batlle, E., J. T. Henderson, H. Beghtel, M. M. van den Born, E. Sancho, G. Huls, J. Meeldijk, J. Robertson, M. van de Wetering, T. Pawson and H. Clevers (2002). Beta-catenin and TCF mediate cell positioning in the intestinal epithelium by controlling the expression of EphB/ephrinB. *Cell* **111**(2): 251-63.

Batlle, E. (2008). A new identity for the elusive intestinal stem cell. *Nat Genet* **40**(7): 818-9.

Battaile, K. P., R. L. Bateman, D. Mortimer, J. Mulcahy, R. K. Rathbun, G. Bagby, W. H. Fleming and M. Grompe (1999). In vivo selection of wild-type hematopoietic stem cells in a murine model of Fanconi anemia. *Blood* **94**(6): 2151-8.

Bhanot, P., M. Brink, C. H. Samos, J. C. Hsieh, Y. Wang, J. P. Macke, D. Andrew, J. Nathans and R. Nusse (1996). A new member of the frizzled family from Drosophila functions as a Wingless receptor. *Nature* **382**(6588): 225-30.

Bhanot, P., M. Fish, J. A. Jemison, R. Nusse, J. Nathans and K. M. Cadigan (1999). Frizzled and Dfrizzled-2 function as redundant receptors for Wingless during Drosophila embryonic development. *Development* **126**(18): 4175-86.

Bienz, M. and H. Clevers (2000). Linking colorectal cancer to Wnt signaling. *Cell* **103**(2): 311-20.

Bjerknes, M. and H. Cheng (1981). The stem-cell zone of the small intestinal epithelium. III. Evidence from columnar, enteroendocrine, and mucous cells in the adult mouse. *Am J Anat* **160**(1): 77-91.

Bjerknes, M. and H. Cheng (1999). Clonal analysis of mouse intestinal epithelial progenitors. *Gastroenterology* **116**(1): 7-14.

Blanpain, C., V. Horsley and E. Fuchs (2007). Epithelial stem cells: turning over new leaves. *Cell* **128**(3): 445-58.

Booth, C. and C. S. Potten (2000). Gut instincts: thoughts on intestinal epithelial stem cells. *J Clin Invest* **105**(11): 1493-9.

Bowen, M. A., D. D. Patel, X. Li, B. Modrell, A. R. Malacko, W. C. Wang, H. Marquardt, M. Neubauer, J. M. Pesando, U. Francke and et al. (1995). Cloning, mapping, and characterization of activated leukocyte-cell adhesion molecule (ALCAM), a CD6 ligand. *J Exp Med* **181**(6): 2213-20.

Brittan, M., T. Hunt, R. Jeffery, R. Poulsom, S. J. Forbes, K. Hodivala-Dilke, J. Goldman, M. R. Alison and N. A. Wright (2002). Bone marrow derivation of pericryptal myofibroblasts in the mouse and human small intestine and colon. *Gut* **50**(6): 752-7.

Bruce, A. G., A. M. Bakke, M. E. Thouless and T. M. Rose (2005). Development of a real-time QPCR assay for the detection of RV2 lineage-specific rhadinoviruses in macaques and baboons. *Virol J* **2**(1): 2.

Bruder, S. P., N. S. Ricalton, R. E. Boynton, T. J. Connolly, N. Jaiswal, J. Zaia and F. P. Barry (1998). Mesenchymal stem cell surface antigen SB-

10 corresponds to activated leukocyte cell adhesion molecule and is involved in osteogenic differentiation. *J Bone Miner Res* **13**(4): 655-63.

Bubner, B. and I. T. Baldwin (2004). Use of real-time PCR for determining copy number and zygosity in transgenic plants. *Plant Cell Rep* **23**(5): 263-71.

Burkhardt, M., E. Mayordomo, K. J. Winzer, F. Fritzsche, T. Gansukh, S. Pahl, W. Weichert, C. Denkert, H. Guski, M. Dietel and G. Kristiansen (2006). Cytoplasmic overexpression of ALCAM is prognostic of disease progression in breast cancer. *J Clin Pathol* **59**(4): 403-9.

Camper, S. (1987). Research Applications of Transgenic Mice. *BioTechniques* **5**(7): 638-650.

Cavallo, R. A., R. T. Cox, M. M. Moline, J. Roose, G. A. Polevoy, H. Clevers, M. Peifer and A. Bejsovec (1998). Drosophila Tcf and Groucho interact to repress Wingless signalling activity. *Nature* **395**(6702): 604-8.

Cayrol, R., K. Wosik, J. L. Berard, A. Dodelet-Devillers, I. Ifergan, H. Kebir, A. S. Haqqani, K. Kreymborg, S. Krug, R. Moumdjian, A. Bouthillier, B. Becher, N. Arbour, S. David, D. Stanimirovic and A. Prat (2008). Activated leukocyte cell adhesion molecule promotes leukocyte trafficking into the central nervous system. *Nat Immunol* **9**(2): 137-45.

Cervantes, S., T. P. Yamaguchi and M. Hebrok (2009). Wnt5a is essential for intestinal elongation in mice. *Dev Biol* **326**(2): 285-94.

Chen, C. M. and G. Struhl (1999). Wingless transduction by the Frizzled and Frizzled2 proteins of Drosophila. *Development* **126**(23): 5441-52.

Cheng, C. W., J. C. Yeh, T. P. Fan, S. K. Smith and D. S. Charnock-Jones (2008). Wnt5a-mediated non-canonical Wnt signalling regulates human endothelial cell proliferation and migration. *Biochem Biophys Res Commun* **365**(2): 285-90.

Cheng, H. (1974). Origin, differentiation and renewal of the four main epithelial cell types in the mouse small intestine. IV. Paneth cells. *Am J Anat* **141**(4): 521-35.

Cheng, H. and C. P. Leblond (1974). Origin, differentiation and renewal of the four main epithelial cell types in the mouse small intestine. I. Columnar cell. *Am J Anat* **141**(4): 461-79.

Cho, R. W. and M. F. Clarke (2008). Recent advances in cancer stem cells. *Curr Opin Genet Dev* **18**(1): 48-53.

Christian, J. L. and R. T. Moon (1993). Interactions between Xwnt-8 and Spemann organizer signaling pathways generate dorsoventral pattern in the embryonic mesoderm of Xenopus. *Genes Dev* **7**(1): 13-28.

Clevers, H. (2006). Wnt/beta-catenin signaling in development and disease. *Cell* **127**(3): 469-80.

Clevers, H. and E. Batlle (2006). EphB/EphrinB receptors and Wnt signaling in colorectal cancer. *Cancer research* **66**(1): 2-5.

Copreni, E., M. Penzo, S. Carrabino and M. Conese (2004). Lentivirus-mediated gene transfer to the respiratory epithelium: a promising approach to gene therapy of cystic fibrosis. *Gene Ther* **11 Suppl 1**: S67-75.

Corbel, C., F. Cormier, O. Pourquie and H. G. Bluestein (1992). BEN, a novel surface molecule of the immunoglobulin superfamily on avian hemopoietic progenitor cells shared with neural cells. *Exp Cell Res* **203**(1): 91-9.

Crosnier, C., D. Stamataki and J. Lewis (2006). Organizing cell renewal in the intestine: stem cells, signals and combinatorial control. *Nat Rev Genet* **7**(5): 349-59.

Dalerba, P., S. J. Dylla, I. K. Park, R. Liu, X. Wang, R. W. Cho, T. Hoey, A. Gurney, E. H. Huang, D. M. Simeone, A. A. Shelton, G. Parmiani, C. Castelli and M. F. Clarke (2007). Phenotypic characterization of human colorectal cancer stem cells. *Proc Natl Acad Sci U S A* **104**(24): 10158-63.

Daley, G. Q., M. A. Goodell and E. Y. Snyder (2003). Realistic prospects for stem cell therapeutics. *Hematology (Am Soc Hematol Educ Program)*: 398-418.

DasGupta, R. and E. Fuchs (1999). Multiple roles for activated LEF/TCF transcription complexes during hair follicle development and differentiation. *Development* **126**(20): 4557-68.

Davidson, G., W. Wu, J. Shen, J. Bilic, U. Fenger, P. Stannek, A. Glinka and C. Niehrs (2005). Casein kinase 1 gamma couples Wnt receptor activation to cytoplasmic signal transduction. *Nature* **438**(7069): 867-72.

Davies, P. S., A. D. Dismuke, A. E. Powell, K. H. Carroll and M. H. Wong (2008). Wnt-reporter expression pattern in the mouse intestine during homeostasis. *BMC Gastroenterol* **8**: 57.

Doane, A. S., M. Danso, P. Lal, M. Donaton, L. Zhang, C. Hudis and W. L. Gerald (2006). An estrogen receptor-negative breast cancer subset characterized by a hormonally regulated transcriptional program and response to androgen. *Oncogene* **25**(28): 3994-4008.

Du, S. J., S. M. Purcell, J. L. Christian, L. L. McGrew and R. T. Moon (1995). Identification of distinct classes and functional domains of Wnts through expression of wild-type and chimeric proteins in Xenopus embryos. *Mol Cell Biol* **15**(5): 2625-34.

Dull, T., R. Zufferey, M. Kelly, R. J. Mandel, M. Nguyen, D. Trono and L. Naldini (1998). A third-generation lentivirus vector with a conditional packaging system. *J Virol* **72**(11): 8463-71.

Dylla, S. J., L. Beviglia, I. K. Park, C. Chartier, J. Raval, L. Ngan, K. Pickell, J. Aguilar, S. Lazetic, S. Smith-Berdan, M. F. Clarke, T. Hoey, J. Lewicki and A. L. Gurney (2008). Colorectal cancer stem cells are enriched in xenogeneic tumors following chemotherapy. *PLoS ONE* **3**(6): e2428.

Fagotto, F., U. Gluck and B. M. Gumbiner (1998). Nuclear localization signal-independent and importin/karyopherin-independent nuclear import of beta-catenin. *Curr Biol* **8**(4): 181-90.

Fassler, R. (2004). Lentiviral transgene vectors. *EMBO Rep* **5**(1): 28-9.

Fevr, T., S. Robine, D. Louvard and J. Huelsken (2007). Wnt/beta-catenin is essential for intestinal homeostasis and maintenance of intestinal stem cells. *Mol Cell Biol* **27**(21): 7551-9.

Flavell, R. B. (1994). Inactivation of gene expression in plants as a consequence of specific sequence duplication. *Proc Natl Acad Sci U S A* **91**(9): 3490-6.

http://www.med.umich.edu/tamc/spike.html.

Fujimoto, K., R. D. Beauchamp and R. H. Whitehead (2002). Identification and isolation of candidate human colonic clonogenic cells based on cell surface integrin expression. *Gastroenterology* **123**(6): 1941-8.

Glinka, A., W. Wu, H. Delius, A. P. Monaghan, C. Blumenstock and C. Niehrs (1998). Dickkopf-1 is a member of a new family of secreted proteins and functions in head induction. *Nature* **391**(6665): 357-62.

Gordon, M. D. and R. Nusse (2006). Wnt signaling: multiple pathways, multiple receptors, and multiple transcription factors. *J Biol Chem* **281**(32): 22429-33.

Gregorieff, A. and H. Clevers (2005). Wnt signaling in the intestinal epithelium: from endoderm to cancer. *Genes Dev* **19**(8): 877-90.

Gregorieff, A., D. Pinto, H. Begthel, O. Destree, M. Kielman and H. Clevers (2005). Expression pattern of Wnt signaling components in the adult intestine. *Gastroenterology* **129**(2): 626-38.

Haegebarth, A. and H. Clevers (2009). Wnt signaling, lgr5, and stem cells in the intestine and skin. *Am J Pathol* **174**(3): 715-21.

Hagemann, R. F., C. P. Sigdestad and S. Lesher (1970). A quantitative description of the intestinal epithelium of the mouse. *Am J Anat* **129**(1): 41-51.

Harada, N., Y. Tamai, T. Ishikawa, B. Sauer, K. Takaku, M. Oshima and M. M. Taketo (1999). Intestinal polyposis in mice with a dominant stable mutation of the beta-catenin gene. *The EMBO journal* **18**(21): 5931-42.

Harris, R. G., E. L. Herzog, E. M. Bruscia, J. E. Grove, J. S. Van Arnam and D. S. Krause (2004). Lack of a fusion requirement for development of bone marrow-derived epithelia. *Science* **305**(5680): 90-3.

Hassan, N. J., A. N. Barclay and M. H. Brown (2004). Frontline: Optimal T cell activation requires the engagement of CD6 and CD166. *Eur J Immunol* **34**(4): 930-40.

He, X. C., J. Zhang, W. G. Tong, O. Tawfik, J. Ross, D. H. Scoville, Q. Tian, X. Zeng, X. He, L. M. Wiedemann, Y. Mishina and L. Li (2004). BMP signaling inhibits intestinal stem cell self-renewal through suppression of Wnt-beta-catenin signaling. *Nat Genet* **36**(10): 1117-21.

He, F., W. Xiong, X. Yu, R. Espinoza-Lewis, C. Liu, S. Gu, M. Nishita, K. Suzuki, G. Yamada, Y. Minami and Y. Chen (2008). Wnt5a regulates directional cell migration and cell proliferation via Ror2-mediated noncanonical pathway in mammalian palate development. *Development* **135**(23): 3871-9.

Hendry, J. H., S. A. Roberts and C. S. Potten (1992). The clonogen content of murine intestinal crypts: dependence on radiation dose used in its determination. *Radiat Res* **132**(1): 115-9.

Herold, M. J., J. van den Brandt, J. Seibler and H. M. Reichardt (2008). Inducible and reversible gene silencing by stable integration of an shRNA-

encoding lentivirus in transgenic rats. *Proceedings of the National Academy of Sciences of the United States of America* **105**(47): 18507-12.

Hoang, B., M. Moos, Jr., S. Vukicevic and F. P. Luyten (1996). Primary structure and tissue distribution of FRZB, a novel protein related to Drosophila frizzled, suggest a role in skeletal morphogenesis. *J Biol Chem* **271**(42): 26131-7.

Hong, D., R. Gupta, P. Ancliff, A. Atzberger, J. Brown, S. Soneji, J. Green, S. Colman, W. Piacibello, V. Buckle, S. Tsuzuki, M. Greaves and T. Enver (2008). Initiating and cancer-propagating cells in TEL-AML1-associated childhood leukemia. *Science* **319**(5861): 336-9.

Hooper, L. V., M. H. Wong, A. Thelin, L. Hansson, P. G. Falk and J. I. Gordon (2001). Molecular analysis of commensal host-microbial relationships in the intestine. *Science* **291**(5505): 881-4.

Houghton, J., C. Stoicov, S. Nomura, A. B. Rogers, J. Carlson, H. Li, X. Cai, J. G. Fox, J. R. Goldenring and T. C. Wang (2004). Gastric cancer originating from bone marrow-derived cells. *Science* **306**(5701): 1568-71.

Huang, S., Y. Chen, K. Podsypanina and Y. Li (2008). Comparison of expression profiles of metastatic versus primary mammary tumors in MMTV-Wnt-1 and MMTV-Neu transgenic mice. *Neoplasia* **10**(2): 118-24.

Ikeda, K. and T. Quertermous (2004). Molecular isolation and characterization of a soluble isoform of activated leukocyte cell adhesion molecule that modulates endothelial cell function. *J Biol Chem* **279**(53): 55315-23.

Ingham, D. J., S. Beer, S. Money and G. Hansen (2001). Quantitative real-time PCR assay for determining transgene copy number in transformed plants. *Biotechniques* **31**(1): 132-4, 136-40.

Ireland, H., R. Kemp, C. Houghton, L. Howard, A. R. Clarke, O. J. Sansom and D. J. Winton (2004). Inducible Cre-mediated control of gene expression in the murine gastrointestinal tract: effect of loss of beta-catenin. *Gastroenterology* **126**(5): 1236-46.

Jezierska, A., W. Matysiak and T. Motyl (2006). ALCAM/CD166 protects breast cancer cells against apoptosis and autophagy. *Med Sci Monit* **12**(8): BR263-73.

Jiang, Y., B. N. Jahagirdar, R. L. Reinhardt, R. E. Schwartz, C. D. Keene, X. R. Ortiz-Gonzalez, M. Reyes, T. Lenvik, T. Lund, M. Blackstad, J. Du, S. Aldrich, A. Lisberg, W. C. Low, D. A. Largaespada and C. M. Verfaillie (2002). Pluripotency of mesenchymal stem cells derived from adult marrow. *Nature* **418**(6893): 41-9.

Kanki, J. P., S. Chang and J. Y. Kuwada (1994). The molecular cloning and characterization of potential chick DM-GRASP homologs in zebrafish and mouse. *J Neurobiol* **25**(7): 831-45.

Kato, Y., Y. Tanaka, M. Hayashi, K. Okawa and N. Minato (2006). Involvement of CD166 in the activation of human gamma delta T cells by tumor cells sensitized with nonpeptide antigens. *J Immunol* **177**(2): 877-84.

Kayahara, T., M. Sawada, S. Takaishi, H. Fukui, H. Seno, H. Fukuzawa, K. Suzuki, H. Hiai, R. Kageyama, H. Okano and T. Chiba (2003).

Candidate markers for stem and early progenitor cells, Musashi-1 and Hes1, are expressed in crypt base columnar cells of mouse small intestine. *FEBS Lett* **535**(1-3): 131-5.

Kennerdell, J. R. and R. W. Carthew (1998). Use of dsRNA-mediated genetic interference to demonstrate that frizzled and frizzled 2 act in the wingless pathway. *Cell* **95**(7): 1017-26.

Kiely, B., R. T. O'Donovan, S. L. McKenna and G. C. O'Sullivan (2007). Beta-catenin transcriptional activity is inhibited downstream of nuclear localisation and is not influenced by IGF signalling in oesophageal cancer cells. *Int J Cancer* **121**(9): 1903-9.

Kinzler, K. W., M. C. Nilbert, L. K. Su, B. Vogelstein, T. M. Bryan, D. B. Levy, K. J. Smith, A. C. Preisinger, P. Hedge, D. McKechnie and et al. (1991). Identification of FAP locus genes from chromosome 5q21. *Science* **253**(5020): 661-5.

Kinzler, K. W. and B. Vogelstein (1996). Lessons from hereditary colorectal cancer. *Cell* **87**(2): 159-70.

Klein, W. M., B. P. Wu, S. Zhao, H. Wu, A. J. Klein-Szanto and S. R. Tahan (2007). Increased expression of stem cell markers in malignant melanoma. *Mod Pathol* **20**(1): 102-7.

Klingensmith, J. and R. Nusse (1994). Signaling by wingless in Drosophila. *Dev Biol* **166**(2): 396-414.

Korbling, M., R. L. Katz, A. Khanna, A. C. Ruifrok, G. Rondon, M. Albitar, R. E. Champlin and Z. Estrov (2002). Hepatocytes and epithelial cells of

donor origin in recipients of peripheral-blood stem cells. *N Engl J Med* **346**(10): 738-46.

Korinek, V., N. Barker, P. Moerer, E. van Donselaar, G. Huls, P. J. Peters and H. Clevers (1998a). Depletion of epithelial stem-cell compartments in the small intestine of mice lacking Tcf-4. *Nat Genet* **19**(4): 379-83.

Korinek, V., N. Barker, K. Willert, M. Molenaar, J. Roose, G. Wagenaar, M. Markman, W. Lamers, O. Destree and H. Clevers (1998b). Two members of the Tcf family implicated in Wnt/beta-catenin signaling during embryogenesis in the mouse. *Mol Cell Biol* **18**(3): 1248-56.

Kosaka, Y., N. Kobayashi, T. Fukazawa, T. Totsugawa, M. Maruyama, C. Yong, T. Arata, H. Ikeda, K. Kobayashi, T. Ueda, Y. Kurabayashi and N. Tanaka (2004). Lentivirus-based gene delivery in mouse embryonic stem cells. *Artif Organs* **28**(3): 271-7.

Krause, D. S., N. D. Theise, M. I. Collector, O. Henegariu, S. Hwang, R. Gardner, S. Neutzel and S. J. Sharkis (2001). Multi-organ, multi-lineage engraftment by a single bone marrow-derived stem cell. *Cell* **105**(3): 369-77.

Kristiansen, G., C. Pilarsky, C. Wissmann, C. Stephan, L. Weissbach, V. Loy, S. Loening, M. Dietel and A. Rosenthal (2003). ALCAM/CD166 is up-regulated in low-grade prostate cancer and progressively lost in high-grade lesions. *Prostate* **54**(1): 34-43.

Kuhl, M., L. C. Sheldahl, C. C. Malbon and R. T. Moon (2000a). Ca(2+)/calmodulin-dependent protein kinase II is stimulated by Wnt and

Frizzled homologs and promotes ventral cell fates in Xenopus. *J Biol Chem* **275**(17): 12701-11.

Kuhl, M., L. C. Sheldahl, M. Park, J. R. Miller and R. T. Moon (2000b). The Wnt/Ca2+ pathway: a new vertebrate Wnt signaling pathway takes shape. *Trends Genet* **16**(7): 279-83.

Kuhnert, F., C. R. Davis, H. T. Wang, P. Chu, M. Lee, J. Yuan, R. Nusse and C. J. Kuo (2004). Essential requirement for Wnt signaling in proliferation of adult small intestine and colon revealed by adenoviral expression of Dickkopf-1. *Proc Natl Acad Sci U S A* **101**(1): 266-71.

Lendrum, A. C. (1947). The phloxine-tartrazine method as a general histological stain for demonstration of inclusion bodies. *Journal of Pathology and Bacteriology* **59**: 399-404.

Li, C., D. G. Heidt, P. Dalerba, C. F. Burant, L. Zhang, V. Adsay, M. Wicha, M. F. Clarke and D. M. Simeone (2007). Identification of pancreatic cancer stem cells. *Cancer Res* **67**(3): 1030-7.

Lickert, H., A. Kispert, S. Kutsch and R. Kemler (2001). Expression patterns of Wnt genes in mouse gut development. *Mech Dev* **105**(1-2): 181-4.

Lipkin, M. (1985). Growth and development of gastrointestinal cells. *Annu Rev Physiol* **47**: 175-97.

Liu, C., Y. Li, M. Semenov, C. Han, G. H. Baeg, Y. Tan, Z. Zhang, X. Lin and X. He (2002). Control of beta-catenin phosphorylation/degradation by a dual-kinase mechanism. *Cell* **108**(6): 837-47.

Liu, P., M. Wakamiya, M. J. Shea, U. Albrecht, R. R. Behringer and A. Bradley (1999). Requirement for Wnt3 in vertebrate axis formation. *Nat Genet* **22**(4): 361-5.

Livak, K. J. and T. D. Schmittgen (2001). Analysis of relative gene expression data using real-time quantitative PCR and the 2(-Delta Delta C(T)) Method. *Methods* **25**(4): 402-8.

Logan, C. Y. and R. Nusse (2004). The Wnt signaling pathway in development and disease. *Annu Rev Cell Dev Biol* **20**: 781-810.

Luna, L. G. (1968). Manual of Histologic Staining Methods of the Armed Forces Institute of Pathology. New York, McGraw-Hill Book Co.

Madison, B. B., L. Dunbar, X. T. Qiao, K. Braunstein, E. Braunstein and D. L. Gumucio (2002). Cis elements of the villin gene control expression in restricted domains of the vertical (crypt) and horizontal (duodenum, cecum) axes of the intestine. *The Journal of biological chemistry* **277**(36): 33275-83.

Maretto, S., M. Cordenonsi, S. Dupont, P. Braghetta, V. Broccoli, A. B. Hassan, D. Volpin, G. M. Bressan and S. Piccolo (2003). Mapping Wnt/beta-catenin signaling during mouse development and in colorectal tumors. *Proc Natl Acad Sci U S A* **100**(6): 3299-304.

Martinez, J. and J. Walker (2004). Real-time and Quantitative PCR. Toxicogenomics: Principles and Applications. H. K. Hamadeh and C. A. Afshari. Indianapolis, IN, John Wiley & Sons**:** 147-163.

Masedunskas, A., J. A. King, F. Tan, R. Cochran, T. Stevens, D. Sviridov and S. F. Ofori-Acquah (2006). Activated leukocyte cell adhesion molecule is a component of the endothelial junction involved in transendothelial monocyte migration. *FEBS Lett* **580**(11): 2637-45.

May, R., T. E. Riehl, C. Hunt, S. M. Sureban, S. Anant and C. W. Houchen (2008). Identification of a novel putative gastrointestinal stem cell and adenoma stem cell marker, doublecortin and CaM kinase-like-1, following radiation injury and in adenomatous polyposis coli/multiple intestinal neoplasia mice. *Stem Cells* **26**(3): 630-7.

McMahon, A. P. and R. T. Moon (1989). Ectopic expression of the proto-oncogene int-1 in Xenopus embryos leads to duplication of the embryonic axis. *Cell* **58**(6): 1075-84.

McMahon, A. P. and A. Bradley (1990). The Wnt-1 (int-1) proto-oncogene is required for development of a large region of the mouse brain. *Cell* **62**(6): 1073-85.

Mezzanzanica, D., M. Fabbi, M. Bagnoli, S. Staurengo, M. Losa, E. Balladore, P. Alberti, L. Lusa, A. Ditto, S. Ferrini, M. A. Pierotti, M. Barbareschi, S. Pilotti and S. Canevari (2008). Subcellular localization of activated leukocyte cell adhesion molecule is a molecular predictor of survival in ovarian carcinoma patients. *Clin Cancer Res* **14**(6): 1726-33.

Mikels, A. J. and R. Nusse (2006). Purified Wnt5a protein activates or inhibits beta-catenin-TCF signaling depending on receptor context. *PLoS Biol* **4**(4): e115.

Molenaar, M., M. van de Wetering, M. Oosterwegel, J. Peterson-Maduro, S. Godsave, V. Korinek, J. Roose, O. Destree and H. Clevers (1996). XTcf-3 transcription factor mediates beta-catenin-induced axis formation in Xenopus embryos. *Cell* **86**(3): 391-9.

Moriyama, A., I. Kii, T. Sunabori, S. Kurihara, I. Takayama, M. Shimazaki, H. Tanabe, M. Oginuma, M. Fukayama, Y. Matsuzaki, Y. Saga and A. Kudo (2007). GFP transgenic mice reveal active canonical Wnt signal in neonatal brain and in adult liver and spleen. *Genesis* **45**(2): 90-100.

Moser, A. R., H. C. Pitot and W. F. Dove (1990). A dominant mutation that predisposes to multiple intestinal neoplasia in the mouse. *Science* **247**(4940): 322-4.

Muncan, V., O. J. Sansom, L. Tertoolen, T. J. Phesse, H. Begthel, E. Sancho, A. M. Cole, A. Gregorieff, I. M. de Alboran, H. Clevers and A. R. Clarke (2006). Rapid loss of intestinal crypts upon conditional deletion of the Wnt/Tcf-4 target gene c-Myc. *Mol Cell Biol*.

Murtaugh, L. C., J. H. Chyung and A. B. Lassar (1999). Sonic hedgehog promotes somitic chondrogenesis by altering the cellular response to BMP signaling. *Genes Dev* **13**(2): 225-37.

Naldini, L., U. Blomer, P. Gallay, D. Ory, R. Mulligan, F. H. Gage, I. M. Verma and D. Trono (1996). In vivo gene delivery and stable transduction of nondividing cells by a lentiviral vector. *Science* **272**(5259): 263-7.

Naldini, L. (1998). Lentiviruses as gene transfer agents for delivery to non-dividing cells. *Curr Opin Biotechnol* **9**(5): 457-63.

Nagy, A. (2003). Manipulating the mouse embryo : a laboratory manual. Cold Spring Harbor, N.Y., Cold Spring Harbor Laboratory Press.

Nishisho, I., Y. Nakamura, Y. Miyoshi, Y. Miki, H. Ando, A. Horii, K. Koyama, J. Utsunomiya, S. Baba and P. Hedge (1991). Mutations of chromosome 5q21 genes in FAP and colorectal cancer patients. *Science* **253**(5020): 665-9.

Nishita, M., S. K. Yoo, A. Nomachi, S. Kani, N. Sougawa, Y. Ohta, S. Takada, A. Kikuchi and Y. Minami (2006). Filopodia formation mediated by receptor tyrosine kinase Ror2 is required for Wnt5a-induced cell migration. *J Cell Biol* **175**(4): 555-62.

Nowell, P. C. (1976). The clonal evolution of tumor cell populations. *Science* **194**(4260): 23-8.

Nusse, R. and H. E. Varmus (1982). Many tumors induced by the mouse mammary tumor virus contain a provirus integrated in the same region of the host genome. *Cell* **31**(1): 99-109.

Nusse, R. and H. E. Varmus (1992). Wnt genes. *Cell* **69**(7): 1073-87.

Nusse, R. (1999). WNT targets. Repression and activation. *Trends Genet* **15**(1): 1-3.

Nusse, R. (2008). The Wnt Homepage. from http://www.stanford.edu/~rnusse/wntwindow.html.

Nygren, J. M., S. Jovinge, M. Breitbach, P. Sawen, W. Roll, J. Hescheler, J. Taneera, B. K. Fleischmann and S. E. Jacobsen (2004). Bone marrow-

derived hematopoietic cells generate cardiomyocytes at a low frequency through cell fusion, but not transdifferentiation. *Nat Med* **10**(5): 494-501.

O'Brien, C. A., A. Pollett, S. Gallinger and J. E. Dick (2007). A human colon cancer cell capable of initiating tumour growth in immunodeficient mice. *Nature* **445**(7123): 106-10.

Ohneda, O., K. Ohneda, F. Arai, J. Lee, T. Miyamoto, Y. Fukushima, D. Dowbenko, L. A. Lasky and T. Suda (2001). ALCAM (CD166): its role in hematopoietic and endothelial development. *Blood* **98**(7): 2134-42.

Okabe, M., M. Ikawa, K. Kominami, T. Nakanishi and Y. Nishimune (1997). 'Green mice' as a source of ubiquitous green cells. *FEBS Lett* **407**(3): 313-9.

Okamoto, R., T. Yajima, M. Yamazaki, T. Kanai, M. Mukai, S. Okamoto, Y. Ikeda, T. Hibi, J. Inazawa and M. Watanabe (2002). Damaged epithelia regenerated by bone marrow-derived cells in the human gastrointestinal tract. *Nat Med* **8**(9): 1011-7.

Pacheco, Il and R. J. Macleod (2008). CaSR stimulates secretion of Wnt5a from colonic myofibroblasts to stimulate CDX2 and sucrase-isomaltase using Ror2 on intestinal epithelia. *Am J Physiol Gastrointest Liver Physiol* **295**(4): G748-59.

Pardal, R., M. F. Clarke and S. J. Morrison (2003). Applying the principles of stem-cell biology to cancer. *Nat Rev Cancer* **3**(12): 895-902.

Patel, D. D., S. F. Wee, L. P. Whichard, M. A. Bowen, J. M. Pesando, A. Aruffo and B. F. Haynes (1995). Identification and characterization of a

100-kD ligand for CD6 on human thymic epithelial cells. *J Exp Med* **181**(4): 1563-8.

Piazza, T., E. Cha, I. Bongarzone, S. Canevari, A. Bolognesi, L. Polito, A. Bargellesi, F. Sassi, S. Ferrini and M. Fabbi (2005). Internalization and recycling of ALCAM/CD166 detected by a fully human single-chain recombinant antibody. *J Cell Sci* **118**(Pt 7): 1515-25.

Picco, V., C. Hudson and H. Yasuo (2007). Ephrin-Eph signalling drives the asymmetric division of notochord/neural precursors in Ciona embryos. *Development* **134**(8): 1491-7.

Pinto, D., A. Gregorieff, H. Begthel and H. Clevers (2003). Canonical Wnt signals are essential for homeostasis of the intestinal epithelium. *Genes Dev* **17**(14): 1709-13.

Pomerantz, J. and H. M. Blau (2004). Nuclear reprogramming: a key to stem cell function in regenerative medicine. *Nat Cell Biol* **6**(9): 810-6.

Potten, C. S. (1974). The epidermal proliferative unit: the possible role of the central basal cell. *Cell Tissue Kinet* **7**(1): 77-88.

Potten, C. S. (1977). Extreme sensitivity of some intestinal crypt cells to X and gamma irradiation. *Nature* **269**(5628): 518-21.

Potten, C. S. and T. D. Allen (1977). Ultrastructure of cell loss in intestinal mucosa. *J Ultrastruct Res* **60**(2): 272-7.

Potten, C. S. and J. C. Bullock (1983). Cell kinetic studies in the epidermis of the mouse. I. Changes in labeling index with time after tritiated thymidine administration. *Experientia* **39**(10): 1125-9.

Potten, C. S. (1990). A comprehensive study of the radiobiological response of the murine (BDF1) small intestine. *Int J Radiat Biol* **58**(6): 925-73.

Potten, C. S., C. Booth, G. L. Tudor, D. Booth, G. Brady, P. Hurley, G. Ashton, R. Clarke, S. Sakakibara and H. Okano (2003). Identification of a putative intestinal stem cell and early lineage marker; musashi-1. *Differentiation* **71**(1): 28-41.

Radtke, F., H. Clevers and O. Riccio (2006). From gut homeostasis to cancer. *Curr Mol Med* **6**(3): 275-89.

Reinisch, C., S. Kandutsch, A. Uthman and J. Pammer (2006). BMI-1: a protein expressed in stem cells, specialized cells and tumors of the gastrointestinal tract. *Histol Histopathol* **21**(11): 1143-9.

Reya, T. and H. Clevers (2005). Wnt signalling in stem cells and cancer. *Nature* **434**(7035): 843-50.

Ringel, M. D., W. F. Schwindinger, M. Saji, M. A. Zeiger and M. A. Levine (1998). Determination of transgene copy number and expression level using denaturing gradient gel electrophoresis. *Biotechniques* **24**(1): 126, 128-31.

Rizvi, A. Z. and M. H. Wong (2005). Epithelial stem cells and their niche: there's no place like home. *Stem Cells* **23**(2): 150-65.

Roarty, K. and R. Serra (2007). Wnt5a is required for proper mammary gland development and TGF-beta-mediated inhibition of ductal growth. *Development* **134**(21): 3929-39.

Roose, J., M. Molenaar, J. Peterson, J. Hurenkamp, H. Brantjes, P. Moerer, M. van de Wetering, O. Destree and H. Clevers (1998). The Xenopus Wnt effector XTcf-3 interacts with Groucho-related transcriptional repressors. *Nature* **395**(6702): 608-12.

Roth, A., D. C. Drummond, F. Conrad, M. E. Hayes, D. B. Kirpotin, C. C. Benz, J. D. Marks and B. Liu (2007). Anti-CD166 single chain antibody-mediated intracellular delivery of liposomal drugs to prostate cancer cells. *Molecular Cancer Therapy* **6**(10): 2737-46.

Sakamoto, I., S. Kishida, A. Fukui, M. Kishida, H. Yamamoto, S. Hino, T. Michiue, S. Takada, M. Asashima and A. Kikuchi (2000). A novel beta-catenin-binding protein inhibits beta-catenin-dependent Tcf activation and axis formation. *Journal of Biological Chemistry* **275**(42): 32871-8.

Sambrook, J. and D. W. Russell (2001). Molecular cloning : a laboratory manual. Cold Spring Harbor, N.Y., Cold Spring Harbor Laboratory Press.

Sangiorgi, E. and M. R. Capecchi (2008). Bmi1 is expressed in vivo in intestinal stem cells. *Nature Genetics* **40**(7): 915-20.

Sansom, O. J., K. R. Reed, A. J. Hayes, H. Ireland, H. Brinkmann, I. P. Newton, E. Batlle, P. Simon-Assmann, H. Clevers, I. S. Nathke, A. R. Clarke and D. J. Winton (2004). Loss of Apc in vivo immediately perturbs Wnt signaling, differentiation, and migration. *Genes & Development* **18**(12): 1385-90.

Sansom, O. J., K. R. Reed, M. van de Wetering, V. Muncan, D. J. Winton, H. Clevers and A. R. Clarke (2005). Cyclin D1 is not an immediate target of

beta-catenin following Apc loss in the intestine. *Journal Biological Chemistry* **280**(31): 28463-7.

Sansom, O. J., V. S. Meniel, V. Muncan, T. J. Phesse, J. A. Wilkins, K. R. Reed, J. K. Vass, D. Athineos, H. Clevers and A. R. Clarke (2007). Myc deletion rescues Apc deficiency in the small intestine. *Nature* **446**(7136): 676-9.

Sato, T., R. G. Vries, H. J. Snippert, M. van de Wetering, N. Barker, D. E. Stange, J. H. van Es, A. Abo, P. Kujala, P. J. Peters and H. Clevers (2009). Single Lgr5 stem cells build crypt-villus structures in vitro without a mesenchymal niche. *Nature*.

Schambony, A. and D. Wedlich (2007). Wnt-5A/Ror2 regulate expression of XPAPC through an alternative noncanonical signaling pathway. *Dev Cell* **12**(5): 779-92.

Scoville, D. H., T. Sato, X. C. He and L. Li (2008). Current view: intestinal stem cells and signaling. *Gastroenterology* **134**(3): 849-64.

Selinger, D. W., R. M. Saxena, K. J. Cheung, G. M. Church and C. Rosenow (2003). Global RNA half-life analysis in Escherichia coli reveals positional patterns of transcript degradation. *Genome Res* **13**(2): 216-23.

Seppen, J., R. van der Rijt, N. Looije, N. P. van Til, W. H. Lamers and R. P. Oude Elferink (2003). Long-term correction of bilirubin UDPglucuronyltransferase deficiency in rats by in utero lentiviral gene transfer. *Mol Ther* **8**(4): 593-9.

Sheldahl, L. C., M. Park, C. C. Malbon and R. T. Moon (1999). Protein kinase C is differentially stimulated by Wnt and Frizzled homologs in a G-protein-dependent manner. *Curr Biol* **9**(13): 695-8.

Shibata, H., K. Toyama, H. Shioya, M. Ito, M. Hirota, S. Hasegawa, H. Matsumoto, H. Takano, T. Akiyama, K. Toyoshima, R. Kanamaru, Y. Kanegae, I. Saito, Y. Nakamura, K. Shiba and T. Noda (1997). Rapid colorectal adenoma formation initiated by conditional targeting of the Apc gene. *Science* **278**(5335): 120-3.

Sierra, J., T. Yoshida, C. A. Joazeiro and K. A. Jones (2006). The APC tumor suppressor counteracts beta-catenin activation and H3K4 methylation at Wnt target genes. *Genes Dev* **20**(5): 586-600.

Silver, L. M. (1995). Mouse genetics : concepts and applications. New York, Oxford University Press.

Skarsgard, E. D., L. Huang, S. C. Reebye, A. Y. Yeung and W. W. Jia (2005). Lentiviral vector-mediated, in vivo gene transfer to the tracheobronchial tree in fetal rabbits. *J Pediatr Surg* **40**(12): 1817-21.

Slusarski, D. C., V. G. Corces and R. T. Moon (1997a). Interaction of Wnt and a Frizzled homologue triggers G-protein-linked phosphatidylinositol signalling. *Nature* **390**(6658): 410-3.

Slusarski, D. C., J. Yang-Snyder, W. B. Busa and R. T. Moon (1997b). Modulation of embryonic intracellular Ca2+ signaling by Wnt-5A. *Dev Biol* **182**(1): 114-20.

Soriano, P. (1999). Generalized lacZ expression with the ROSA26 Cre reporter strain. *Nat Genet* **21**(1): 70-1.

Spyridonidis, A., A. Schmitt-Graff, T. Tomann, A. Dwenger, M. Follo, D. Behringer and J. Finke (2004). Epithelial tissue chimerism after human hematopoietic cell transplantation is a real phenomenon. *Am J Pathol* **164**(4): 1147-55.

Staal, F. J. and H. C. Clevers (2005). WNT signalling and haematopoiesis: a WNT-WNT situation. *Nat Rev Immunol* **5**(1): 21-30.

Stappenbeck, T. S., L. V. Hooper, J. K. Manchester, M. H. Wong and J. I. Gordon (2002). Laser capture microdissection of mouse intestine: characterizing mRNA and protein expression, and profiling intermediary metabolism in specified cell populations. *Methods Enzymol* **356**: 167-96.

Stappenbeck, T. S., J. C. Mills and J. I. Gordon (2003). Molecular features of adult mouse small intestinal epithelial progenitors. *Proc Natl Acad Sci U S A* **100**(3): 1004-9.

Su, L. K., K. W. Kinzler, B. Vogelstein, A. C. Preisinger, A. R. Moser, C. Luongo, K. A. Gould and W. F. Dove (1992). Multiple intestinal neoplasia caused by a mutation in the murine homolog of the APC gene. *Science* **256**(5057): 668-70.

Sweetser, D. A., S. M. Hauft, P. C. Hoppe, E. H. Birkenmeier and J. I. Gordon (1988). Transgenic mice containing intestinal fatty acid-binding protein-human growth hormone fusion genes exhibit correct regional and cell-specific expression of the reporter gene in their small intestine.

Proceedings of the National Academy of Sciences of the United States of America **85**(24): 9611-5.

Takada, S., K. L. Stark, M. J. Shea, G. Vassileva, J. A. McMahon and A. P. McMahon (1994). Wnt-3a regulates somite and tailbud formation in the mouse embryo. *Genes Dev* **8**(2): 174-89.

Takemaru, K., S. Yamaguchi, Y. S. Lee, Y. Zhang, R. W. Carthew and R. T. Moon (2003). Chibby, a nuclear beta-catenin-associated antagonist of the Wnt/Wingless pathway. *Nature* **422**(6934): 905-9.

Tomita, K., A. van Bokhovenâ€ , C. F. J. Jansen, L. A. Kiemeney, H. F. M. Karthaus, J. Vriesema, M. J. G. Bussemakers, J. A. Witjes and J. A. Schalken (2003). Activated Leukocyte Cell Adhesion Molecule (ALCAM) Expression is Associated with a Poor Prognosis for Bladder Cancer Patients. *Urooncology* **3**(3): 121 - 129.

Topol, L., X. Jiang, H. Choi, L. Garrett-Beal, P. J. Carolan and Y. Yang (2003). Wnt-5a inhibits the canonical Wnt pathway by promoting GSK-3-independent beta-catenin degradation. *J Cell Biol* **162**(5): 899-908.

Torres, M. A., J. A. Yang-Snyder, S. M. Purcell, A. A. DeMarais, L. L. McGrew and R. T. Moon (1996). Activities of the Wnt-1 class of secreted signaling factors are antagonized by the Wnt-5A class and by a dominant negative cadherin in early Xenopus development. *J Cell Biol* **133**(5): 1123-37.

Uchida, N., Z. Yang, J. Combs, O. Pourquie, M. Nguyen, R. Ramanathan, J. Fu, A. Welply, S. Chen, G. Weddell, A. K. Sharma, K. R. Leiby, D.

Karagogeos, B. Hill, L. Humeau, W. B. Stallcup, R. Hoffman, A. S. Tsukamoto, D. P. Gearing and B. Peault (1997). The characterization, molecular cloning, and expression of a novel hematopoietic cell antigen from CD34+ human bone marrow cells. *Blood* **89**(8): 2706-16.

van de Wetering, M., E. Sancho, C. Verweij, W. de Lau, I. Oving, A. Hurlstone, K. van der Horn, E. Batlle, D. Coudreuse, A. P. Haramis, M. Tjon-Pon-Fong, P. Moerer, M. van den Born, G. Soete, S. Pals, M. Eilers, R. Medema and H. Clevers (2002). The beta-catenin/TCF-4 complex imposes a crypt progenitor phenotype on colorectal cancer cells. *Cell* **111**(2): 241-50.

Van der Flier, L. G., J. Sabates-Bellver, I. Oving, A. Haegebarth, M. De Palo, M. Anti, M. E. Van Gijn, S. Suijkerbuijk, M. Van de Wetering, G. Marra and H. Clevers (2007). The Intestinal Wnt/TCF Signature. *Gastroenterology* **132**(2): 628-32.

van Es, J. H., P. Jay, A. Gregorieff, M. E. van Gijn, S. Jonkheer, P. Hatzis, A. Thiele, M. van den Born, H. Begthel, T. Brabletz, M. M. Taketo and H. Clevers (2005). Wnt signalling induces maturation of Paneth cells in intestinal crypts. *Nat Cell Biol* **7**(4): 381-6.

van Kempen, L. C., J. J. van den Oord, G. N. van Muijen, U. H. Weidle, H. P. Bloemers and G. W. Swart (2000). Activated leukocyte cell adhesion molecule/CD166, a marker of tumor progression in primary malignant melanoma of the skin. *Am J Pathol* **156**(3): 769-74.

Vassilopoulos, G., P. R. Wang and D. W. Russell (2003). Transplanted bone marrow regenerates liver by cell fusion. *Nature* **422**(6934): 901-4.

Vaucheret, H., C. Beclin, T. Elmayan, F. Feuerbach, C. Godon, J. B. Morel, P. Mourrain, J. C. Palauqui and S. Vernhettes (1998). Transgene-induced gene silencing in plants. *Plant J* **16**(6): 651-9.

Verma, A., N. K. Shukla, S. V. Deo, S. D. Gupta and R. Ralhan (2005). MEMD/ALCAM: a potential marker for tumor invasion and nodal metastasis in esophageal squamous cell carcinoma. *Oncology* **68**(4-6): 462-70.

Vermeulen, L., M. R. Sprick, K. Kemper, G. Stassi and J. P. Medema (2008). Cancer stem cells--old concepts, new insights. *Cell Death Differ* **15**(6): 947-58.

Wagers, A. J. and I. L. Weissman (2004). Plasticity of adult stem cells. *Cell* **116**(5): 639-48.

Wang, X., H. Willenbring, Y. Akkari, Y. Torimaru, M. Foster, M. Al-Dhalimy, E. Lagasse, M. Finegold, S. Olson and M. Grompe (2003). Cell fusion is the principal source of bone-marrow-derived hepatocytes. *Nature* **422**(6934): 897-901.

Wehkamp, J., G. Wang, I. Kubler, S. Nuding, A. Gregorieff, A. Schnabel, R. J. Kays, K. Fellermann, O. Burk, M. Schwab, H. Clevers, C. L. Bevins and E. F. Stange (2007). The Paneth cell alpha-defensin deficiency of ileal Crohn's disease is linked to Wnt/Tcf-4. *J Immunol* **179**(5): 3109-18.

Wehrli, M., S. T. Dougan, K. Caldwell, L. O'Keefe, S. Schwartz, D. Vaizel-Ohayon, E. Schejter, A. Tomlinson and S. DiNardo (2000). arrow encodes an LDL-receptor-related protein essential for Wingless signalling. *Nature* **407**(6803): 527-30.

Weichert, W., T. Knosel, J. Bellach, M. Dietel and G. Kristiansen (2004). ALCAM/CD166 is overexpressed in colorectal carcinoma and correlates with shortened patient survival. *J Clin Pathol* **57**(11): 1160-4.

Weiser, M. M. (1973a). Intestinal epithelial cell surface membrane glycoprotein synthesis. I. An indicator of cellular differentiation. *J Biol Chem* **248**(7): 2536-41.

Weiser, M. M. (1973b). Intestinal epithelial cell surface membrane glycoprotein synthesis. II. Glycosyltransferases and endogenous acceptors of the undifferentiated cell surface membrane. *J Biol Chem* **248**(7): 2542-8.

Weiss, L. (2000). Metastasis of cancer: a conceptual history from antiquity to the 1990s. *Cancer Metastasis Rev* **19**(3-4): I-XI, 193-383.

Willenbring, H. and M. Grompe (2004). Delineating the hepatocyte's hematopoietic fusion partner. *Cell Cycle* **3**(12): 1489-91.

Willert, K., J. D. Brown, E. Danenberg, A. W. Duncan, I. L. Weissman, T. Reya, J. R. Yates, 3rd and R. Nusse (2003). Wnt proteins are lipid-modified and can act as stem cell growth factors. *Nature* **423**(6938): 448-52.

Wilson, J. P. (1967). Surface area of the small intestine in man. *Gut* **8**(6): 618-21.

Wolda, S. L., C. J. Moody and R. T. Moon (1993). Overlapping expression of Xwnt-3A and Xwnt-1 in neural tissue of Xenopus laevis embryos. *Dev Biol* **155**(1): 46-57.

Wong, G. T., B. J. Gavin and A. P. McMahon (1994). Differential transformation of mammary epithelial cells by Wnt genes. *Mol Cell Biol* **14**(9): 6278-86.

Wong, M. H., M. L. Hermiston, A. J. Syder and J. I. Gordon (1996). Forced expression of the tumor suppressor adenomatosis polyposis coli protein induces disordered cell migration in the intestinal epithelium. *Proc Natl Acad Sci U S A* **93**(18): 9588-93.

Wong, M. H., B. Rubinfeld and J. I. Gordon (1998). Effects of forced expression of an NH2-terminal truncated beta-Catenin on mouse intestinal epithelial homeostasis. *J Cell Biol* **141**(3): 765-77.

Wong, M. H., J. R. Saam, T. S. Stappenbeck, C. H. Rexer and J. I. Gordon (2000). Genetic mosaic analysis based on Cre recombinase and navigated laser capture microdissection. *Proc Natl Acad Sci U S A* **97**(23): 12601-6.

Wright, N. A. (2000). Epithelial stem cell repertoire in the gut: clues to the origin of cell lineages, proliferative units and cancer. *Int J Exp Pathol* **81**(2): 117-43.

Yamaguchi, T. P., A. Bradley, A. P. McMahon and S. Jones (1999). A Wnt5a pathway underlies outgrowth of multiple structures in the vertebrate embryo. *Development* **126**(6): 1211-23.

Yamanaka, H., T. Moriguchi, N. Masuyama, M. Kusakabe, H. Hanafusa, R. Takada, S. Takada and E. Nishida (2002). JNK functions in the non-canonical Wnt pathway to regulate convergent extension movements in vertebrates. *EMBO Rep* **3**(1): 69-75.

Yanagawa, S., Y. Matsuda, J. S. Lee, H. Matsubayashi, S. Sese, T. Kadowaki and A. Ishimoto (2002). Casein kinase I phosphorylates the Armadillo protein and induces its degradation in Drosophila. *EMBO J* **21**(7): 1733-42.

Zeng, X., K. Tamai, B. Doble, S. Li, H. Huang, R. Habas, H. Okamura, J. Woodgett and X. He (2005). A dual-kinase mechanism for Wnt co-receptor phosphorylation and activation. *Nature* **438**(7069): 873-7.

Zhu, S., L. Liu, V. Korzh, Z. Gong and B. C. Low (2006). RhoA acts downstream of Wnt5 and Wnt11 to regulate convergence and extension movements by involving effectors Rho kinase and Diaphanous: use of zebrafish as an in vivo model for GTPase signaling. *Cell Signal* **18**(3): 359-72.

Zufferey, R., D. Nagy, R. J. Mandel, L. Naldini and D. Trono (1997). Multiply attenuated lentiviral vector achieves efficient gene delivery in vivo. *Nat Biotechnol* **15**(9): 871-5.

Zufferey, R., T. Dull, R. J. Mandel, A. Bukovsky, D. Quiroz, L. Naldini and D. Trono (1998). Self-inactivating lentivirus vector for safe and efficient in vivo gene delivery. *J Virol* **72**(12): 9873-80.